WRC RESEARCH REPORT NO. 182

MODELING STREAMLINES AND MASS TRANSPORT IN CIRCULATING FLOW

by

Vahid Alavian
Sally M. Broeren
David W. Bintz

Department of Civil Engineering
University of Illinois at Urbana-Champaign
Urbana, IL 61801

FINAL REPORT

Project No. A-112-ILL

This project was partially supported by funds provided by the United States Department of the Interior as authorized under the Water Resources Research and Development Act of 1978.

UNIVERSITY OF ILLINOIS
WATER RESOURCES CENTER
Urbana, Illinois 61801

October 1983

ABSTRACT

State-of-the-art of hydraulic and water quality modeling in streams and rivers does not include the role of large, slowly circulating regions in dilution and transport of effluents discharged in such water bodies. Examples of circulating regions include meander, blocked arms of the stream, and flow behind engineering structures such as jetties, wing dams, and bridge piers as well as flow within small marinas and fleeting areas.

Numerical schemes have been developed to simulate streamline patterns and mass transport within a circulating region approximated by a square cavity on the side of a channel. The circulating flow is assumed two-dimensional (depth averaged) and is generated and maintained by a known main flow at the open boundary. Results are given for characteristic Reynolds numbers ranging from 500 to 30,000.

The equation governing the mixing and transport of a finite quantity of conservative tracer instantaneously introduced at any location in the flow field has been numerically solved. The numerical scheme is based on the finite element approximation of the governing differential equation and uses the method of weighted residuals. The flow geometry is represented by triangular elements, and a linear basis function is used in the interpolation scheme. The unsteady term is approximated by finite differencing in full-forward time steps. Dispersion coefficient has been represented as a first-order tensor, the components of which are functions of the dispersion coefficients along and normal to the streamlines. Results are given for scalar and vectorized dispersion coefficients as well as a range of computation time steps.

Alavian, Vahid, Sally M. Broeren, and David W. Bintz
MODELING STREAMLINES AND MASS TRANSPORT IN CIRCULATING FLOW
Final report to the U.S. Department of the Interior
Project A-112-ILL, October 1983, 128 pages.

KEYWORDS: *mass transport/*mixing/flow pattern/circulating flow
*dispersion/*finite element/fluid mechanics

TABLE OF CONTENTS

LIST OF FIGURES

LIST OF TABLES

LIST OF SYMBOLS

Symbols of secondary importance which appear only briefly in the text are not included in this list.

a	time dependent portion of local concentration
A	finite element area
B	global boundary matrix
BigM	global matrix assembled from sum of $\frac{1}{\Delta t}M$ over all elements
c	local concentration
$\hat{c}$	approximate value of c
C_{MAX}	maximum concentration in the flow field
e	error vector $\hat{c} - c$
e	maximum value of error, e, in the flow field
E	dispersion coefficient
E_L	streamwise dispersion coefficient
E_T	transverse dispersion coefficient
E_{xx}	dispersion coefficient along x-axis
E_{yy}	dispersion coefficient along y-axis
E_{xy}	cross product of E_{xx} and E_{yy}
g_x	body force x-direction
g_y	body force y-direction
G	global matrix assembled from the sum of $\frac{1}{\Delta t}M$, K, and H over all elements
h	depth of flow
H	coefficient matrix for dispersive approximation of concentration
i,j,k,l,m,n	summation indices
K	coefficient matrix for dispersive approximation of concentration

L	characteristic length scale
M	coefficient matrix for temporal approximation of concentration
p	local pressure
P	derivative of the basis function
R	residual error from approximation of concentration equation
R_e	characteristic Reynolds number
t	time
u	velocity component along x-axis
u	approximate value of u
U	uniform main flow velocity; not applicable to equation (68)
U_a	characteristic velocity in the circulating flow
$\overline{U}$	velocity vector
v	velocity component along y-axis
$\underline{V}$	magnitude of the velocity vector
x,y,z	coordinate axes
ν	kinematic viscosity
ρ	local density
τ	turbulent shear stress
ϕ	basis function for finite element approximation
ψ	stream function
ω	local vorticity
$\overline{\omega}$	vorticity vector
ω_z	vorticity component in the z-direction

1. INTRODUCTION

1.1 General

Mixing and transport of substances in the environment are an integral part of the overall environmental management. Fate of the effluents and sediments entering streams and rivers depends on their physical, chemical, and biological nature as well as the hydraulic characteristics of the body of water. Not all mechanisms responsible for dilution, transport of effluents and movement of sediments are adequately understood and modeled. Among them is mass and momentum exchange between the main flow and a slowly circulating flow adjacent to it.

Banks of streams and rivers are always irregular with regions of flow separation and circulation formed due to meandering, sudden changes in the cross-sectional area, or presence of engineering structures such as wing dams, bridge piers, and navigation facilities. Water motion within such regions is different from the main flow, though induced by it, and is generally referred to as secondary or circulating motion. Depending on the size, geometry, and zone of influence; circulating flows can significantly affect transport and deposition of sediments, mixing and transport of contaminants, and dissipation of heated effluent from cooling facilities.

When pollutants and hazardous substances are, accidentally or by design, released into a stream they spread out due to the combined effects of advection, diffusion (molecular and turbulent), and dispersion. The latter phenomenon, dispersion, is a mechanical process caused by the spatial variation in the mean velocity distribution. Research has shown (e.g., Fischer [6]) that the transverse velocity distribution in low gradient streams, which are common in Illinois, is the dominant factor in controlling the longitudinal dispersion of substances in the stream.

Presence of circulating regions in streams forces the transverse velocity distribution to deviate from a basically parablic profile to a complicated shape. In some cases, considerable portion of a cross-section of a stream may experience reversed flow. As a consequence of a highly varied transverse velocity, a solute released in a stream mixes in and out of the circulating regions in a presently unknown fashion.

The existing water quality and quantity models are limited to estimating the dispersion component of solute transport and mixing in basically prismatic streams and generally ignore the circulating regions. Once the physics of the interaction between the main flow and the circulating (secondary) flow is investigated and understood, the behavior of such flows can be accurately modeled. This information, in turn, is useful in evaluating the significance of induced circulating flows in mixing and transport of sediments and pollutants in a stream -- a knowledge which will ultimately contribute to the overall objective of developing better water resources policy and management programs.

1.2 Objectives

The overall objective of this study is to contribute to the development of better management programs for the available water resources through furthering the scientific understanding of the processes governing mixing and transport of substances in water. The specific objectives are:

1. To develop a numerical model capable of simulating flow pattern (i.e., streamlines, vorticity, and velocity) associated with shear induced circulating flows. Figure 1 shows an idealized schematic drawing of the flow situation under study.

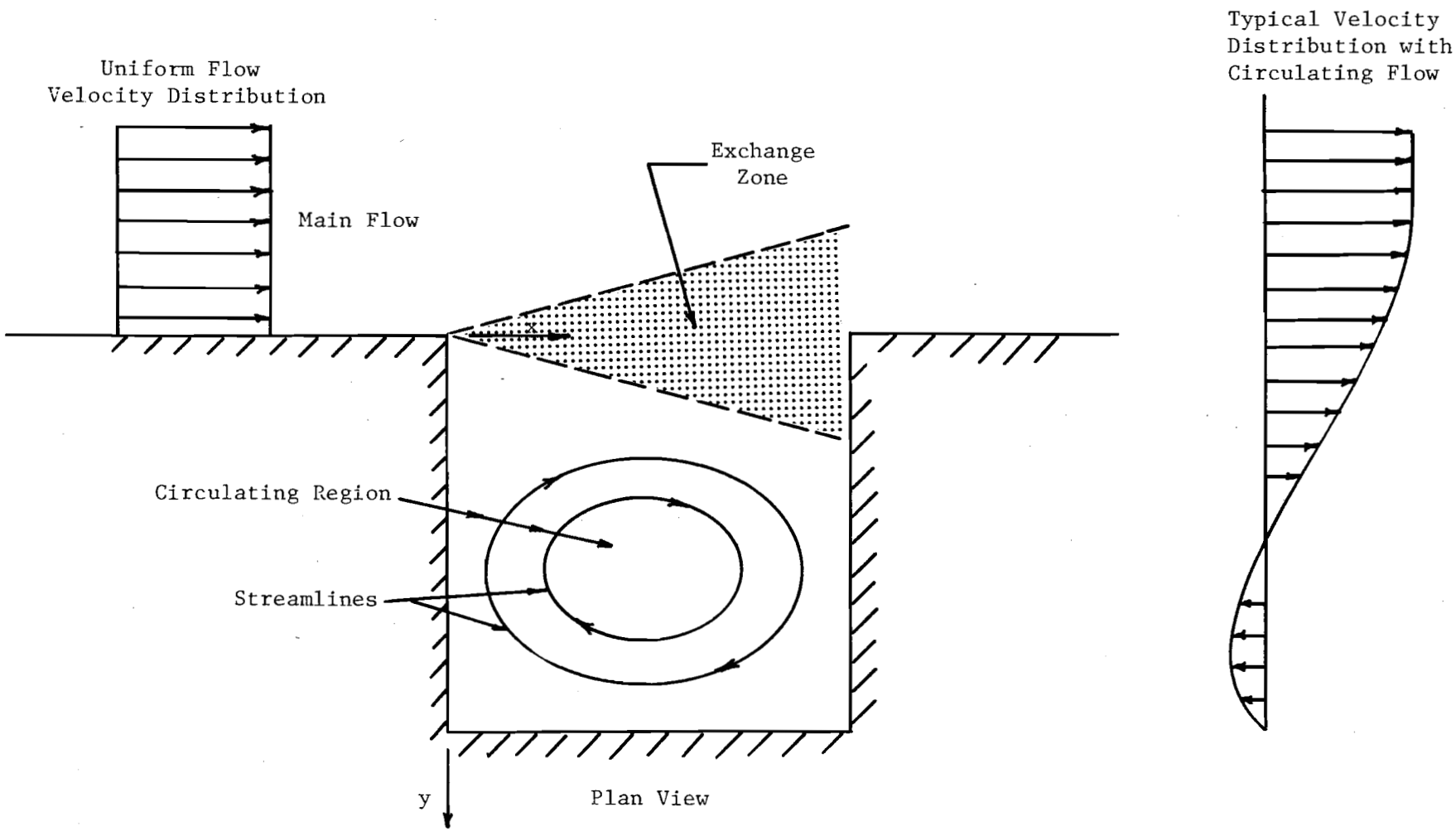

Fig. 1. Idealized Sketch of Circulating Region Driven by Constant Uniform Flow

2. To develop a numerical model capable of predicting concentration distribution and mass transport and diffusion in circulating flows using results from objective 1 as input.

3. To investigate the dispersive and diffusive characteristics of shear induced circulating flows by formulating the dispersion coefficient as a scalar, vector, and a tensor. In addition, a criteria will be developed to minimize loss of mass due to numerical diffusion and other factors present in numerical solution of the mass transport equation.

2. REVIEW OF RELATED LITERATURE

Presence of circulating regions or "dead water" zones on banks of streams and rivers has significant effect on the mixing and transport of substances. Exchange of mass between the circulating region and the main flow has come to sharper focus in the past decade or so because in addition to changing the hydraulic characteristics of flow, it controls the quality of water in the circulating regions or "dead water" zones.

Literature related to the study of circulation induced by a steady main flow has been reviewed in this chapter. Effort has been made to review representative works on shear-induced circulation patterns, concentration distribution in circulating flow, and mass exchange mechanisms between the main flow and the circulating flow. Emphasis has been placed on the latter two areas.

Fishcher [5,6] and others have shown that in rivers and streams turbulent diffusion resulting from velocity fluctuations along with the differential advection are the basic mechanisms responsible for longitudinal dispersion. Furthermore, Fischer [4,5] has specifically shown that in natural streams the transverse variation of velocity across the stream is the dominant factor in estimating the longitudinal dispersion. Channel boundaries, particularly the banks, in natural streams are often irregular with regions of flow separation and circulation. Presence of such regions significantly alters the transverse velocity profile.

Day [3], Pedersen [18], and Valentine and Wood [29] have speculated that the interaction between the main flow and the circulating regions can significantly affect the dispersion characteristics of natural streams. In addition, depending on their size and geometry, the circulating regions can serve as temporary storage and subsequent slow release of dispersing

substances. This process can cause concentration distributions markedly different from those predicted by simple advection-diffusion models presently available.

Flokstria [9] analyzed the relative importance of viscous shear stresses, Reynolds stresses and momentum transfer due to secondary currents. Extending Flokstria's work Lean and Weare [14] examined the contribution of shear layer turbulence, bed-generated turbulence and secondary flow to the effective lateral shear stress in steady, turbulent, two-dimensional circulating flow. They concluded that the relative significance of each mixing mechanism depends on the flow depth, bed roughness, radius of curvature of the flow and the distance downstream from the point of flow separation.

A depth-averaged numerical model for circulating flow has been developed by Ponce and Yabusaki [20]. The model is premised upon the simulation of turbulence using a velocity averaging routine with an empirical weighting factor to simulate effective shear stresses. They state that at the present no comprehensive analysis of the various mechanisms leading to generation of circulation has been attempted using numerical models. However, they do not address the mass exchange between the circulating flow and the main flow, nor do they address mixing and transport of a solute released in the recirculating flow. The authors used the model to test several hypotheses concerning the modeling of circulating flow. Their tests indicate the necessity of including effective shear stress and convective inertia in the model in order to generate circulation. They were able to achieve circulating flow without specifying a no-slip boundary condition. However, the authors reflect upon the sensitivity of the model to the choice of the empirical velocity weighting

coefficient. The empirical basis of their model makes it difficult to judge the generality of their conclusions.

Findikakis and Street [8] have extended the large eddy simulation concept to modeling two-dimensional uniform density and thermally stratified flows in a vertical plane. Flow parameters are described in terms of space averages, and the time history of the large scale motions are simulated. A filtering function separates the large scale component of the flow variables from the "sub-grid" or "small scale" components. The spacial average of the large scale motions are simulated in time, and the small scale motions are accounted for using Smagorinsky's eddy viscosity model and the vorticity gradient eddy viscosity model.

Shen and Lokrov [15] have analytically investigated the velocity patterns generated by a sudden expansion using the similarity approach. Comparisons of the numerical solutions obtained from simplified Navier-Stokes equations to the available laboratory data have supported the hypothesis of self preserving behavior to some degree. Their work lends insight to the geometry of the mass exchange (mixing) zone and the rate of expansion of the zone.

Westrich [30] developed a spatially one-dimensional model predicting the mixing process of a conservative tracer mass between a main flow and an adjacent circulating region. He verified the analytical results by physical modeling and found an exponential decrease of the tracer concentration with time for steady flows. His approach is limited in that concentration is assumed constant in the circulating region. This is not the case in practical situations.

Tsai and Holley [28] conducted analytical and experimental study of longitudinal mixing process in prismatic channels with storage in separation

zones. They determined a dimensionless mass exchange coefficient for separation zones at the bottom of a channel. Their values were in some cases up to five times higher than those obtained by direct measurement suggesting a possible problem in formulation of the exchange mechanism.

Sabol and Nordin [22] investigated the longitudinal dispersion in rivers with periodic storage zones. They proposed a three parameter model in which particles are trapped in storage zones through a stochastic random travel time. The model predicts concentration distributions as a function of initial concentration, longitudinal position, and convective velocity.

McGuirk and Rodi [17] have studied square cavity circulation driven by a main stream flow. Their depth-averaged finite difference flow model rigorously computes the velocity and eddy viscosity distribution from the basic concentration and momentum equations and the energy transport equation. The mass transport equation is solved independently using the flow parameters input. The mass transport model is detailed to reveal the concentration distribution within the cavity as well as the mass exchange with the main stream. Turbulent mixing is modeled using the concentration gradient approach and computing the varying eddy diffusivity from the eddy viscosity distribution. The eddy viscosity is related to the diffusivity via a turbulent Schmidt number. The numerical solution of the flow field parameters requires substantial computational time and the assignment of values to seven empirical coefficients. Their results are supported by comparison with laboratory data. The authors do not discuss the effects of numerical dispersion in their finite difference approximation scheme.

Lam [12] addresses the problem of devising a numerical solution scheme which does not mask the physical mixing processes. This is particularly important in hydrodynamic flow fields for which mean velocity patterns and

mixing processes have not been delineated. He reports that the linear Galerkin finite element method has difficulty handling steep gradients but may be applied to this problem with proper choice of grid spacing.

Application of various numerical methods to the Navier-Stokes equations governing incompressible flow in a driven cavity flow has been examined at Langley Research Center [13]. These are a series of papers presenting solutions for both primitive variables (i.e., velocity and pressure) and vorticity-stream function systems of equations. The individual papers will not be discussed in this review.

Zelazny and Baker [32] and Baker [1] use the Galerkin form of the method of weighted residuals to develop a finite element solution for numerous hydrological phenomena including large scale recirculating regions. Their work demonstrates the wide range of application of the finite element approximation method. Results show generally stable solutions with somewhat less numerical dispersion than their finite difference counterparts.

Loziuk, Anderson, and Belytchko [16] successfully applied the finite element method to analysis of two-dimensional temperature distributions in moving bodies of water. The dispersion and convection terms in the equations for heat transfer are analogous to those in the mass transport equation. The Galerkin method of weighted residuals was applied and linear basis functions were used to approximate the velocity field distribution. The model results agreed well with the analytical solution of the one-dimensional transport equation. The two-dimension simulation of heated effluent discharged into a river system produced results agreeable with field data.

Smith, Farraday, and O'Connor [27] performed a series of tests comparing the Galerkin finite element method to several optimized finite difference models. Finite element results for the two-dimensional convection-diffusion problem were found to be as conservative as Siemons [26] iterative alternating direction implicit finite difference method. The authors compare the Galerkin finite element solution for a two-dimensional convection to the solution obtained from Robert and Weise's [21] fourth order finite difference model. The Galerkin finite element results for this problem were sensitive to the time step selected but had somewhat less distortion of contours than the finite difference model. The Galerkin form of the finite element method is reported by Grove [11] to be less subject to numerical dispersion than many standard finite difference schemes.

Pinder and Gray [19] evaluate several numerical schemes and conclude that "It is apparent that the finite element scheme provides consistently more accurate solutions in that both numerical dispersion and numerical dissipation are less apparent in the finite element curves."

Review of the previous work on mixing and transport within and in the vicinity of circulating flows reveals the limitations of the existing knowledge and points the researcher in the direction of overcoming some of the shortcomings. One-dimensional models, while instructive, ignore the concentration distribution within the circulating region and only deal with uniform concentrations. The dynamics of the mass exchange zone are difficult to describe mathematically and, therefore, are not accounted for in most models. Rigorous numerical solutions of the governing equations require extensive computation time and effort. Further, their application requires specification of empirical coefficients, specified by intuition more than scientific basis due to lack of data.

More realistic numerical simulation of mass exchange can be achieved from a better understanding of the dynamics of mass and momentum exchange between circulating and main flows. The convective character of the circulating region can then be modeled and flow patterns determined. Subsequently, the mass transport equation governing the fate of the pollutants discharged in the circulating regions can be solved. The results will help evaluate the impact of such regions on the hydraulic and water quality characteristics of flow in rivers and streams.

3. THEORETICAL ANALYSIS

3.1 Objective

The objective of the theoretical analysis was to mathematically describe the physics of circulating flow and the mass transport associated with it. The governing differential equations were written in approximate form and solved numerically. The analysis was carried out in two parts: flow modeling and mass transport modeling.

3.2 Flow Model

The basic flow situation under study is illustrated in Fig. 1. The main flow passing the expansion area develops a free shear zone through which energy is transferred from the main flow to the circulating area, setting it into motion. A dividing streamline is formed between the edge of the circulating area and the opposite wall. There is no net flow across this streamline, but mass and momentum are indeed transported in and out of the circulation area. The problem will be simplified by assuming motions in the vertical direction are small and the flow field can be represented by a depth-averaged mathematical model - a common approach in study of this type of flow. Casting the problem in two-dimensions has the added advantage of reducing the computational costs without great loss of generality.

3.2.1 Governing Equations

Steady, depth-averaged continuity and momentum equations for turbulent flow must be solved in order to established the horizontal components of the velocity. These equations, in their primitive form are:

$$\frac{\partial u}{\partial x} + \frac{\partial v}{\partial y} = 0, \tag{1}$$

$$u \frac{\partial u}{\partial x} + v \frac{\partial u}{\partial y} = \frac{\partial}{\partial x} \left(\frac{\tau_{xx}}{\rho}\right) + \frac{\partial}{\partial y} \left(\frac{\tau_{xy}}{\rho}\right) - \frac{\tau_{bx}}{\rho h}, \tag{2}$$

$$u \frac{\partial v}{\partial x} + v \frac{\partial v}{\partial y} = \frac{\partial}{\partial x} \left(\frac{\tau_{xy}}{\rho}\right) + \frac{\partial}{\partial y} \left(\frac{\tau_{yy}}{\rho}\right) - \frac{\tau_{by}}{\rho h}. \tag{3}$$

In the above equations u and v are the time averaged components of the velocity in the x and y directions, respectively. The τ terms represent turbulent shear stresses in their respective directions. The subscript b refers to the shear stress along the bottom and h is the depth of water in the circulating region. Each stress term can be written in terms of a coefficient times the appropriate mean velocity gradients. For turbulent shear stresses, the coefficient is known as the eddy viscosity (generally determined experimentally), and for bottom shear the coefficient is an empirical friction factor. Details of the mathematical manipulations will not be given here in the interest of brevity. Some details can be found in a publication by McGuirk and Rodi [17].

Since the main objective of the study was to model transport of mass in a known circulating flow, a more simplified flow situation was considered in order to provide the required velocity distribution. Two-dimensional motion of an incompressible viscous fluid in a circulating region generated and maintained by a known uniform flow was considered as a first approximation. The continuity and Navier-Stokes equations governing such flows and written in their primitive form are:

continuity

$$\frac{\partial u}{\partial x} + \frac{\partial v}{\partial y} = 0 \tag{4}$$

x-momentum

$$\frac{\partial u}{\partial t} + u \frac{\partial u}{\partial x} + v \frac{\partial u}{\partial y} = g_x - \frac{1}{\rho} \frac{\partial p}{\partial x} + \nu \left(\frac{\partial^2 u}{\partial x^2} + \frac{\partial^2 u}{\partial y^2}\right) \tag{5}$$

y-momentum

$$\frac{\partial v}{\partial t} + u \frac{\partial v}{\partial x} + v \frac{\partial v}{\partial y} = g_y - \frac{1}{\rho} \frac{\partial p}{\partial y} + \nu \left(\frac{\partial^2 v}{\partial x^2} + \frac{\partial^2 v}{\partial y^2}\right) \tag{6}$$

where x and y are the cartesian coordinate system; u and v are the x and y components of the velocity, respectively; p is the pressure; ν is the kinematic viscosity; g_x and g_y are the x and y components of the body force, respectively; and t is time. Solution to equations (4-6) for given boundary conditions gives u, v, and p.

It is possible to transform equations (4-6) with 3 unknowns to one equation and one unknown by cross-differentiating equations (5) and (6), to eliminate the pressure and body force terms, and introducing the stream function to replace u and v. Letting

$$u = \frac{\partial \psi}{\partial y} \quad \text{and} \quad v = -\frac{\partial \psi}{\partial x} \tag{7}$$

which automatically satisfies the continuity equation (4) will simplify the equation resulting from cross-differentiation of equations (5) and (6) to

$$\frac{\partial \nabla^2 \psi}{\partial t} + \frac{\partial \psi}{\partial y} \frac{\partial \nabla^2 \psi}{\partial x} - \frac{\partial \psi}{\partial x} \frac{\partial \nabla^2 \psi}{\partial y} = \nu \nabla^4 \psi. \tag{8}$$

Equation (8) is a fourth order partial differential equation with the stream function, ψ, as the only unknown. Boundary conditions for the problem under study are:

$$\begin{aligned} &\text{at the stationary walls} \quad \frac{\partial \psi}{\partial x} = \frac{\partial \psi}{\partial y} = 0; \text{ and} \\ &\text{at the open boundary} \quad \frac{\partial \psi}{\partial y} = U \text{ and } \frac{\partial \psi}{\partial x} = 0 \end{aligned} \tag{9}$$

where U is the uniform main flow velocity.

Equation (8) is sometimes written in terms of the vorticity vector defined as the curl of the velocity vector. For the two-dimensional flow under consideration, the x and y components of the vorticity vector vanish (vorticity vector is perpendicular to the gradient of the velocity vector). Thus, the vorticity vector, ω, reduces to only the component about the z-axis:

$$\frac{1}{2}\,\bar{\omega} = \omega_z = \omega = \frac{1}{2}\left(\frac{\partial v}{\partial x} - \frac{\partial u}{\partial y}\right). \tag{10}$$

Combination of equations (7) and (10) gives

$$\omega = -\frac{1}{2}\nabla^2\psi \tag{11}$$

which tranforms equation (8) to

$$\frac{\partial \omega}{\partial t} + u\frac{\partial \omega}{\partial x} + v\frac{\partial \omega}{\partial y} = \nu\left(\frac{\partial^2 \omega}{\partial x^2} + \frac{\partial^2 \omega}{\partial y^2}\right). \tag{12}$$

The vector form of equation (12) is

$$\frac{\partial \omega}{\partial t} - \nabla \cdot (\bar{U}\omega) = \nu\nabla^2\omega \tag{13}$$

where $U = ui + vj$ is the velocity vector. Equation (13) can be written in a dimensionless form using the ratios:

$$x' = \frac{x}{L} \; ; \; y' = \frac{y}{L} \; ; \; t' = \frac{t}{L/U} \; ; \; \omega' = \frac{\omega}{U/L} \; ; \text{ and } \bar{U} = \frac{\bar{U}}{U} \; .$$

Substituting the dimensionless form of the variables into equation (13) and dropping the prime for convenience gives

$$\frac{\partial \omega}{\partial t} - \nabla \cdot (\bar{U}\omega) = \frac{1}{R_e} \nabla^2 \omega \tag{14}$$

where $R_e = UL/\nu$ is the characteristic Reynolds number for the flow. Equation (14) is known as the vorticity transport equation. Alternatively, equation (14) can be derived by taking the curl of the equation resulting from cross-differentiation of equations (5) and (6). Details of the development of equation (14) can be found in any intermediate or advanced text on viscous fluid flow including Schlichting [24] and White [31].

3.2.2 Finite Difference Approximation

Solution to the vorticity transport equation (14) subject to the appropriate boundary conditions gives the desired velocity pattern for input to the mass transport model. Unfortunately, equation (14) cannot be solved analytically and must be approximated and solved numerically. Many numerical schemes exist for solving such equations as indicated in the report published by Langley Research Center [13] and others. However, a second upwind finite differencing scheme was found most suitable for the problem under study. The solution domain is discritized in space as shown in Fig. 2. Computation time step of 1/30 second, based on the grid spacing and the range of Reynolds numbers, gave stable steady state solutions.

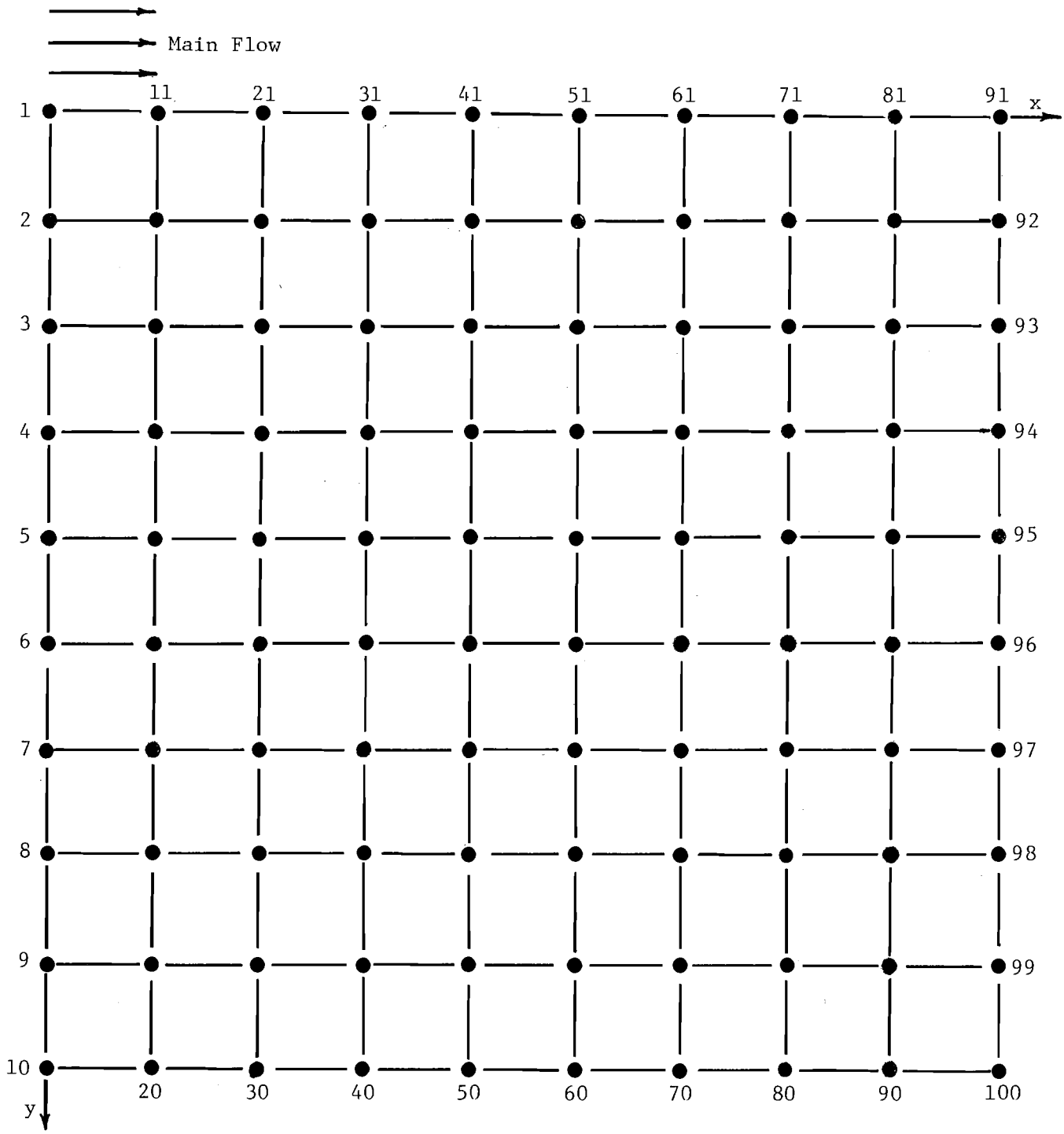

Fig. 2. Finite Difference Node Network

Equation (14) can be written in approximate form:

$$\frac{\omega_{i,j}^{n+1} - \omega_{i,j}^{n}}{\Delta t} = - \frac{u_{r,j}\,\omega_{r,j} - u_{l,j}\,\omega_{l,j}}{\Delta x} - \frac{v_{i,r}\,\omega_{l,r} - v_{i,l}\,\omega_{i,l}}{\Delta y}$$

$$+ \frac{1}{Re} \left[\omega_{i+1,j}^{n} + \omega_{i-1,j}^{n} + \omega_{i,j+1}^{n} + \omega_{i,j-1}^{n} - 4\omega_{i,j}^{n} \right] \qquad (15)$$

where n is the time step;

$$\omega_{r,j} = \begin{cases} \omega_{i,j} & \text{for } u_{r,j} > 0 \\ \omega_{i+1,j} & \text{for } u_{r,j} < 0 \end{cases} = \frac{1+p}{2}\,\omega_{i,j} + \frac{1-p}{2}\,\omega_{i+1,j} \; ; \qquad (16)$$

$$\omega_{l,j} = \begin{cases} \omega_{i-1,j} & \text{for } u_{s,j} > 0 \\ \omega_{i,j} & \text{for } u_{s,j} < 0 \end{cases} = \frac{1+p}{2}\,\omega_{i-1,j} + \frac{1-p}{2}\,\omega_{i,j} \; ; \qquad (17)$$

$$\omega_{i,r} = \begin{cases} \omega_{i,j} & \text{for } v_{i,r} > 0 \\ \omega_{i,j+1} & \text{for } v_{i,r} < 0 \end{cases} = \frac{1+p}{2}\,\omega_{i,j} + \frac{1-p}{2}\,\omega_{i,j+1} \; ; \text{ and} \qquad (18)$$

$$\omega_{i,l} = \begin{cases} \omega_{j,j-1} & \text{for } v_{i,s} > 0 \\ \omega_{i,j} & \text{for } v_{i,s} < 0 \end{cases} = \frac{1+p}{2}\,\omega_{i,j-1} + \frac{1-p}{2}\,\omega_{i,j} \qquad (19)$$

in which

$$u_{r,j} = \frac{1}{2} (u_{i+1,j} + u_{i,j}) \; ; \tag{20}$$

$$u_{s,j} = \frac{1}{2} (u_{i,j} + u_{i-1,j}) \; ; \tag{21}$$

$$v_{i,r} = \frac{1}{2} (v_{i,j+1} + v_{i,j}) \; ; \quad \text{and} \tag{22}$$

$$v_{i,s} = \frac{1}{2} (v_{i,j} + v_{i,j-1}) \; . \tag{23}$$

In equations (16-19) variable p has the value +1 for velocities in the positive direction of the axes and -1 for velocities in the negative direction of the axes, respectively.

Product of velocity and vorticity in equation (15) can be represented by one variable, g. For example:

$$g_{i+1/2,j} = u_{r,j} \, \omega_{r,j} \; . \tag{24}$$

Substituting equation (16) into (24) gives

$$g_{i+1/2,j} = u_{r,j} \left(\frac{\omega_{i,j} + \omega_{i+1,j}}{2} \right) - |u_{r,j}| \left(\frac{\omega_{i+1,j} - \omega_{i,j}}{2} \right) . \tag{25}$$

which upon rearranging yields

$$g_{i+1/2,j} = \frac{u_{r,j} + |u_{r,j}|}{2} \omega_{i,j} + \frac{u_{r,j} - |u_{r,j}|}{2} \omega_{i+1,j} \; . \tag{26}$$

In equation (26) absolute value of the velocity has replaced the variable p.

Similarly:

$$g_{i-1/2,j} = u_{s,j} \left(\frac{\omega_{i-1,j} + \omega_{i,j}}{2} \right) - \left|u_{s,j}\right| \left(\frac{\omega_{i,j} - \omega_{i-1,j}}{2} \right) ; \qquad (27)$$

$$g_{i,j+1/2} = v_{i,r} \left(\frac{\omega_{i,j} + \omega_{i,j+1}}{2} \right) - \left|v_{i,r}\right| \left(\frac{\omega_{i,j+1} - \omega_{i,j}}{2} \right) ; \text{ and} \qquad (28)$$

$$g_{i,j-1/2} = v_{i,s} \left(\frac{\omega_{i,j-1} + \omega_{i,j}}{2} \right) - \left|v_{i,s}\right| \left(\frac{\omega_{i,j} - \omega_{i,j-1}}{2} \right) . \qquad (29)$$

Substituting equations (22-25) into equation (15) gives the final approximate form of the vorticity transport equation:

$$\omega_{i,j}^{n+1} = \omega_{i,j}^{n} - \frac{\Delta t}{\Delta} \left[g_{i+1/2,j} - g_{i-1/2,j} + g_{i,j+1/2} - g_{i,j-1/2} \right]$$

$$+ \frac{\Delta t}{Re\Delta^2} \left[\omega_{i+1,j}^{n} + \omega_{i-1,j}^{n} + \omega_{i,j+1}^{n} + \omega_{i,j-1}^{n} - 4\omega_{i,j}^{n} \right] \qquad (30)$$

where $\Delta = \Delta x = \Delta y$ is the grid size.

The boundary conditions can be specified in terms of the stream function,

$$u_{i,j} = \frac{1}{2\Delta} \left(\psi_{i,j+1} - \psi_{i,j} \right) ; \qquad (31)$$

$$v_{i,j} = - \frac{1}{2\Delta} \left(\psi_{i+1,j} - \psi_{i,j} \right) ; \qquad (32)$$

and

$$\omega = \frac{2}{\Delta^2} \psi_b \qquad \text{at solid boundaries; and} \tag{33}$$

$$\omega = \frac{2}{\Delta^2} (\psi_b + \Delta) \qquad \text{at the open boundary.} \tag{34}$$

ψ_b is the value of the streamline at the solid boundaries and can be set equal to any convenient constant, including zero.

3.3 Mass Transport Model

Mixing and transport of conservative pollutants discharged into a moving body of water is caused by the combined effects of advection, diffusion (molecular and turbulent), and dispersion. For non-conservative substances, the process must also include any gain or loss of mass of the substance due to chemical, biological, and mechanical (e.g., settling or adsorption).

3.3.1 Dispersion in Two-Dimensional Circulating Flow

Dispersion is a mechanical process caused by the spatial variation in the mean velocity distribution. In rivers and streams the transverse velocity distribution is known to be the dominant process responsible for the dispersion of mass. The problem is, therefore, treated by assuming one or two-dimensional motion with the main flow along one of the coordinate axes.

In circulating flows the direction of flow does not coincide with one of the cartesian coordinate axes. Velocity vector in such flows is still decomposed into components along the cartesian coordinate axes for analysis. Unlike the velocity vector, dispersion coefficient is a first order tensor in the two-dimensional flow and has 4 components defined as:

$$E = \begin{vmatrix} E_{xx} & E_{xy} \\ E_{xy} & E_{yy} \end{vmatrix} \tag{36}$$

In equation (36), E_{xx} and E_{yy} are components of the dispersion tensor along the x and y coordinate axes, respectively. E_{xy} and E_{yx} are cross-product terms and account of the interaction between the E_{xx} and E_{yy}. In circulating flow, it is difficult, if not impossible, to define meaningful values for dispersion coefficients in the x and y directions because direction of flow changes with both x and y. Subsequently, dispersion must be defined by other physically meaningful constants. These are the streamwise dispersion coefficient, E_L, and the transverse dispersion coefficient, E_T. The values of dispersion coefficient along the cartesian coordinates can now be written in terms of E_L and E_T as a function of the relative magnitude of the velocity components as discussed by Scheidegger [23] and Bear [2]:

$$E_{xx} = E_L \frac{u^2}{\underline{V}^2} + E_T \frac{v^2}{\underline{V}^2} \quad ; \tag{37}$$

$$E_{yy} = E_T \frac{u^2}{\underline{V}^2} + E_L \frac{v^2}{\underline{V}^2} \quad ; \text{ and} \tag{38}$$

$$E_{xy} = E_{yx} = (E_L - E_T) \frac{uv}{\underline{V}^2} \tag{39}$$

where $\underline{V}$ is the magnitude of velocity vector at each point; and u and v are the components of the velocity vector. Note that even though E_{xx} and E_{yy} always have positive values, E_{xy} and E_{yx} may have positive or negative values depending on the position in the flow field and the direction of flow. In

two-dimensional flows in which one of the axes coincides with the mean direction of flow, one of the velocity components will be zero and subsequently the cross-product components of the dispersion coefficient vanish.

Since E_T is much smaller than E_L, the two constants can be related by another constant $k \leq 1$:

$$E_T = kE_L \ . \tag{40}$$

Equations (37-39) can be rewritten to include k:

$$E_{xx} = E_L \left[\frac{u^2 + kv^2}{\underline{V}^2}\right] \ ; \tag{41}$$

$$E_{yy} = E_L \left[\frac{ku^2 + v^2}{\underline{V}^2}\right] \ ; \text{ and} \tag{42}$$

$$E_{xy} = E_{yx} = E_L(1-k) \frac{uv}{\underline{V}^2} \ . \tag{43}$$

Once E_L and k are specified, components of the dispersion tensor transformed to the cartesian coordinate system can be evaluated.

3.3.2 Governing Equations

The unsteady mass transport equation for a conservative substance released in a two-dimensional (depth-averaged) flow is:

$$\frac{\partial c}{\partial t} + u \frac{\partial c}{\partial y} + v \frac{\partial c}{\partial y} = \frac{\partial}{\partial x}\left[E_{xx} \frac{\partial c}{\partial x}\right] + \frac{\partial}{\partial y}\left[E_{yy} \frac{\partial c}{\partial y}\right] + \frac{\partial}{\partial x}\left[E_{xy} \frac{\partial c}{\partial y}\right]$$

$$+ \frac{\partial}{\partial y}\left[E_{yx} \frac{\partial c}{\partial x}\right] \tag{44}$$

where c is the time dependent, depth-averaged concentration; and E_{xx}, E_{yy}, E_{xy}, and E_{yx} are defined by equations (41-43). Components of the velocity, u and v, are provided by the flow model. For two dimensional flows in which one coordinate axis is aligned with the mean flow velocity, the last two terms of equation (44) drop out.

Two cases have been investigated and are reported here:

1. For constant dispersion throughout the flow field, the dispersion tensor equation (36) reduces to a scalar

$$E_{xx} = E_{yy} = E_L = E \ . \tag{45}$$

The same result can be obtained by setting k in equation (40) equal to 1. Equation (45) simplifies equation (44) to

$$\frac{\partial c}{\partial t} + u \frac{\partial c}{\partial x} + v \frac{\partial c}{\partial y} = E\left[\frac{\partial^2 c}{\partial x^2} + \frac{\partial^2 c}{\partial y^2}\right] \ . \tag{46}$$

2. For the case of no dispersion transverse to the direction of rotation (i.e., $E_T = 0$), the dispersion tensor equation (36) reduces to a vector parallel to the velocity vector with components

$$E_{xx} = E_L \frac{u^2}{\underline{v}^2} \ ; \quad E_{yy} = E_L \frac{v^2}{\underline{v}^2} \ ; \text{ and } E_{xy} = E_{yx} = E_L \frac{uv}{\underline{v}^2} \ . \tag{47}$$

Substitution of equation (47) into equation (44) gives

$$\frac{\partial c}{\partial t} + u \frac{\partial c}{\partial x} + v \frac{\partial c}{\partial y} = E_L \left[\frac{u^2}{\underline{v}^2} \frac{\partial^2 c}{\partial x^2} + \frac{v^2}{\underline{v}^2} \frac{\partial^2 c}{\partial y^2} + 2 \frac{uv}{\underline{v}^2} \frac{\partial^2 c}{\partial x \partial y}\right] \ . \tag{48}$$

Equation (46) has been numerically solved and solutions are given later in this report. Equation (48) without the last term on the right hand side and with the first order velocity ratio (instead of square of the ratio) has also been solved and results are given later in this report. This equation is now being solved to include the last term. The results will be compared with the limited case and will appear in the second report in the series. The boundary conditions for equations (46) and (48) are:

1. No concentration gradient across the solid boundary: $\frac{\partial c}{\partial x} = \frac{\partial c}{\partial y} = 0$ and

2a. No concentration across the open boundary: $\frac{\partial c}{\partial y} = 0$; or

2b. Concentration specified with time within the mixing zone at the open boundary.

3.3.3 Finite Element Approximation

Partial differential equations (46) and the simplified version of (48) have been numerically solved by finite-element approximation using the Galerkin method of weighted residuals. Choice of finite element approximation of the mass transport equations is based on the intent to use the model for simulating mixing and transport in natural waterways with irregular boundaries. This method is suitable for approximation of irregular shapes. Furthermore, the method has been shown to converge to solution rapidly and is numerically quite stable in comparison to finite difference schemes.

The finite element approximation equations have been developed using triangular elements and linear basis functions. This formulation allows use of the area coordinates as given by Pinder and Gray [19]. Basis functions representing area coordinates can be integrated explicitly circumventing the need for numerical integration. This eliminates

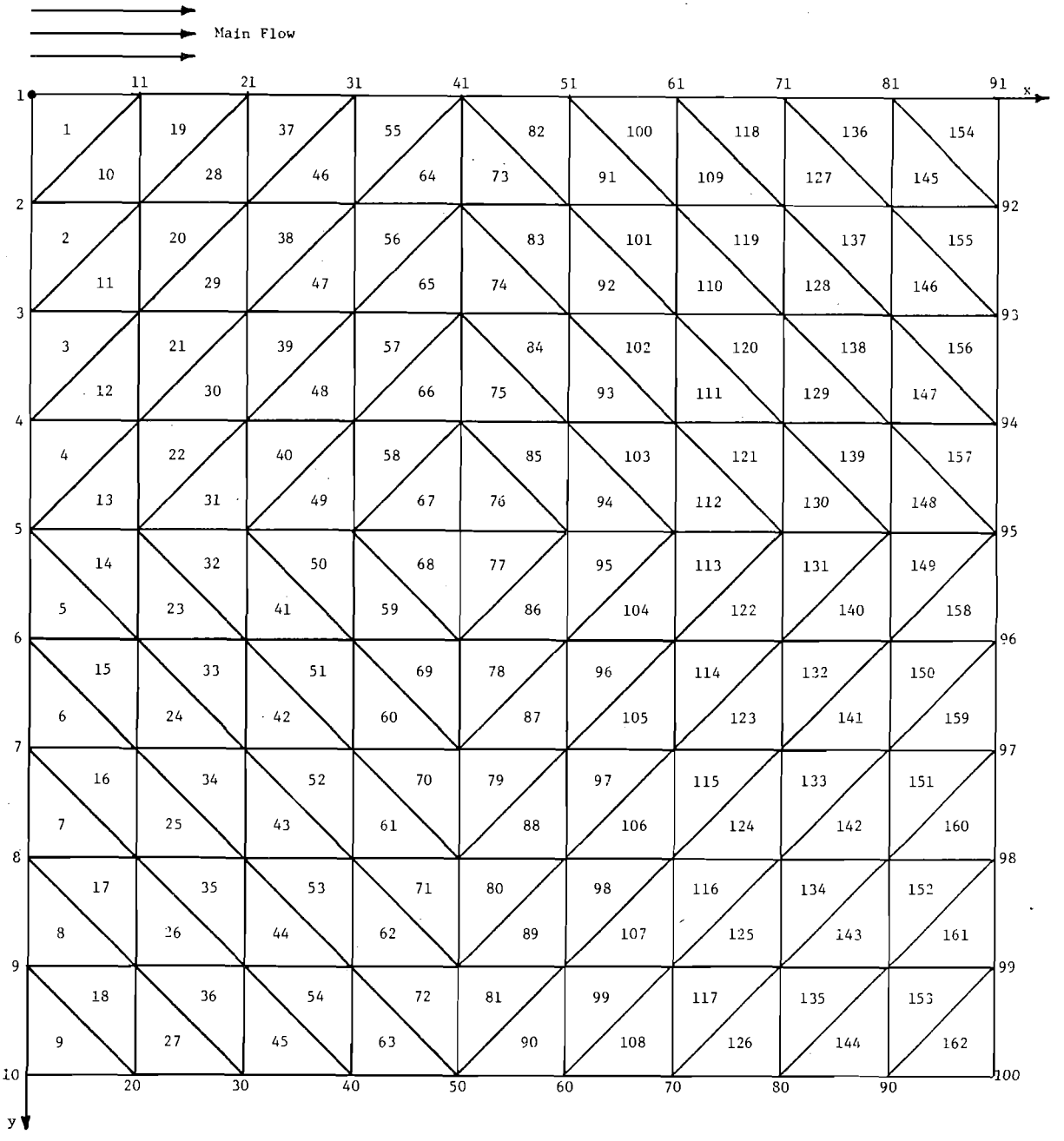

Fig. 3. Finite Element Network

computational inaccuracies and saves computing time. Figure 3 shows the flow field discritized by triangular elements.

Concentration is approximated in the following manner:

$$c(x,y,t) \approx \hat{c}(x,y,t) = \sum_{j=1}^{3} a_j(t)\ \phi_j(x,y) \tag{49}$$

where c is the approximate value of c represented by the product of a time dependent function, a_j, and a space dependent function, ϕ_j, summed over the three nodes of each element. Substituting equation (49) into equation (44) and rearranging gives

$$\frac{\partial \hat{c}}{\partial t} + u\frac{\partial \hat{c}}{\partial x} + v\frac{\partial \hat{c}}{\partial y} - \frac{\partial}{\partial x}E_{xx}\frac{\partial \hat{c}}{\partial x} - \frac{\partial}{\partial y}E_{yy}\frac{\partial \hat{c}}{\partial y} - 2\frac{\partial}{\partial x}E_{xy}\frac{\partial \hat{c}}{\partial y} = R(x,y) \tag{50}$$

where R(x,y) is the residual error generated by the approximation of c. The Galerkin method of weighted residuals uses the basis function used to approximate c to force the weighted integral of the residual to go to zero over each element, viz:

$$\int_A R(x,y)\ \phi_i(x,y)dA = 0\ . \tag{51}$$

Thus, equation (50) integrated over an element becomes

$$\underbrace{\int_A \phi_i \frac{\partial c}{\partial t}\,dA}_{1} + \underbrace{\int_A u\phi_i \frac{\partial c}{\partial x}\,dA}_{2} + \underbrace{\int_A v\phi_i \frac{\partial \hat{c}}{\partial y}\,dA}_{3} - \underbrace{\int_A \phi_i \frac{\partial}{\partial x}E_{xx}\frac{\partial \hat{c}}{\partial x}\,dA}_{4}$$

$$- \underbrace{\int_A \phi_i \frac{\partial}{\partial y}E_{yy}\frac{\partial \hat{c}}{\partial y}\,dA}_{5} - \underbrace{\int_A 2\phi_i \frac{\partial}{\partial x}E_{xy}\frac{\partial \hat{c}}{\partial y}\,dA}_{6} = 0 \tag{52}$$

Now, terms 1-5 are considered one at a time and expanded using the right hand side of equation (49).

Term 1

$$\int_A \phi_i \frac{\partial \hat{c}}{\partial t} \, dA = \int_A \phi_i \frac{\partial}{\partial t} \sum_{j=1}^{3} a_j \phi_j dA \tag{53}$$

$$= \sum_{j=1}^{3} \frac{\partial a_j}{\partial t} \int_A \phi_i \phi_j \, dA \tag{54}$$

Equation (54) is expanded into a matrix:

$$\begin{bmatrix} \frac{\partial a_1}{\partial t} \int_A \phi_1 \phi_1 \, dA & \frac{\partial a_2}{\partial t} \int_A \phi_1 \phi_2 \, dA & \frac{\partial a_3}{\partial t} \int_A \phi_1 \phi_3 \, dA & i=1 \\ \frac{\partial a_1}{\partial t} \int_A \phi_2 \phi_1 \, dA & \frac{\partial a_2}{\partial t} \int_A \phi_2 \phi_2 \, dA & \frac{\partial a_3}{\partial t} \int_A \phi_2 \phi_3 \, dA & i=2 \\ \frac{\partial a_1}{\partial t} \int_A \phi_3 \phi_1 \, dA & \frac{\partial a_2}{\partial t} \int_A \phi_3 \phi_2 \, dA & \frac{\partial a_3}{\partial t} \int_A \phi_3 \phi_3 \, dA & i=3 \end{bmatrix} \tag{55}$$

Pinder and Gray [19] give the values of the integrals in equation (55) according to the following formulas:

$$\int_A \phi_m \phi_n \, dA = \frac{1}{12} A \qquad \begin{array}{l} m = 1,2,3 \\ n = 1,2,3 \\ m \neq n \end{array} \tag{56}$$

$$\int_A \phi_m \phi_m \, dA = \frac{1}{6} A \qquad m = 1,2,3 \tag{57}$$

Substituting for the integrals in equation (55) and simplifying gives the final form of term 1:

$$\int_A \phi_1 \frac{\partial \hat{c}}{\partial t} \, dA = \frac{A}{6} \begin{bmatrix} 1 & 1/2 & 1/2 \\ 1/2 & 1 & 1/2 \\ 1/2 & 1/2 & 1 \end{bmatrix} \begin{bmatrix} \frac{\partial a_1}{\partial t} \\ \frac{\partial a_2}{\partial t} \\ \frac{\partial a_3}{\partial t} \end{bmatrix} \tag{58}$$

The coefficient matrix will be referred to as the M matrix from here on for convenience.

Term 2

Velocity in this term can be approximated similar to the concentration using a linear basis function ϕ_k:

$$u \approx \hat{u} = \sum_{k=1}^{3} u_k \, \phi_k \, . \tag{59}$$

Substitute for c and u in term 2

$$\int_A u \phi_i \frac{\partial \hat{c}}{\partial x} \, dA = \int_A [\sum_{k=1}^{3} u_k \, \phi_k][\phi_i \sum_{j=1}^{3} a_j \frac{\partial \phi_j}{\partial x}] \, dA \tag{60}$$

Again, Pinder and Gray [19] work out the derivatives of a linear basis function for triangular elements:

$$\frac{\partial \phi_j}{\partial x} = P_j = \begin{bmatrix} P_1 \\ P_2 \\ P_3 \end{bmatrix} = \frac{1}{2A} \begin{bmatrix} y_2 - y_3 \\ y_3 - y_1 \\ y_1 - y_2 \end{bmatrix} \tag{61}$$

Note that because of the choice of basis function, P_j is independent of the index i. The right hand side of equation (60) can now be rearranged to

$$\sum_{j=1}^{3} a_j P_j \sum_{k=1}^{3} u_k \int_A \phi_k \phi_i \, dA \, . \tag{62}$$

For i = 1

$$\sum_{k=1}^{3} u_k \int_A \phi_k \phi_i dA = u_1 \int_A \phi_1 \phi_1 dA + u_2 \int_A \phi_2 \phi_1 dA + u_3 \int_A \phi_3 \phi_1 dA \tag{63}$$

$$= u_1 \frac{A}{6} + u_2 \frac{A}{12} + u_3 \frac{A}{12} \tag{64}$$

$$= \frac{A}{6} \left(u_1 + \frac{u_2}{2} + \frac{u_3}{2}\right) \tag{65}$$

Similarily;

for i = 2 $$= \frac{A}{6} \left(\frac{u_1}{2} + u_2 + \frac{u_3}{2}\right) \text{ ; and} \tag{66}$$

for i = 3 $$= \frac{A}{6} \left(\frac{u_1}{2} + \frac{u_2}{2} + u_3\right) \, . \tag{67}$$

Let $$u_1 + u_m + u_n = U \, , \tag{68}$$

then $$u_1 + \frac{u_m}{2} + \frac{u_n}{2} = \frac{1}{2} (U + u_1) \tag{69}$$

Similar expressions can be written for other permutations of the 1 and 1/2 multipliers of u. Substituting equations (61) and (65-67) into equation (62) and making use of equation (69) lead to the final evaluation of term 2 in matrix form:

$$\int_A u\phi_i \frac{\partial \hat{c}}{\partial x}\, dA = \frac{1}{24}\begin{bmatrix} (U+u_1)(y_2-y_3) & (U+u_1)(y_3-y_1) & (U+u_1)(y_1-y_2) \\ (U+u_2)(y_2-y_3) & (U+u_2)(y_3-y_1) & (U+u_2)(y_1-y_2) \\ (U+u_3)(y_2-y_3) & (U+u_3)(y_3-y_1) & (U+u_3)(y_3-y_1) \end{bmatrix} \begin{bmatrix} a_1 \\ a_2 \\ a_3 \end{bmatrix} \qquad (70)$$

The coefficient matrix in equation (70) will be referred to as K_x from here on for convenience.

Term 3

Evaluation of term 3 is similar to term 2. The final equation in this case is:

$$\int_A v\phi_i \frac{\partial \hat{c}}{\partial y}\, dA = \frac{1}{24}\begin{bmatrix} (V+v_1)(x_3-x_2) & (V+v_1)(x_1-x_3) & (V+v_1)(x_2-x_1) \\ (V+v_2)(x_3-x_2) & (V+v_2)(x_1-x_3) & (V+v_2)(x_2-x_1) \\ (V+v_3)(x_3-x_2) & (V+v_3)(x_1-x_3) & (V+v_3)(x_2-x_1) \end{bmatrix} \begin{bmatrix} a_1 \\ a_2 \\ a_3 \end{bmatrix} \qquad (71)$$

Definition of V is similar to that given for U in equation (68) with v replacing u. The coefficient matrix in equation (71) will be referred to as K_y from here on for convenience. Order of indexing for x and y in equations (70) and (71) can be found in Pinder and Gray [19].

Term 4

This term of equation (52) can be integrated by parts using Green's theorem:

$$\int_A \phi_i \frac{\partial}{\partial x} E_{xx} \frac{\partial \hat{c}}{\partial x}\, dA = \phi_i E_{xx} \frac{\partial \hat{c}}{\partial x}\bigg|_b - \int_A E_{xx} \frac{\partial \hat{c}}{\partial x} \frac{\partial \phi_i}{\partial x}\, dA \,. \qquad (72)$$

where b denotes term evaluated at the element boundaries. For interior element boundaries this term and its counterpart in term 5 are zero. At the closed exterior boundaries, the boundary term is still zero because the dispersion coefficient is zero. At the open boundary this term and its counterpart in term 5 of equation (52) have values specified by the exchange model. These values will appear in the "B" matrix of the final equation. Therefore, the boundary term will not be expanded here and only the second term on the right hand side of equation (72) will be considered.

The dispersion coefficient can be represented similar to the velocity in term 2 of equation (52) as:

$$E_{xx} \approx \hat{E}_{xx} = \sum_{m=1}^{3} E_m \phi_m \,. \tag{73}$$

Substituting for c and E_{xx} in equation (72) and rearranging:

$$- \int_A E_{xx} \frac{\partial c}{\partial x} \frac{\partial \phi_i}{\partial x} \, dA = - \int_A [\sum_{m=1}^{3} E_m \phi_m][\sum_{j=1}^{3} a_j \frac{\partial \phi_j}{\partial x}] \frac{\partial \phi_i}{\partial x} \, dA. \tag{74}$$

Since the basis functions are linear, the derivative of ϕ is constant and can be represented as P with proper indexing. Thus, right hand side of equation (74) becomes

$$= - [\sum_{j=1}^{3} a_j P_j P_i] \sum_{m=1}^{3} E_m \int_A \phi_m \, dA \tag{75}$$

$$= - \frac{A}{3} [\sum_{j=1}^{3} a_j P_j P_i] \sum_{m=1}^{3} E_m \tag{76}$$

where integral of ϕ_m over the element area has been evaluated as A/3 according to Pinder and Gray [19]. Equation (76) can be written in a matrix form using the expansion for P given in equation (61). Thus, term 4 becomes

$$\int_A \phi_i \frac{\partial}{\partial x} E_{xx} \frac{\partial \hat{c}}{\partial x} dA = -\frac{1}{12A} \sum_{m=1}^{3} E_{mxx} \begin{bmatrix} (y_2-y_3)(y_2-y_3) & (y_3-y_1)(y_2-y_3) & (y_1-y_2)(y_2-y_3) \\ (y_2-y_3)(y_3-y_1) & (y_3-y_1)(y_3-y_1) & (y_1-y_2)(y_3-y_1) \\ (y_2-y_3)(y_1-y_2) & (y_3-y_2)(y_1-y_2) & (y_1-y_2)(y_1-y_2) \end{bmatrix} \begin{bmatrix} a_1 \\ a_2 \\ a_3 \end{bmatrix} \qquad (77)$$

in which E_m has been replaced by E_{mxx} to indicate the xx-component of the dispersion tensor. The coefficient matrix will be referred to as H_x from here on for convenience.

Term 5

This term is the counterpart of term 4 in the y-direction. Performing similar tasks on this term leads to a final equation as follows:

$$\int_A 2\phi_i \frac{\partial}{\partial x} E_{xy} \frac{\partial \hat{c}}{\partial y} dA = -\frac{1}{6A} \sum_{m=1}^{3} E_{mxy} \begin{bmatrix} (y_2-y_3)(x_3-x_2) & (y_2-y_3)(x_1-x_3) & (y_2-y_3)(x_2-x_1) \\ (y_3-y_1)(x_3-x_2) & (y_3-y_1)(x_1-x_3) & (y_3-y_1)(x_2-x_1) \\ (y_1-y_2)(x_3-x_2) & (y_1-y_2)(x_1-x_3) & (y_1-y_2)(x_2-x_1) \end{bmatrix} \begin{bmatrix} a_1 \\ a_2 \\ a_3 \end{bmatrix} \qquad (78)$$

in which E_m has been replaced by E_{myy} to indicate the yy-component of the dispersion tensor. The coefficient matrix will be referred to as H_y from here on for convenience.

Term 6

Similar to terms 4 and 5 this term expands to

$$\int_A \phi_i \frac{\partial}{\partial y} E_{yy} \frac{\partial c}{\partial y} dA = -\frac{1}{12A} \sum_{m=1}^{3} E_{myy} \begin{bmatrix} (x_3-x_2)(x_3-x_2) & (x_1-x_3)(x_3-x_2) & (x_2-x_1)(x_3-x_2) \\ (x_3-x_2)(x_1-x_3) & (x_1-x_3)(x_1-x_3) & (x_2-x_1)(x_1-x_3) \\ (x_3-x_2)(x_2-x_1) & (x_1-x_3)(x_2-x_1) & (x_2-x_1)(x_2-x_1) \end{bmatrix} \begin{bmatrix} a_1 \\ a_2 \\ a_3 \end{bmatrix} \quad (79)$$

where E_{mxy} indicates the cross product of dispersion coefficients E_{xx} and E_{yy}. The coefficient matrix will be referred to as H_{xy} from this point on for convenience. Note that in terms 4-6 the dispersion coefficients are related to the transverse and longitudinal dispersion coefficients through velocity.

Combining the integrated forms of the 6 terms in equation (52) will give

$$[M] \sum_{j=1}^{3} \frac{\partial a_j}{\partial t} + [K_x + K_y] \sum_{j=1}^{3} a_j + [H_x + H_y + H_{xy}] \sum_{j=1}^{3} a_j = [B] \quad (80)$$

where B is the residual matrix and includes the boundary conditions. For a case where dispersion is the same in all directions H_{xy} vanishes and H_x and H_y can be replaced by the matrix H which is the algebraic sum of equations (76) and (77). The time derivative of a_j can be approximated by letting

$$\frac{\partial a_j}{\partial t} = \frac{a_j^{n+1} - a_j^n}{\Delta t} \quad (81)$$

where n denotes time step and Δt is the time interval of computation. Substituting equation (81) into equation (80) and rearranging gives the final finite element approximation of the mass transport equation for any

element in the flow field:

$$[\frac{1}{\Delta t} M + K_x + K_y + H] \sum_{j=1}^{3} a_j^{n+1} = [B] + [\frac{1}{\Delta t} M] \sum_{j=1}^{3} a_j^{n} \quad . \tag{82}$$

Since equation (82) holds for every element, a global equation can be assembled by summing this equation over the number of elements in the flow field using a global numbering scheme. The element matrices M, K_x, K_y, and H are then assembled into the Global matrix, G with (kxk) components where k is the number of nodes in the discretized flow field. The element matrices M and B are similarly assembled into the global matrix BigM (kxk) and the global boundary matrix B (kx1), respectively. Thus, the final finite element approximation of the mass transport equation for the entire flow field is

$$[G] \sum_{j=1}^{k} a_j = [B] + [BigM] \sum_{j=1}^{k} a_j \quad . \tag{83}$$

The system of simultaneous equations (83) is solved using the iterative scheme described in the next chapter.

4. COMPUTATION PROCEDURES FOR FLOW AND MASS TRANSPORT MODELS

4.1 General

The purpose of this chapter is to describe the procedure for translation of the approximated differential equation describing flow and mass transport into a series of computer compatible statements for numerical solution. Since the emphasis of the study has been on the mass transport in known circulating flow, the computer program for solution of the flow model is not as general as one would like. It simply provides a rotating flow field as input to the mass transport algorithm by solving the unsteady vorticity equation in time until steady-state solution is obtained. The mass transport program, on the other hand, is user interactive and quite versatile in specification of parameters.

In developing the solution procedure, effort has been made to make the computer programs, particularly the mass transport program "user friendly" with minimum requirements for familiarity with the structure of the programs. Steps have been taken to reduce computation time and storage space required by the program. Documented solution procedure to differential equations and subroutines available on the University of Illinois Cyber 175 system have been used as much as possible.

Limitations on use of the programs are the same as those of the solution procedure. Scope of the flow model is limited to computation of a circulating flow field verifiable by published results obtained by others. Accuracy, stability, variation in grid size, and time step were not investigated in detail for the flow model as long as results compared favorably with the work of others. Numerical procedure for solution of the mass transport model has been treated with more care and attention than the flow model. Potential problems arising from the numerical procedure are

instabilty, "condition" of the matrices, and numerical diffusion. These problems are addressed in detail later in the chapter.

4.2 Numerical Procedure for the Flow Model

The numerical procedure developed to solve equation (30) has two major components -- solution procedure and contour plot of the flow pattern. A listing of the program is given in Appendix 1. The solution procedure, which repeatedly solves the governing equation in time until steady-state solution is found, is as follows:

a. Initial conditions of the problem are specified at t=0. These conditions include characteristic Reynolds number, grid spacing along the axes, time step for computations, and the criteria for achieving a steady-state solution.

b. Equation (30) is solved for the vorticity, ω, using a library routine available on the University of Illinois Cyber 175 computer. This routine solves the standard fine-point finite difference approximation to the Helmholtz equation

$$\nabla^2( ) + b( ) = f(x,y) \tag{84}$$

where ( ) denotes the dependent variable, b is a constant, and f(x,y) is specified. The variables x and y are bounded by rectangular or square boundary specified by constants A, B, C, and D where

$$A < x < B \text{ and } C < y < D \, . \tag{85}$$

c. Once the vorticity is computed, a modified version of the library routine used in (b) above is called to compute the stream function, ψ, from the equation

$$\nabla^2\psi = \omega \tag{86}$$

subject to the boundary conditions:

$$\begin{aligned} &\psi = 0 \quad \text{and} \quad \frac{\partial\psi}{\partial x} = 0 \qquad \text{on solid boundary; and} \\ &\psi = 0 \quad \text{and} \quad \frac{\partial\psi}{\partial y} = 0 \qquad \text{on moving boundary.} \end{aligned} \tag{87}$$

d. The current solution for ψ is tested against the solution for the previous time step. If the difference is larger than the specified criteria, computation is repeated. If the difference is equal to or less than the specified criteria, the steady-state solution is reached and results are printed out.

4.3 Numerical Procedure for the Mass Transport Model

Details of the numerical procedure developed to solve equation (83) are provided in this section. The procedure requires specification of the local and global geometry of the flow field as well as the components of velocity along the axes. This information is provided through an input file prepared by the user. Additional information concerning mass transport properties of the flow and computation time step are specified interactively.

The procedure makes use of two routines available through the Illinois Math and Science Library (IMSL) of the University of Illinois Cyber 175. One routine is used to decompose the global matrix into triangular matrices, and another is used to solve the system of equations. Documentation for both routines are available through the Computer Services Office at the University of Illinois and will not be included in this report.

4.3.1 Solution Scheme Organization

The solution scheme is user interactive allowing specification of some of the variables during the computing session. The program asks a series of questions to set up the problem under study and proceeds to solve the mass transport equation.

Initial conditions of the model are created through the use of both data files and user input. The model is dimensionally homogeneous, and the user is responsible for entering all values in the proper units. The user has the option of varying the geometric scale of the problem through the data entry. Components of velocity, node positions, and node numbering are supplied by the user through input files read by the main program. A cartesian coordinate system is assumed with x-axis along the mainflow and y-axis normal to it.

The computer "visualizes" the shape of all elements shown in Fig. 3 by reading the NODE data specifying the three global nodes associated with each element and the GEO data establishing the geographical position of each global node with respect to the origin of the coordinate system. The computer receives velocity information through VEL data, which are user-supplied velocity vector components in orthogonal directions at each global node. This file is the output of the flow model discussed earlier.

The user has the opportunity to specify the dispersion coefficient, the finite difference time step, the location and method of mass injection (instantaneous or continuous) and the elapse time between concentration level readouts during program execution.

All parameters and concentration levels are stored after each elapse time for later documentation of results. The user has the option, after each specified elapse time, to continue with the experiment, try another run with new interactive input parameters or terminate the execution of the program. The stored output can be claimed upon termination of the program execution.

During the program execution the user is supplied with pertinent information at the end of each elapse time, (see Fig. 4). At this point in the execution the user may request certain additional output. The user may request a plot of the normalized concentrations, C/C_{MAX}, at each node, (see Fig. 4). The unscaled character plot is printed on the user's terminal. Additionally, a scaled contour plot may be requested, (see Fig. 4). This plot is also printed on the user's terminal. These two plots are not stored and, if not requested during program execution, cannot be retrieved later.

4.3.2 The Computer Program

The computation scheme has been coded using Fortran Version IV. The program is divided into a series of independently operating subroutines performing specific tasks regarding solution of the approximate equation for mass transport. Information required by each subroutine is made available through use of common block data statements. A brief description of each subroutine is given below. The listing of the program appears in the Appendix II.

```
 E =   .100E-01          OUTER VEL=1.000        MAX CONC. =  .144E+02

 DELTA T=  .500E-01      *SLUG*=  .100E+01      TOTAL MASS=  .99111E+00

      ELAPSED TIME FROM LAST READING:           .20 TIME UNITS
      CLOCK TIME                                .45 TIME UNITS

  DO YOU WANT C/CMAX AT EACH NODE?? Y


 ALL CONCENTRATIONS FOR RUN  215

    1 11 21 31 41 51 61 71 81 91

 1  0  0  0  0  0  0  0  0  0  0
 2  0  0  0  0  0  0  0  0  0  0
 3  0  0  0  0  0  0  0  0  0  0
 4  0  0  0  0  0  0  0  0  0  0
 5  0  0  0  0  0  1  1  0  0  0
 6  0  0  0  0  1  4  6  3  0  0
 7  0  0  0  0  3  8  *  4  1  0
 8  0  0  0  0  2  5  6  2  0  0
 9  0  0  0  0  0  1  1  0  0  0
10  0  0  0  0  0  0  0  0  0  0
  DO YOU WANT A CONTOUR PLOT OF CONC. ? Y


 MAX CONCENTRATION=  .144E+02
 ORIGIN AT X=    0.0 Y=    0.0 SCALE=  .111E+02
```

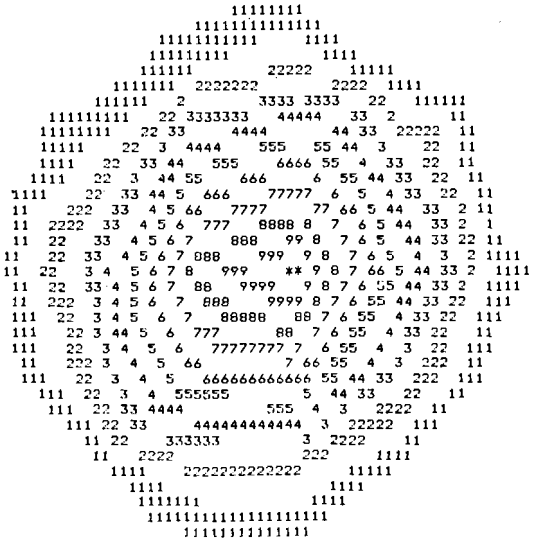

Fig. 4. Typical Printout of Solution

Subroutine INIT

Subroutine INIT reads the input data file and sets up the initial conditions for computations. The current program versions have the capability of accepting a 100 node network partitioned into 162 triangular elements, see Fig. 3 for details. The two principle axis geographical coordinates are stored by global node number in the array PT(2,100). For example, node 37 (Fig. 3) has x-coordinate 3 and y-coordinate 7, this information is stored in the array as PT(1,37)=3 and PT(2,37)=7. The velocity data is stored in the array VEL(2,100). For example, node 37 (Fig. 3) has a velocity component in the x-direction of 2.0 and velocity component in the y-direction of 4.0. This information is stored as: VEL(1,37)=2.0 and VEL(2,37)=4.0. The global node numbers associated with each element are stored in the array NODE(162,3). The local node numbering system is implicitly recorded in this array. For example, for element 85 (Fig. 3):

global node no.	local node no.
44	1
54	2
55	3

This information is stored as: NODE(85,1)=44;
NODE(85,2)=54;
NODE(85,3)=55.

Subroutine INIT contains the user interactive portion of the program where the value of parameters not transmitted through the attached data file are requested and must be provided by the user during program execution.

The initial concentration for the node where the tracer is injected and the initial area affected are calculate by subroutine INIT. The area

and concentration calculations are premised on the assumption that triangular elements are established such that two sides of the triangle are parallel to the coordinate axes. The area of an element is calculated using the following formula:

$$\text{AREA} = (x_2 - x_1)(y_3 - y_1)/2 - (x_3 - x_1)(y_2 - y_1)/2 \quad .$$

Subscripts denote local node numbers.

Subroutine MATRIX

This subroutine assembles the Global matrix which is the sum of the element matrices M, K_x, K_y, H_x, and H_y in equation (82). It serves as the coefficient matrix for the unknown or new concentration matrix to be computed at the next time step. The element M matrices are summed to form the BigM matrix which is multiplied by the current concentration values to form part of the solution matrix.

One version of the the model has the subroutine MATRIX coded to assign variable magnitudes to the dispersion coefficient in the x and y directions. The direction cosines are computed in subroutine MATRIX, and the dispersion coefficient E_x and E_y are calculated for each element within the same program loop that computes the element matrices.

Subroutine MIX

In subroutine MIX the right hand side of solution matrix, equation (83) is assembled. The program array name is B(100). For instantaneous mass injection at a node, B is simply the BigM coefficient matrix multiplied by the "current" concentration values.

The University of Illinois Math and Science Library (IMSL) subroutine LUDAFT and LUELMF are called by subroutine MIX to solve the set of simultaneous equations for the time dependent concentrations. The

subroutine LUDAFT has an optimal accuracy test for the decomposed matrix which can be used to determine "condition" of the matrix as discussed later in this chapter. A discussion of the relevance of the accuracy test can be found in Shapine & Allen [25]. Subroutine LUELMF performs the elimination portion of the solution. New concentration values are determined by forward then back substitution.

Subroutine SUMASS

Subroutine SUMASS calculates the total mass in the flow field. The scheme averages the three nodal concentrations of an element then multiplies the average element concentration by the element area. The area computations scheme assumes two sides of the element are parallel to the respective coordinate axis. The flow area and total mass are printed during program execution as a check on conservation of mass.

Subroutine OUTPUT

Subroutine OUTPUT, along with subroutines CMAX and PLOT (described below), provides the output for the program. Concentration levels and other pertinent data are stored on "TAPE7" at the end of the elapse time specified by the user. Concentration levels and other data computed during intermediate time steps are not stored.

Subroutine OUTPUT is automatically invoked by the main program. It prints the run number, dispersion coefficient, main flow velocity, time step, amount of mass injected, total mass currently in the flow field, maximum concentration, elapsed time and the accumulated time from the start of the run (clock time).

Subroutine CMAX

Subroutine CMAX is called by subroutine OUTPUT at the user's discretion. It produces unscaled character plot of concentrations normalized by the maximum concentration in the flow field. See Fig. 4 for an example of CMAX output.

Subroutine PLOT

Subroutine PLOT prints a scaled character contour plot for the concentration in the flow field.

The equation of the plane defined by element node positions and concentration values is computed. A linear interpolation procedure computes concentration values interior to the plane at points scaled to the printer type dimensions. The program proceeds element by element and assigns concentration values to an array, PICTUR, dimensioned to the scaled vertical and horizontal proportions of the printer. A ratio of 6 horizontal to 10 vertical spacing is common for line printers.

After all elements have been analyzed and a concentration level assigned to the appropriate positions in array PICTUR the concentrations in PICTUR are normalized. Then a single digit number is assigned to each position in PICTUR indicative of the relative values of the concentrations relative to the maximum concentration present in the flow field. The printout appears as a contour plot of normalized concentration (Fig. 4).

4.3.3 Stability Guidelines

Pinder and Gray and Smith et al. state that the forward difference time step, also known as implicit time difference method, yields a recurrence relation which is usually "unconditionally stable." A generally accepted criteria for stability is the bounded oscillation of results in

the early iterations with eventual convergence to the "solution." A more restrictive definition would require that seed errors in the problem diminish monotonically (e.g. truncation errors cancel out). A stability criteria expressing the more restrictive definition is derived here and a procedure to apply it to the transport model is developed.

4.3.3.1 Derivation of Stability Criteria

Consider the final finite element global matrix equation (83) for simulation of mass transport:

$$[G] \sum_{j=1}^{k} a_j^{n+1} = [B] + [BigM] \sum_{j=1}^{k} a_j^{n+1} \qquad (88)$$

with an all zero B matrix. The analysis can be readily generalized for the case of a non-zero B matrix.

Define the error vector $[e]^n$ such that

$$[e]^n = [\hat{c}]^n - [c]^n \qquad (89)$$

where

$[\hat{c}]^n$ is the vector of computed concentration values;

$[c]^n$ is the vector of the true concentration values; and

n is the time step.

Also, define $[\bar{e}]^n$ such that $[\bar{e}]^n = \max \left| [e]^n \right|$. (90)

Substituting equations (89) and (90) in the finite element matrix equation (88) gives:

$$[G] \{ [c]^{n+1} + [\bar{e}]^{n+1} \} = [BigM] \{ [c]^n + [\bar{e}]^n \} \qquad (91)$$

Rearranging equation (91):

$$[G]\ [\bar{e}]^{n+1} = [BigM]\ [\bar{e}]^{n} + [BigM]\ [c]^{n} - [G]\ [c]^{n+1} . \qquad (92)$$

By definition $[c]^{n+1}$ and $[c]^{n}$ are exact. Thus, the last two terms on the right hand side of equation (92) cancel and the error in the n+1 time step becomes a function of the error in the nth time step as:

$$[G]\ [\bar{e}]^{n+1} = [BigM]\ [\bar{e}]^{n} . \qquad (93)$$

The propagation of error depends on the form of this relationship. Note that all the entries in the error vector [e] are equal and the error can be treated as a scalar. In order to eliminate error magnification, the error in the n+1 time step must be less than or equal to the error in the nth time step. Written mathematically,

$$\bar{e}^{n+1} \leq \bar{e}^{n} \text{ or } \frac{\bar{e}^{n+1}}{\bar{e}^{n}} \leq 1 . \qquad (94)$$

Let $[G] = \sum_{i=1}^{k} \sum_{j=1}^{k} g_{ij}$ and $[BigM] = \sum_{i=1}^{k} \sum_{j=1}^{k} m_{ij}$.

Then for the ith row of equation (93), we can write:

$$\left(\sum_{j=1}^{k} g_{ij} \right) \bar{e}^{n+1} = \left(\sum_{j=1}^{k} m_{ij} \right) \bar{e}^{n}, \quad i = 1, k . \qquad (95)$$

By observation, the requirement of equation (94) can be met if

$$\frac{(\text{MAX} \sum_{j=1}^{k} m_{ij})}{(\text{MIN} \sum_{j=1}^{k} g_{ij})} = \frac{\bar{e}^{n+1}}{\bar{e}^{n}} \leq 1 , \quad i = 1, k . \tag{96}$$

Rewriting equation (96)

$$\text{MAX} \sum_{j=1}^{k} m_{ij} \leq \text{MIN} \sum_{j=1}^{k} g_{ij} , \quad i = 1, k \tag{97}$$

Thus, stability is assured if the maximum sum of the ith row of the BigM matrix is less than the minimum sum of the ith row of the Global matrix, G, for each time step.

4.3.3.2 Application of the Stability Criteria

Lack of symmetry or regularity of the finite element global matrices encumbers the exact prediction of the matrices' row component sums. The procedure developed here serves to approximate the matrix row sums. The approximations substituted in the stability criteria form a guideline for designing parameter bounds. For the purpose of this discussion the term "component" will signify the final value in a position of a matrix and "entry" will refer to one of possibly several values summed to form the components of a matrix.

There are two principal steps in the procedure. First, the general assembly of the global matrices is visualized. Then the row sum of global matrix components is approximated by examining the element matrix components. Every component of a global matrix will be some combination of the corresponding element matrix components. A linear, triangular finite element network has the characteristic that for every element to which a node is common, each component of the element matrix row corresponding to the local element node number will be entered into the row of the global

matrix corresponding to the node's global number. Thus, a row sum of a global matrix is the aggregate of row sums of element matrices. Figure 5 illustrates the assembly of a global matrix for a regular grid spacing finite element network.

The element matrix rows (1, 2, or 3) entered in the global matrix row is determined by each local node numbering scheme. Note in Fig. 5, that row 1 of the element matrix is entered twice, row 3 once, and row 2 not at all. Given a particular finite element network all the row sums of an element matrix may be approximated by a common expression. The row sum of a global matrix can then be represented by a multiple of the aggregate row sum approximations of the element matrices from which it is assembled.

The Global matrix, G, neglecting the cross product terms (E_{xy}) is assembled from the element matrices M, K_x, K_y, H_x, and H_y equations (58), (70), (71), (77), and (78), respectively. Figure 6 is a compilation of the matrices.

Let the sum of the ith row be defined as:

$$[\frac{1}{\Delta t} M] = \sum_{j=1}^{3} M_{ij} , \quad i = 1, 3 ;$$

$$[K_x] = \sum_{j=1}^{3} k_{xij} , \quad i = 1, 3 ;$$

$$[K_y] = \sum_{j=1}^{3} k_{yij} , \quad i = 1, 3 ; \tag{98}$$

$$[H_x] = \sum_{j=1}^{3} h_{xij} , \quad i = 1, 3 ; \text{ and}$$

$$[H_y] = \sum_{j=1}^{3} h_{yij} , \quad i = 1, 3 .$$

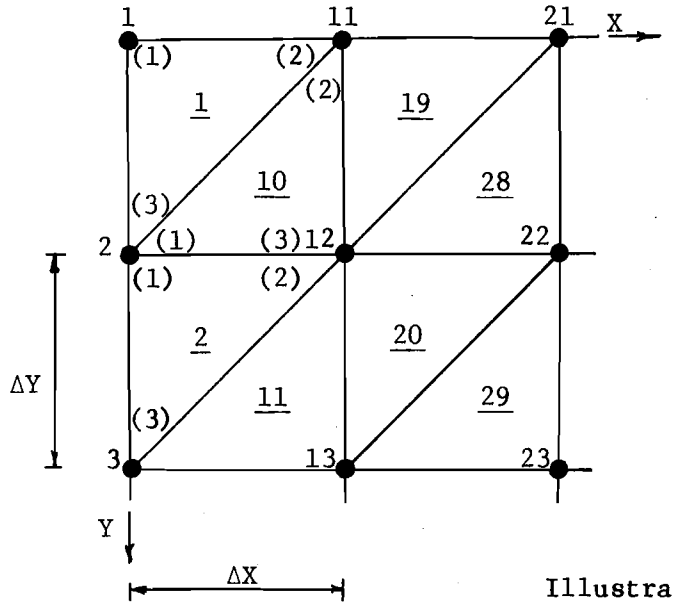

LEGEND

xx	global node #
(xx)	local node #
xx	element #

Element #	Local Node #	Global Node #	Illustrative Element Matrix Positions	Corresponding Global Matrix Positions	
			(2,3)	(11,2)	
1	1	1	(3,1)	(2,1)	Entered in
	2	11	(3,2)	(2,11)	Row 2 of
	3	2	(3,3)	(2,2)	global
					matrix
10	1	2	(1,1)	(2,2)	Entered in
	2	11	(1,2)	(2,11)	Row 2 of
	3	12	(1,3)	(2,12)	global
					matrix
2	1	2	(1,1)	(2,2)	Entered in
	2	12	(1,2)	(2,12)	Row 2 of
	3	3	(1,3)	(2,3)	global
					matrix
				(2,4)	No element
				(2,5)	matrix
				(2,6)	entries in
				.	the global
				.	matrix,
				(2,10)	nodes have
				(2,13)	no common
				.	elements
				.	
				(2,k)	

Note:
Node 2 is common to 3 elements, thus the components of 3 element matrix rows are entered in the global Row 2.

Fig. 5. Global Matrix Assembly

$$
\begin{bmatrix}
\frac{A}{6\Delta t} + \frac{1}{24}(U+u_1)(y_2-y_3) + \frac{1}{24}(V+v_1)(x_3-x_2) + \frac{\bar{E}_x}{4A}(y_2-y_3)(y_2-y_3) + \frac{\bar{E}_y}{4A}(x_3-x_2)(x_3-x_2) & \frac{A}{12\Delta t} + \frac{1}{24}(U+u_1)(y_3-y_1) + \frac{1}{24}(V+v_1)(x_1-x_3) + \frac{\bar{E}_x}{4A}(y_2-y_3)(y_3-y_1) + \frac{\bar{E}_y}{4A}(x_3-x_2)(x_1-x_3) & \frac{A}{12\Delta t} + \frac{1}{24}(U+u_1)(y_1-y_2) + \frac{1}{24}(V+v_1)(x_2-x_1) + \frac{\bar{E}_x}{4A}(y_2-y_3)(y_1-y_2) + \frac{\bar{E}_y}{4A}(x_3-x_2)(x_2-x_1) \\
\frac{A}{12\Delta t} + \frac{1}{24}(U+u_2)(y_2-y_3) + \frac{1}{24}(V+v_2)(x_3-x_2) + \frac{\bar{E}_x}{4A}(y_3-y_1)(y_2-y_3) + \frac{\bar{E}_y}{4A}(x_1-x_3)(x_3-x_2) & \frac{A}{6\Delta t} + \frac{1}{24}(U+u_2)(y_3-y_1) + \frac{1}{24}(V+v_2)(x_1-x_3) + \frac{\bar{E}_x}{4A}(y_3-y_1)(y_3-y_1) + \frac{\bar{E}_y}{4A}(x_1-x_3)(x_1-x_3) & \frac{A}{12\Delta t} + \frac{1}{24}(U+u_2)(y_1-y_2) + \frac{1}{24}(V+v_2)(x_2-x_1) + \frac{\bar{E}_x}{4A}(y_3-y_1)(y_1-y_2) + \frac{\bar{E}_y}{4A}(x_1-x_3)(x_2-x_1) \\
\frac{A}{12\Delta t} + \frac{1}{24}(U+u_3)(y_2-y_3) + \frac{1}{24}(V+v_3)(x_3-x_2) + \frac{\bar{E}_x}{4A}(y_1-y_2)(y_2-y_3) + \frac{\bar{E}_y}{4A}(x_2-x_1)(x_3-x_2) & \frac{A}{12\Delta t} + \frac{1}{24}(U+u_3)(y_3-y_1) + \frac{1}{24}(V+v_3)(x_1-x_3) + \frac{\bar{E}_x}{4A}(y_1-y_2)(y_3-y_1) + \frac{\bar{E}_y}{4A}(x_2-x_1)(x_1-x_3) & \frac{A}{6\Delta t} + \frac{1}{24}(U+u_3)(y_1-y_2) + \frac{1}{24}(V+v_3)(x_2-x_1) + \frac{\bar{E}_x}{4A}(y_1-y_2)(y_1-y_2) + \frac{\bar{E}_y}{4A}(x_2-x_1)(x_2-x_1)
\end{bmatrix}
$$

Fig. 6 Sum of Element Matrices M, K and H

The sum of the ith row of the $[K_x]$ and $[K_y]$ matrices can be written:

$$\sum_{j=1}^{3} k_{xij} = \frac{1}{24} (U+u_i)[(y_2-y_3) + (y_3-y_1) + (y_1-y_2)] = 0 \qquad (99)$$

and

$$\sum_{j=1}^{3} k_{xij} = \frac{1}{24} (V+v_1)[(x_3-x_2) + (x_1-x_3) + (x_2-x_1)] = 0 \qquad (100)$$

where $U = u_1 + u_2 + u_3$ and $V = v_1 + v_2 + v_3$. The y and x coordinate terms cancel. Thus, the contribution of the K matrices to the row sum of the Global matrix is nil.

The sum of the ith row of the H_x matrix can be written as:

$$\sum_{j=1}^{3} h_{xij} = \frac{\sum_{m=1}^{3} E_{xm}}{4A} [(y_t-y_r)(y_s-y_t) + (y_s-y_r)(y_t-y_r) + (y_s-y_t)(y_r-y_s)] \qquad (101)$$

Similarly for the H_y matrix:

$$\sum_{j=1}^{3} h_{yij} = \frac{\sum_{m=1}^{3} E_{ym}}{4A} [(x_t-x_s)(x_t-x_r) + (x_r-x_t)(x_r-x_s) + (x_s-x_r)(x_s-x_t)] \qquad (102)$$

In equations (101) and (102) r, s, and t cycle from 1-3.

Given a uniform grid spacing and a triangular element mesh with two sides of each triangle parallel to the two coordinate axes, Fig. 5, the following generalizations can be made:

$$y_s - y_r = \begin{matrix} \pm\Delta y \\ 0 \end{matrix} \quad , \quad s = 1, 3 \; , \quad r = 1, 3$$

$$x_s - x_r = \begin{matrix} \pm\Delta x \\ 0 \end{matrix} \quad , \quad s = 1, 3 \quad r = 1, 3 \tag{103}$$

$\pm\Delta x = \pm\Delta y = \pm\Delta L$ for $\Delta y \neq 0$, $\Delta x \neq 0$; $A = \frac{1}{2} (\Delta L)^2$ where A = element area.

Assume the dispersion coefficient summed over each element is a constant and is written as equation (15) below:

$$\sum_{m=1}^{3} E_{xm} = \bar{E}_x \quad \text{and} \quad \sum_{m=1}^{3} E_{ym} = \bar{E}_y \tag{104}$$

Substituting equations (103) and (104) in equations (101) and (102) the row sums of the H_x and H_y matrices reduce to:

$$\sum_{j=1}^{3} h_{xij} = \begin{matrix} \pm \bar{E}_x \\ \text{or} \\ 0 \end{matrix} \tag{105}$$

and

$$\sum_{j=1}^{3} h_{yij} = \begin{matrix} \pm \bar{E}_y \\ \text{or} \\ 0 \end{matrix} \tag{106}$$

$$\begin{bmatrix} \frac{A}{6\Delta T} & \frac{A}{12\Delta T} & \frac{A}{12\Delta T} \\ \frac{A}{12\Delta T} & \frac{A}{6\Delta T} & \frac{A}{12\Delta T} \\ \frac{A}{12\Delta T} & \frac{A}{12\Delta T} & \frac{A}{6\Delta T} \end{bmatrix}$$

Fig. 7 The M Matrix for Each Element

From Fig. 7, the ith row sum of the $\frac{1}{\Delta t}$ M matrix is exactly:

$$\sum_{j=1}^{3} m_{ij} = \frac{(\Delta L)^2}{6\Delta t} \tag{107}$$

The possible minimum of any row sum of the Global matrix can be approximated by a multiple of the sum of equations (99), (100), and (105-107). Similarly, the sum of any row of the BigM matrix is a multiple of equation (107). For a given row, the multiple factor is the same for both matrices.

Inspection of element orientations reveals that if the row sum of the element H_x matrix equation (105) is zero, the corresponding row sum of the H_y matrix equation (106) will be nonzero. Furthermore, E_x and E_y in equations (105) and (106) could be of equal magnitude and opposite sign, summing to 0. The minimum row sum of the Global matrix will be equal to equation (107) plus $\pm E_x$, $\pm E_y$, or 0.

If dispersion is uniform throughout the region, $\pm E_x = \pm E_y = \pm E$. Substituting in the stability criterion (94) we have

$$\frac{(\Delta L)^2}{6\Delta t} \leq \frac{(\Delta L)^2}{6\Delta t} + \begin{cases} \pm E \\ \text{or} \\ 0 \end{cases} \tag{108}$$

The value of the dispersion coefficient, E, is always positive. Stability will be assured therefore if the row sums of the H_x and H_y matrices reduce to +E. However if $+E << \frac{(\Delta L)^2}{6\Delta t}$ or 0, stability is marginal and subject to computational errors such as internal representation, rounding and truncation. Computation will be unstable if the row sums of the H_x and H_y matrices reduce to -E since condition in equation (108) will become invalid.

The node numbering scheme determines the sign of equations (105) and (106) and thereby may cause computations associated with an element or a region of the flow field to be unstable.

The stability guideline derived here is applicable to a square flow field approximated by triangular elements. The methodology may be applied to flow field of other geometry with some care. The analysis may be applied piecewise to regions of a network if the grid spacing is not uniform throughout. In situations where dispersion coefficient is not uniform throughout the flow field, an approximate minimum value of E might be used in equation (108). However, as more variables are introduced, more generalized approximations will be necessary which will subsequently weaken the power of the criteria presented here.

4.3.4 Condition of the Coefficient Matrix

"Condition" of a matrix has a direct bearing on the errors that may be generated when the matrix is decomposed. Further, judicious choice of the algorithm to solve the system of equations can minimize rounding and truncation errors, storage space, and computation time. A preliminary review of the method of elimination for the solution of simultaneous non-singular problems is given in Shapine and Allen [25]. A complete discussion of the methodology can be found in Forsyth & Moler [10].

The Crout algorithm is employed to solve the system of equations. This algorithm uses partial pivoting, which chooses the largest element in the column as a pivot in the matrix decomposition in order to reduce round off error. However, the 'size' of the elements in the various equations must be comparable for the partial pivoting strategy to be useful.

For the problem of circulating flow the velocities may be positive or negative. Also, dependent upon the local numbering scheme and element orientation the dispersion terms may be positive or negative. The M matrix terms are a product of the element area and time step and, therefore, are always positive. The relative magnitudes of the H, K, and M matrix terms will play a roll in the conditioning of the Global matrix. If the M matrix terms $A/\Delta t$ are much larger than the velocity and dispersion terms, the components of the Global matrix will be of the same order and the matrix is considered well conditioned. However, if the M matrix terms are much larger than the other terms, there will be little change in the concentrations after each time step. Numerous time steps may be required to produce meaningful results. The calculations may or may not remain stable for sufficiently long time to produce results. The relative magnitude of the terms can be manipulated by varying the grid spacing and by choice of the finite difference time step.

4.3.5 Numerical Diffusion

Numerical diffusion occurs when the numerical scheme transports a discritized mass (represented by a concentration) to a position between the discritized points of a flow field. The mass must then be proportionately assigned to the grid points, effectively diffusing it. Typical test for numerical diffusion is to solve the mass transport equation without the dispersion terms (i.e., set dispersion coefficient equal to zero) and

examine the solution to the pure advection problem for artificial spreading of mass. This is not always easy to do since finite element method is subject to instability problems for purely advecting flows, as discussed in section 4.3.3 earlier.

Pinder and Gray [19], Grove [11], and Smith [27] have shown that the Galerkin form of the finite element method is less subject to numerical diffusion than many standard finite difference schemes for the numerical solution of the one-dimensional mass transport equation. The Galerkin finite element method has also compared favorably with optimized finite difference schemes for the numerical solution of the two-dimensional transport problems.

If grid spacing, ΔL, and time step, Δt, are related to the characteristic velocity, U_a, of the flow field, the artificial spreading of the mass can be reduced but not eliminated. This is achieved when the dimensionless group $U_a(\Delta t/\Delta L)$ is kept close to unity. For $(U_a\ \Delta t) << \Delta L$, the flow field is dispersion dominated, and numerous iterations must be conducted before significant advection can be observed. For $(U_a\ \Delta t) >> \Delta L$, the flow is advection dominated and the center of mass (peak concentration) leaps around the flow field and it is not possible to observe the gradual transport of mass. These observations have been supported by numerical experiments conducted on the scheme used in this study. A series of tests comparing the dispersion properties of flow for various values of $U_a(\Delta t/\Delta L)$ will be incorporated in future investigations.

5. PRESENTATION AND DISCUSSION OF RESULTS

5.1 General

Preliminary results from the flow and the mass transport model are presented in this chapter. The flow model has been tested for a range of characteristic Reynolds numbers to establish the lower limit at which the viscous flow assumption in the model formulation is no longer valid. The velocity pattern for a characteristic Reynolds number of 10,000 has been used as input to the mass transport model. At this Reynolds number the solution was stable and comparable to the circulation pattern obtained by other researchers.

Two versions of the mass transport model have been tested and results are given. Version I simulates mixing and transport of a finite amount of mass injected instantaneously at a rate using a constant dispersion coefficient throughout the flow field. Version II simulates the same condition subject to a vectorized dispersion coefficient with components along and normal to the streamlines, respectively. The components of the dispersion coefficient at each node are the product of the direction cosines of the velocity vector at that node and a constant coefficient, E, assigned interactively by the user.

Input file preparation and conditions for numerical stability have been discussed in the previous section and will not be repeated here. However, the velocity data file from the flow model was scaled up by a factor of 10 in order to make it compatible with the grid spacing ($\Delta L=1.0$) and time step in the mass transport model. The general shape of the circulation remained the same. All scales have been selected to minimize potential numerical problems discussed in the previous chapter. The units used in presentation of results are arbitrary, but consistent.

5.2 Results from the Flow Model

A standard data set containing the finite difference grid spacing, time step, and the accuracy criteria was established and used for each simulation run. Calculations have been performed for characteristic Reynolds numbers of 500; 1,000; 2,000; 5,000; 10,000; 15,000; 20,000; and 30,000. The results for each run have been presented in tabular form in the following pages (Tables 1-8). The tables list computed values of the stream function, vorticity, and x and y components of the velocity at each node. The format for each table follows the node numbering scheme shown in Fig. 2 earlier. Simulation parameters for each run appear at the top of each table for identification purposes.

Plot of the flow pattern for each run follows the tabulated results for that run (Figs. 8-15). The plots are generated by line printer using the program CONTOUR listed in Appendix I. This program interpolates the values of the stream function among adjacent nodes and developes a character contour plot of the data.

PROBLEM PARAMETERS

NUMBER OF SUBDIVITIONS IN EACH DIRECTION = 9
TIME INTERVALS = .0333
SPACE INTERVALS IN EACH DIRECTION = .1000
NUMBER OF ITERATIONS = 656
ITERATION CRITERIA = .00005000
DIFFERENCE OF Z(T) AND Z(T-1) = .498E-04
REYNOLDS NUMBER RE = 500.00

TABLE OF THE STREAMFUNCTION

0.	0.	0.	0.	0.	0.	0.	0.	0.	0.
0.	-.12E-01	-.22E-01	-.31E-01	-.38E-01	-.45E-01	-.49E-01	-.50E-01	-.42E-01	0.
0.	-.10E-01	-.24E-01	-.37E-01	-.49E-01	-.59E-01	-.65E-01	-.64E-01	-.48E-01	0.
0.	-.92E-02	-.23E-01	-.37E-01	-.50E-01	-.60E-01	-.65E-01	-.60E-01	-.38E-01	0.
0.	-.78E-02	-.20E-01	-.33E-01	-.44E-01	-.52E-01	-.53E-01	-.45E-01	-.25E-01	0.
0.	-.57E-02	-.15E-01	-.24E-01	-.32E-01	-.37E-01	-.36E-01	-.28E-01	-.13E-01	0.
0.	-.33E-02	-.90E-02	-.15E-01	-.20E-01	-.22E-01	-.21E-01	-.15E-01	-.56E-02	0.
0.	-.13E-02	-.40E-02	-.70E-02	-.95E-02	-.11E-01	-.96E-02	-.61E-02	-.16E-02	0.
0.	-.15E-03	-.82E-03	-.17E-02	-.26E-02	-.30E-02	-.26E-02	-.15E-02	-.10E-03	0.
0.	0.	0.	0.	0.	0.	0.	0.	0.	0.

TABLE OF THE VORTICITY

0.	.18E+02	.16E+02	.14E+02	.12E+02	.11E+02	.10E+02	.10E+02	.12E+02	.20E+02
-.23E+01	.11E+01	.18E+01	.21E+01	.24E+01	.26E+01	.29E+01	.37E+01	.56E+01	-.84E+01
-.21E+01	-.31E+00	.31E+00	.64E+00	.95E+00	.13E+01	.18E+01	.28E+01	.40E+01	-.97E+01
-.18E+01	-.37E+00	.16E+00	.48E+00	.84E+00	.13E+01	.18E+01	.21E+01	.17E+01	-.77E+01
-.16E+01	-.30E+00	.12E+00	.39E+00	.68E+00	.97E+00	.12E+01	.11E+01	.19E+00	-.49E+01
-.11E+01	-.25E+00	.29E-01	.19E+00	.34E+00	.46E+00	.48E+00	.31E+00	-.47E+00	-.26E+01
-.67E+00	-.22E+00	-.86E-01	-.21E-01	.33E-01	.63E-01	.49E-01	-.11E+00	-.58E+00	-.11E+01
-.26E+00	-.18E+00	-.17E+00	-.18E+00	-.17E+00	-.15E+00	-.16E+00	-.25E+00	-.43E+00	-.33E+00
-.30E-01	-.12E+00	-.21E+00	-.28E+00	-.32E+00	-.31E+00	-.28E+00	-.25E+00	-.22E+00	-.20E-01
0.	-.30E-01	-.16E+00	-.34E+00	-.51E+00	-.60E+00	-.53E+00	-.29E+00	-.20E-01	0.

TABLE 1--Flow Model Results

Reynolds No. = 500

TABLE OF VELOCITY U IN X-DIRECTION

.10E+01	.10E+01	.10E+01	.10E+01	.10E+01	.10E+01	.10E+01	.10E+01	.10E+01	.10E+01
0.	.51E-01	.12E+00	.19E+00	.25E+00	.29E+00	.32E+00	.32E+00	.24E+00	0.
0.	-.12E-01	.44E-02	.31E-01	.59E-01	.80E-01	.82E-01	.48E-01	-.17E-01	0.
0.	-.13E-01	-.22E-01	-.25E-01	-.27E-01	-.36E-01	-.59E-01	-.97E-01	-.12E+00	0.
0.	-.17E-01	-.42E-01	-.66E-01	-.90E-01	-.12E+00	-.14E+00	-.16E+00	-.13E+00	0.
0.	-.22E-01	-.55E-01	-.88E-01	-.12E+00	-.15E+00	-.16E+00	-.15E+00	-.95E-01	0.
0.	-.22E-01	-.54E-01	-.86E-01	-.11E+00	-.13E+00	-.13E+00	-.11E+00	-.58E-01	0.
0.	-.16E-01	-.41E-01	-.66E-01	-.86E-01	-.97E-01	-.91E-01	-.67E-01	-.28E-01	0.
0.	-.65E-02	-.20E-01	-.35E-01	-.47E-01	-.53E-01	-.48E-01	-.31E-01	-.82E-02	0.
0.	0.	0.	0.	0.	0.	0.	0.	0.	0.

TABLE OF VELOCITY V IN Y-DIRECTION

0.	0.	0.	0.	0.	0.	0.	0.	0.	0.
0.	-.11E+00	-.98E-01	-.81E-01	-.67E-01	-.52E-01	-.28E-01	.35E-01	.25E+00	0.
0.	-.12E+00	-.14E+00	-.12E+00	-.11E+00	-.78E-01	-.27E-01	.82E-01	.32E+00	0.
0.	-.12E+00	-.14E+00	-.14E+00	-.12E+00	-.74E-01	.43E-02	.13E+00	.30E+00	0.
0.	-.10E+00	-.12E+00	-.12E+00	-.95E-01	-.46E-01	.34E-01	.14E+00	.22E+00	0.
0.	-.74E-01	-.93E-01	-.87E-01	-.64E-01	-.20E-01	.44E-01	.12E+00	.14E+00	0.
0.	-.45E-01	-.58E-01	-.54E-01	-.37E-01	-.53E-02	.37E-01	.76E-01	.74E-01	0.
0.	-.20E-01	-.28E-01	-.27E-01	-.18E-01	-.43E-03	.22E-01	.40E-01	.31E-01	0.
0.	-.41E-02	-.78E-02	-.87E-02	-.63E-02	-.46E-03	.76E-02	.13E-01	.73E-02	0.
0.	0.	0.	0.	0.	0.	0.	0.	0.	0.

TABLE 1 (cont.)--Flow Model Results

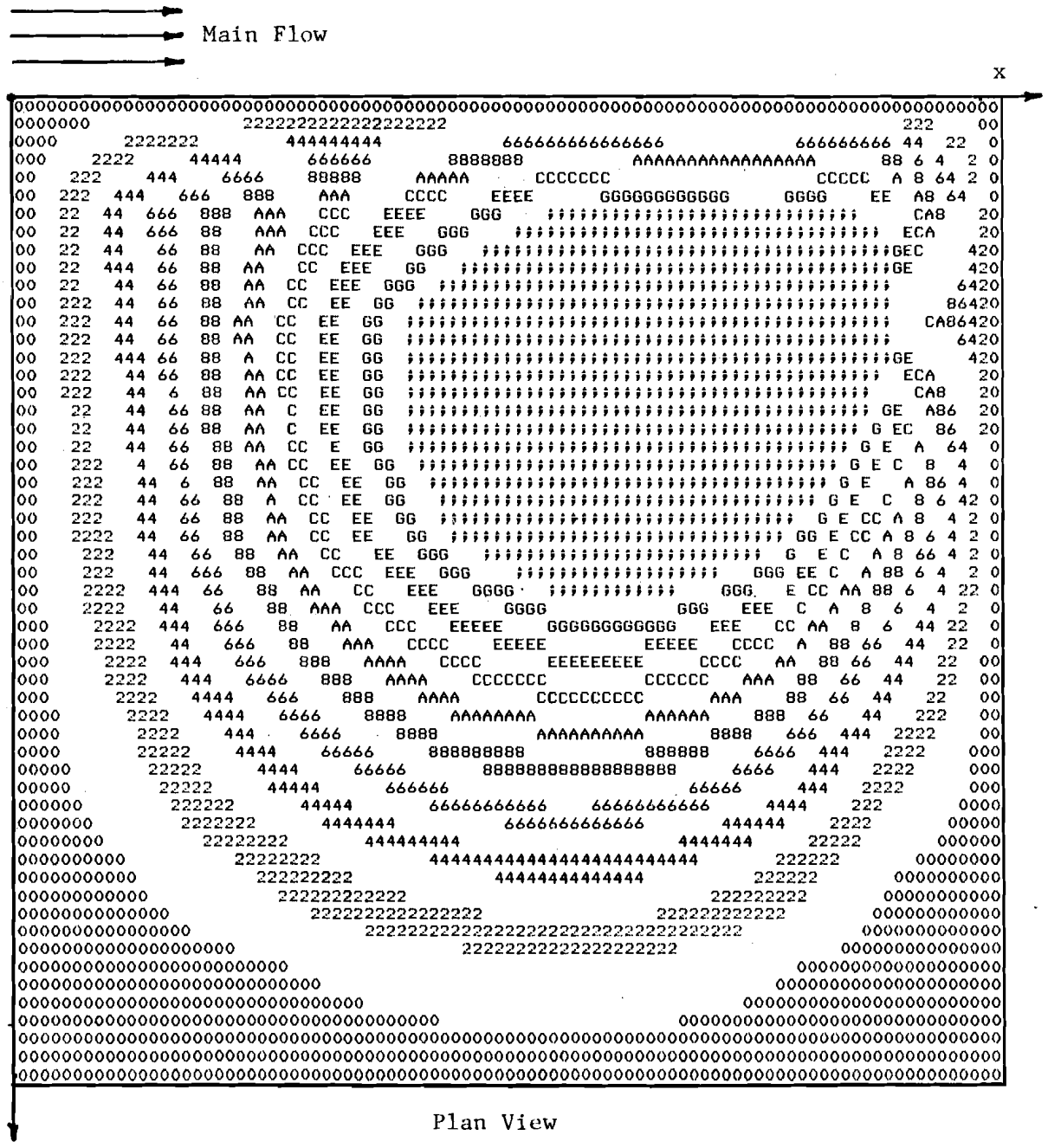

Plan View

Reynolds No. = 500

Fig. 8. Contour Plot of Streamlines

PROBLEM PARAMETERS

NUMBER OF SUBDIVITIONS IN EACH DIRECTION = 9
TIME INTERVALS = .0333
SPACE INTERVALS IN EACH DIRECTION = .1000
NUMBER OF ITERATIONS = 947
ITERATION CRITERIA = .00005000
DIFFERENCE OF Z(T) AND Z(T-1) = .498E-04
REYNOLDS NUMBER RE = 1000.00

TABLE OF THE STREAMFUNCTION

0.	0.	0.	0.	0.	0.	0.	0.	0.	0.
0.	-.87E-02	-.17E-01	-.24E-01	-.30E-01	-.35E-01	-.39E-01	-.41E-01	-.38E-01	0.
0.	-.81E-02	-.19E-01	-.30E-01	-.39E-01	-.48E-01	-.53E-01	-.54E-01	-.45E-01	0.
0.	-.77E-02	-.19E-01	-.31E-01	-.42E-01	-.51E-01	-.57E-01	-.53E-01	-.37E-01	0.
0.	-.69E-02	-.17E-01	-.28E-01	-.38E-01	-.46E-01	-.48E-01	-.42E-01	-.25E-01	0.
0.	-.53E-02	-.13E-01	-.22E-01	-.29E-01	-.34E-01	-.34E-01	-.28E-01	-.14E-01	0.
0.	-.32E-02	-.82E-02	-.14E-01	-.18E-01	-.21E-01	-.20E-01	-.15E-01	-.64E-02	0.
0.	-.12E-02	-.36E-02	-.65E-02	-.90E-02	-.10E-01	-.97E-02	-.65E-02	-.20E-02	0.
0.	-.95E-04	-.68E-03	-.16E-02	-.25E-02	-.30E-02	-.28E-02	-.17E-02	-.19E-03	0.
0.	0.	0.	0.	0.	0.	0.	0.	0.	0.

TABLE OF THE VORTICITY

0.	.18E+02	.17E+02	.15E+02	.14E+02	.13E+02	.12E+02	.12E+02	.12E+02	.20E+02
-.17E+01	.79E+00	.13E+01	.16E+01	.17E+01	.19E+01	.22E+01	.27E+01	.53E+01	-.76E+01
-.16E+01	-.25E+00	.19E+00	.43E+00	.66E+00	.95E+00	.12E+01	.19E+01	.42E+01	-.91E+01
-.15E+01	-.26E+00	.13E+00	.37E+00	.67E+00	.11E+01	.16E+01	.19E+01	.21E+01	-.75E+01
-.14E+01	-.20E+00	.12E+00	.35E+00	.63E+00	.93E+00	.11E+01	.12E+01	.55E+00	-.50E+01
-.11E+01	-.17E+00	.45E-01	.19E+00	.35E+00	.49E+00	.54E+00	.43E+00	-.23E+00	-.28E+01
-.63E+00	-.17E+00	-.69E-01	-.55E-02	.59E-01	.10E+00	.11E+00	-.14E-01	-.47E+00	-.13E+01
-.24E+00	-.16E+00	-.16E+00	-.16E+00	-.14E+00	-.12E+00	-.12E+00	-.20E+00	-.41E+00	-.41E+00
-.19E-01	-.12E+00	-.21E+00	-.27E+00	-.30E+00	-.28E+00	-.25E+00	-.23E+00	-.24E+00	-.37E-01
0.	-.19E-01	-.14E+00	-.31E+00	-.50E+00	-.61E+00	-.57E+00	-.33E+00	-.37E-01	0.

TABLE 2--Flow Model Results

Reynolds No. = 1,000

TABLE OF VELOCITY U IN X-DIRECTION

.10E+01	.10E+01	.10E+01	.10E+01	.10E+01	.10E+01	.10E+01	.10E+01	.10E+01	.10E+01
0.	.41E-01	.95E-01	.15E+00	.20E+00	.24E+00	.27E+00	.27E+00	.23E+00	0.
0.	-.48E-02	.11E-01	.34E-01	.60E-01	.81E-01	.87E-01	.62E-01	-.24E-02	0.
0.	-.58E-02	-.92E-02	-.79E-02	-.59E-02	-.91E-02	-.24E-01	-.59E-01	-.10E+00	0.
0.	-.12E-01	-.29E-01	-.46E-01	-.64E-01	-.86E-01	-.11E+00	-.13E+00	-.12E+00	0.
0.	-.19E-01	-.45E-01	-.72E-01	-.99E-01	-.12E+00	-.14E+00	-.14E+00	-.94E-01	0.
0.	-.20E-01	-.48E-01	-.76E-01	-.10E+00	-.12E+00	-.12E+00	-.11E+00	-.61E-01	0.
0.	-.15E-01	-.38E-01	-.61E-01	-.80E-01	-.91E-01	-.88E-01	-.68E-01	-.31E-01	0.
0.	-.61E-02	-.18E-01	-.32E-01	-.45E-01	-.52E-01	-.48E-01	-.33E-01	-.10E-01	0.
0.	0.	0.	0.	0.	0.	0.	0.	0.	0.

TABLE OF VELOCITY V IN Y-DIRECTION

0.	0.	0.	0.	0.	0.	0.	0.	0.	0.
0.	-.85E-01	-.76E-01	-.65E-01	-.56E-01	-.46E-01	-.29E-01	.65E-02	.21E+00	0.
0.	-.95E-01	-.11E+00	-.10E+00	-.90E-01	-.69E-01	-.31E-01	.40E-01	.27E+00	0.
0.	-.96E-01	-.12E+00	-.11E+00	-.10E+00	-.73E-01	-.10E-01	.96E-01	.27E+00	0.
0.	-.86E-01	-.11E+00	-.11E+00	-.89E-01	-.50E-01	.18E-01	.12E+00	.21E+00	0.
0.	-.66E-01	-.82E-01	-.80E-01	-.63E-01	-.26E-01	.32E-01	.10E+00	.14E+00	0.
0.	-.41E-01	-.53E-01	-.51E-01	-.37E-01	-.10E-01	.29E-01	.70E-01	.76E-01	0.
0.	-.18E-01	-.26E-01	-.27E-01	-.19E-01	-.33E-02	.19E-01	.38E-01	.33E-01	0.
0.	-.34E-02	-.74E-02	-.90E-02	-.74E-02	-.17E-02	.69E-02	.13E-01	.83E-02	0.
0.	0.	0.	0.	0.	0.	0.	0.	0.	0.

TABLE 2 (cont.)--Flow Model Results

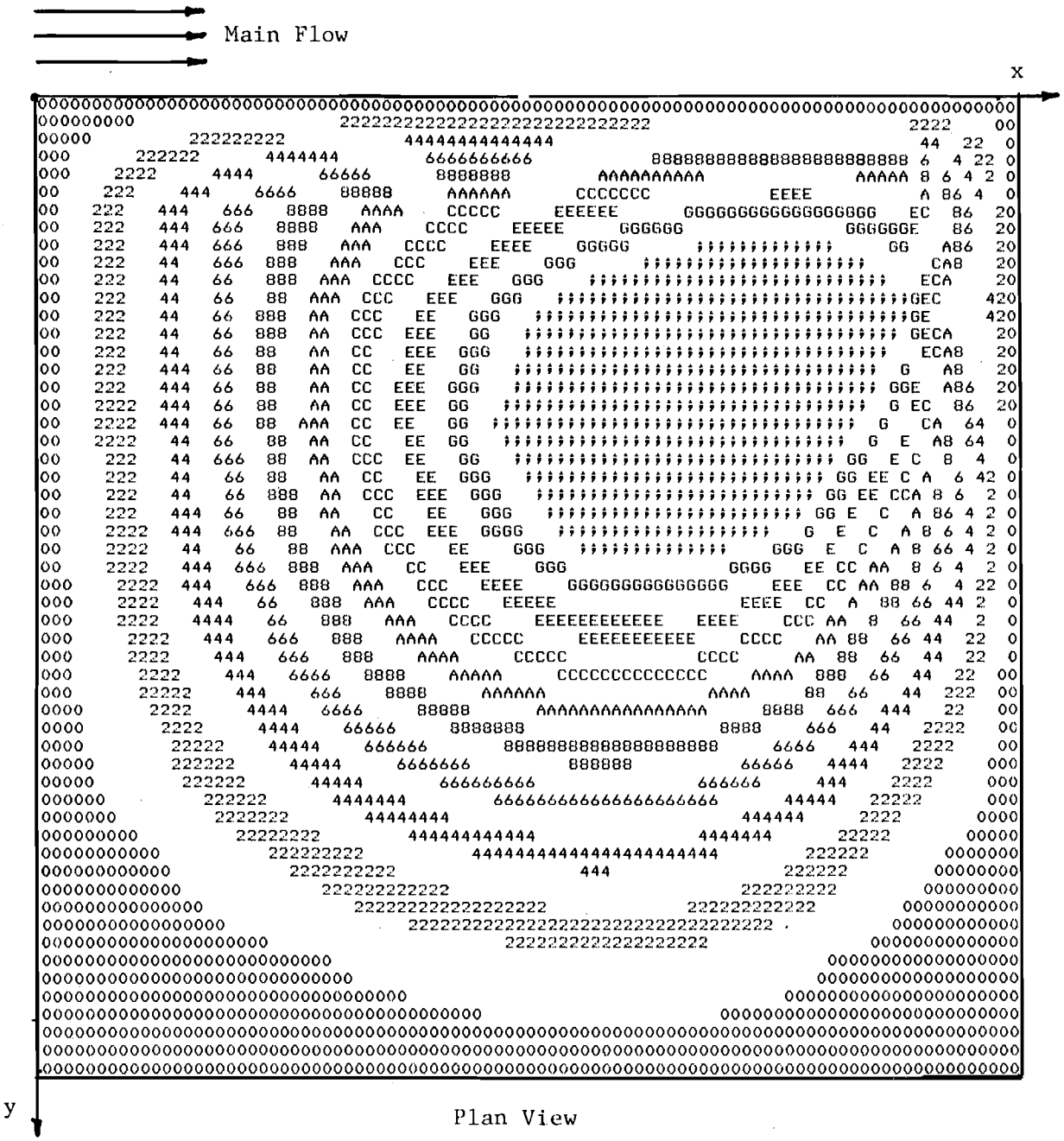

Plan View

Reynolds No. = 1,000

Fig. 9. Contour Plot of Streamlines

PROBLEM PARAMETERS

NUMBER OF SUBDIVITIONS IN EACH DIRECTION = 9
TIME INTERVALS = .0333
SPACE INTERVALS IN EACH DIRECTION = .1000
NUMBER OF ITERATIONS = 1056
ITERATION CRITERIA = .00005000
DIFFERENCE OF Z(T) AND Z(T-1) = .498E-04
REYNOLDS NUMBER RE = 2000.00

TABLE OF THE STREAMFUNCTION

0.	0.	0.	0.	0.	0.	0.	0.	0.	0.
0.	-.65E-02	-.13E-01	-.18E-01	-.23E-01	-.27E-01	-.31E-01	-.33E-01	-.34E-01	0.
0.	-.64E-02	-.15E-01	-.24E-01	-.32E-01	-.38E-01	-.43E-01	-.44E-01	-.41E-01	0.
0.	-.66E-02	-.16E-01	-.26E-01	-.35E-01	-.43E-01	-.48E-01	-.47E-01	-.35E-01	0.
0.	-.62E-02	-.15E-01	-.24E-01	-.33E-01	-.40E-01	-.43E-01	-.39E-01	-.24E-01	0.
0.	-.49E-02	-.12E-01	-.19E-01	-.26E-01	-.31E-01	-.32E-01	-.27E-01	-.14E-01	0.
0.	-.30E-02	-.76E-02	-.13E-01	-.17E-01	-.20E-01	-.20E-01	-.15E-01	-.69E-02	0.
0.	-.12E-02	-.34E-02	-.61E-02	-.87E-02	-.10E-01	-.97E-02	-.69E-02	-.24E-02	0.
0.	-.47E-04	-.61E-03	-.15E-02	-.25E-02	-.32E-02	-.31E-02	-.19E-02	-.31E-03	0.
0.	0.	0.	0.	0.	0.	0.	0.	0.	0.

TABLE OF THE VORTICITY

0.	.19E+02	.17E+02	.16E+02	.15E+02	.15E+02	.14E+02	.13E+02	.13E+02	.20E+02
-.13E+01	.54E+00	.91E+00	.11E+01	.13E+01	.14E+01	.16E+01	.19E+01	.50E+01	-.67E+01
-.13E+01	-.19E+00	.12E+00	.30E+00	.49E+00	.68E+00	.87E+00	.11E+01	.40E+01	-.81E+01
-.13E+01	-.18E+00	.11E+00	.31E+00	.55E+00	.83E+00	.13E+01	.17E+01	.22E+01	-.69E+01
-.12E+01	-.13E+00	.11E+00	.31E+00	.57E+00	.88E+00	.11E+01	.11E+01	.74E+00	-.48E+01
-.98E+00	-.11E+00	.55E-01	.20E+00	.36E+00	.51E+00	.58E+00	.51E+00	-.50E-01	-.29E+01
-.60E+00	-.13E+00	-.50E-01	.18E-01	.92E-01	.15E+00	.17E+00	.68E-01	-.35E+00	-.14E+01
-.23E+00	-.15E+00	-.15E+00	-.14E+00	-.11E+00	-.83E-01	-.79E-01	-.15E+00	-.37E+00	-.48E+00
-.94E-02	-.13E+00	-.21E+00	-.26E+00	-.27E+00	-.24E+00	-.21E+00	-.21E+00	-.25E+00	-.62E-01
0.	-.94E-02	-.12E+00	-.30E+00	-.50E+00	-.64E+00	-.61E+00	-.38E+00	-.62E-01	0.

TABLE 3--Flow Model Results

Reynolds No. = 2,000

TABLE OF VELOCITY U IN X-DIRECTION

.10E+01	.10E+01	.10E+01	.10E+01	.10E+01	.10E+01	.10E+01	.10E+01	.10E+01	.10E+01
0.	.32E-01	.75E-01	.12E+00	.16E+00	.19E+00	.21E+00	.22E+00	.20E+00	0.
0.	.50E-03	.15E-01	.37E-01	.59E-01	.78E-01	.85E-01	.67E-01	.41E-02	0.
0.	-.12E-02	-.57E-03	.37E-02	.88E-02	.10E-01	.91E-03	-.28E-01	-.82E-01	0.
0.	-.83E-02	-.20E-01	-.31E-01	-.43E-01	-.58E-01	-.79E-01	-.99E-01	-.10E+00	0.
0.	-.16E-01	-.37E-01	-.58E-01	-.80E-01	-.10E+00	-.12E+00	-.12E+00	-.86E-01	0.
0.	-.19E-01	-.42E-01	-.66E-01	-.89E-01	-.11E+00	-.11E+00	-.99E-01	-.59E-01	0.
0.	-.15E-01	-.35E-01	-.56E-01	-.74E-01	-.85E-01	-.84E-01	-.67E-01	-.33E-01	0.
0.	-.58E-02	-.17E-01	-.31E-01	-.43E-01	-.51E-01	-.49E-01	-.34E-01	-.12E-01	0.
0.	0.	0.	0.	0.	0.	0.	0.	0.	0.

TABLE OF VELOCITY V IN Y-DIRECTION

0.	0.	0.	0.	0.	0.	0.	0.	0.	0.
0.	-.64E-01	-.59E-01	-.52E-01	-.46E-01	-.38E-01	-.28E-01	-.15E-01	.17E+00	0.
0.	-.75E-01	-.86E-01	-.83E-01	-.74E-01	-.57E-01	-.30E-01	.12E-01	.22E+00	0.
0.	-.79E-01	-.95E-01	-.96E-01	-.87E-01	-.64E-01	-.18E-01	.66E-01	.23E+00	0.
0.	-.74E-01	-.90E-01	-.92E-01	-.81E-01	-.49E-01	.87E-02	.95E-01	.19E+00	0.
0.	-.59E-01	-.73E-01	-.73E-01	-.59E-01	-.28E-01	.23E-01	.89E-01	.13E+00	0.
0.	-.38E-01	-.48E-01	-.48E-01	-.37E-01	-.13E-01	.24E-01	.65E-01	.76E-01	0.
0.	-.17E-01	-.25E-01	-.26E-01	-.20E-01	-.52E-02	.17E-01	.37E-01	.34E-01	0.
0.	-.30E-02	-.74E-02	-.96E-02	-.83E-02	-.27E-02	.64E-02	.14E-01	.95E-02	0.
0.	0.	0.	0.	0.	0.	0.	0.	0.	0.

TABLE 3 (cont.)--Flow Model Results

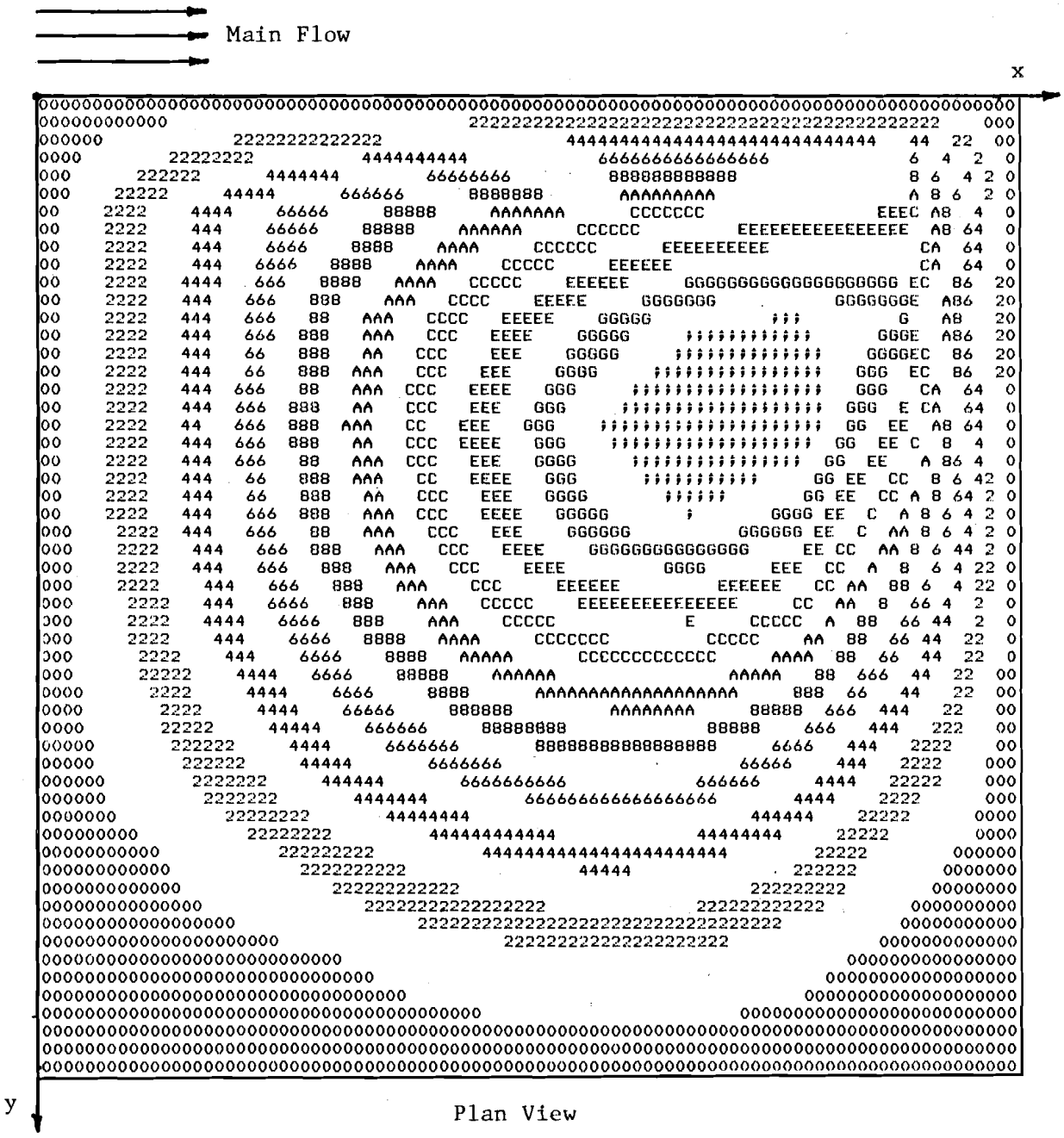

Plan View

Reynolds No. = 2,000

Fig. 10. Contour Plot of Streamlines

PROBLEM PARAMETERS

NUMBER OF SUBDIVITIONS IN EACH DIRECTION = 9
TIME INTERVALS = .0333
SPACE INTERVALS IN EACH DIRECTION = .1000
NUMBER OF ITERATIONS = 1296
ITERATION CRITERIA = .00005000
DIFFERENCE OF Z(T) AND Z(T-1) = .499E-04
REYNOLDS NUMBER RE = 5000.00

TABLE OF THE STREAMFUNCTION

0.	0.	0.	0.	0.	0.	0.	0.	0.	0.
0.	-.42E-02	-.86E-02	-.13E-01	-.17E-01	-.20E-01	-.23E-01	-.25E-01	-.29E-01	0.
0.	-.46E-02	-.11E-01	-.18E-01	-.24E-01	-.30E-01	-.34E-01	-.36E-01	-.35E-01	0.
0.	-.52E-02	-.13E-01	-.21E-01	-.28E-01	-.35E-01	-.39E-01	-.40E-01	-.31E-01	0.
0.	-.53E-02	-.12E-01	-.20E-01	-.28E-01	-.35E-01	-.38E-01	-.35E-01	-.23E-01	0.
0.	-.44E-02	-.10E-01	-.17E-01	-.24E-01	-.28E-01	-.29E-01	-.25E-01	-.14E-01	0.
0.	-.28E-02	-.69E-02	-.12E-01	-.16E-01	-.19E-01	-.19E-01	-.15E-01	-.71E-02	0.
0.	-.11E-02	-.32E-02	-.58E-02	-.84E-02	-.10E-01	-.97E-02	-.71E-02	-.27E-02	0.
0.	.17E-05	-.56E-03	-.15E-02	-.26E-02	-.34E-02	-.33E-02	-.22E-02	-.47E-03	0.
0.	0.	0.	0.	0.	0.	0.	0.	0.	0.

TABLE OF THE VORTICITY

0.	.19E+02	.18E+02	.17E+02	.17E+02	.16E+02	.15E+02	.15E+02	.14E+02	.20E+02
-.84E+00	.29E+00	.52E+00	.65E+00	.75E+00	.87E+00	.98E+00	.11E+01	.45E+01	-.58E+01
-.92E+00	-.16E+00	.50E-01	.20E+00	.35E+00	.50E+00	.60E+00	.70E+00	.36E+01	-.70E+01
-.10E+01	-.12E+00	.75E-01	.24E+00	.45E+00	.69E+00	.84E+00	.15E+01	.21E+01	-.62E+01
-.11E+01	-.78E-01	.90E-01	.26E+00	.50E+00	.80E+00	.11E+01	.11E+01	.86E+00	-.45E+01
-.88E+00	-.70E-01	.58E-01	.20E+00	.36E+00	.52E+00	.61E+00	.57E+00	.90E-01	-.28E+01
-.56E+00	-.97E-01	-.32E-01	.42E-01	.12E+00	.19E+00	.22E+00	.14E+00	-.25E+00	-.14E+01
-.22E+00	-.13E+00	-.13E+00	-.11E+00	-.72E-01	-.40E-01	-.31E-01	-.91E-01	-.31E+00	-.54E+00
.31E-03	-.13E+00	-.20E+00	-.23E+00	-.23E+00	-.19E+00	-.16E+00	-.18E+00	-.24E+00	-.94E-01
0.	.31E-03	-.11E+00	-.31E+00	-.52E+00	-.68E+00	-.66E+00	-.44E+00	-.94E-01	0.

TABLE 4--Flow Model Results

Reynolds No. = 5,000

TABLE OF VELOCITY U IN X-DIRECTION

.10E+01	.10E+01	.10E+01	.10E+01	.10E+01	.10E+01	.10E+01	.10E+01	.10E+01	.10E+01
0.	.23E-01	.55E-01	.89E-01	.12E+00	.15E+00	.17E+00	.18E+00	.17E+00	0.
0.	.51E-02	.20E-01	.39E-01	.60E-01	.76E-01	.82E-01	.72E-01	.89E-02	0.
0.	.32E-02	.70E-02	.13E-01	.21E-01	.26E-01	.21E-01	-.41E-02	-.62E-01	0.
0.	-.42E-02	-.11E-01	-.17E-01	-.25E-01	-.35E-01	-.49E-01	-.73E-01	-.84E-01	0.
0.	-.12E-01	-.28E-01	-.44E-01	-.62E-01	-.80E-01	-.95E-01	-.99E-01	-.77E-01	0.
0.	-.17E-01	-.36E-01	-.56E-01	-.76E-01	-.92E-01	-.98E-01	-.89E-01	-.56E-01	0.
0.	-.14E-01	-.32E-01	-.50E-01	-.67E-01	-.78E-01	-.78E-01	-.64E-01	-.33E-01	0.
0.	-.54E-02	-.16E-01	-.29E-01	-.42E-01	-.50E-01	-.49E-01	-.36E-01	-.14E-01	0.
0.	0.	0.	0.	0.	0.	0.	0.	0.	0.

TABLE OF VELOCITY V IN Y-DIRECTION

0.	0.	0.	0.	0.	0.	0.	0.	0.	0.
0.	-.43E-01	-.43E-01	-.40E-01	-.36E-01	-.31E-01	-.27E-01	-.32E-01	.13E+00	0.
0.	-.55E-01	-.65E-01	-.66E-01	-.60E-01	-.47E-01	-.29E-01	-.63E-02	.18E+00	0.
0.	-.63E-01	-.77E-01	-.80E-01	-.74E-01	-.54E-01	-.22E-01	.42E-01	.20E+00	0.
0.	-.62E-01	-.76E-01	-.80E-01	-.73E-01	-.48E-01	.11E-02	.77E-01	.17E+00	0.
0.	-.52E-01	-.63E-01	-.66E-01	-.56E-01	-.29E-01	.16E-01	.77E-01	.13E+00	0.
0.	-.34E-01	-.44E-01	-.46E-01	-.37E-01	-.15E-01	.19E-01	.59E-01	.75E-01	0.
0.	-.16E-01	-.24E-01	-.26E-01	-.21E-01	-.68E-02	.14E-01	.35E-01	.36E-01	0.
0.	-.28E-02	-.77E-02	-.10E-01	-.92E-02	-.35E-02	.60E-02	.14E-01	.11E-01	0.
0.	0.	0.	0.	0.	0.	0.	0.	0.	0.

TABLE 4 (cont.)--Flow Model Results

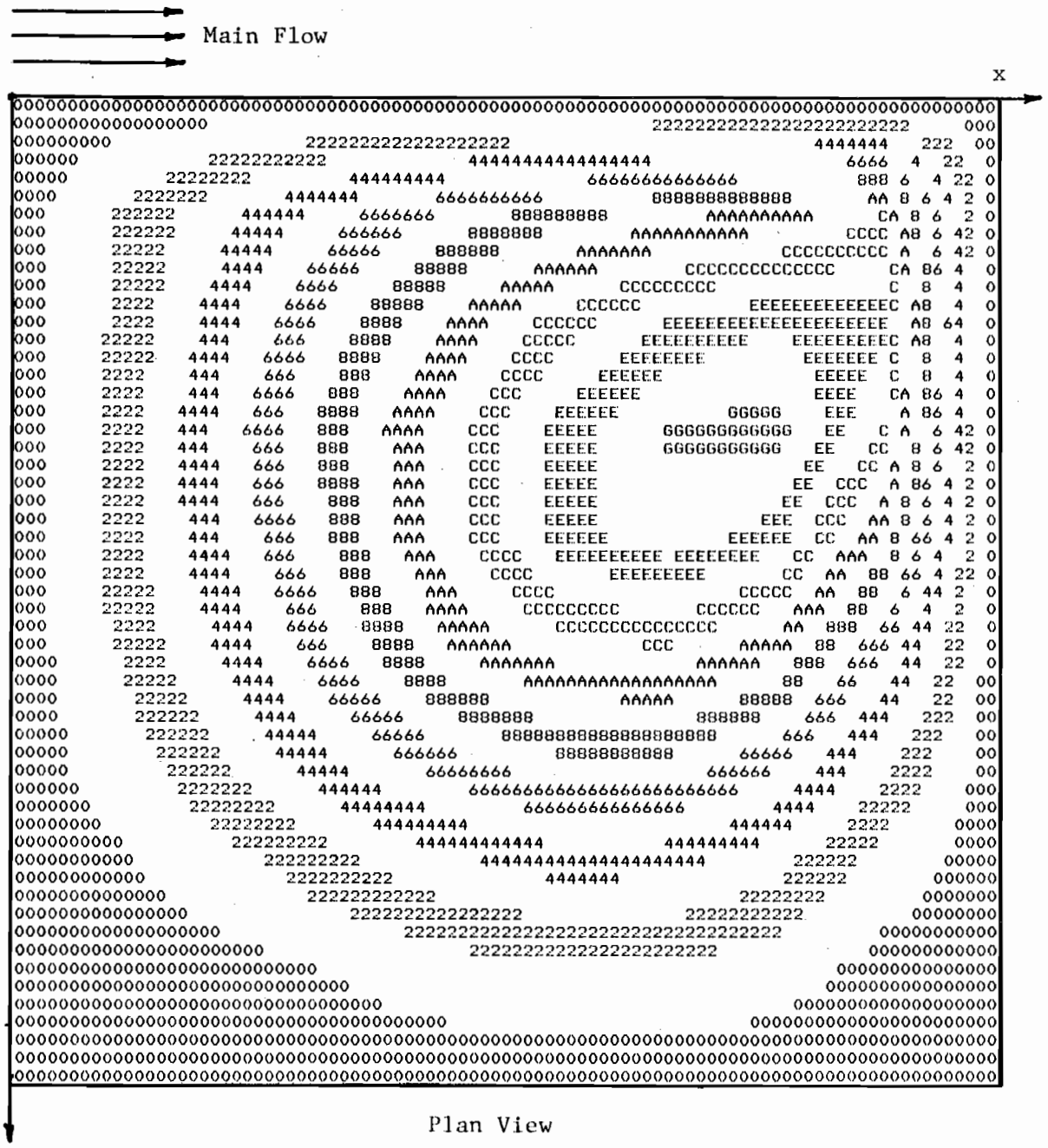

Plan View

Reynolds No. = 5,000

Fig. 11. Contour Plot of Streamlines

PROBLEM PARAMETERS

NUMBER OF SUBDIVITIONS IN EACH DIRECTION = 9
TIME INTERVALS = .0333
SPACE INTERVALS IN EACH DIRECTION = .1000
NUMBER OF ITERATIONS = 1513
ITERATION CRITERIA = .00005000
DIFFERENCE OF Z(T) AND Z(T-1) = .499E-04
REYNOLDS NUMBER RE = 10000.00

TABLE OF THE STREAMFUNCTION

0.	0.	0.	0.	0.	0.	0.	0.	0.	0.
0.	-.30E-02	-.64E-02	-.98E-02	-.13E-01	-.16E-01	-.19E-01	-.21E-01	-.27E-01	0.
0.	-.36E-02	-.88E-02	-.15E-01	-.20E-01	-.26E-01	-.29E-01	-.31E-01	-.32E-01	0.
0.	-.44E-02	-.11E-01	-.18E-01	-.25E-01	-.31E-01	-.35E-01	-.36E-01	-.29E-01	0.
0.	-.46E-02	-.11E-01	-.18E-01	-.25E-01	-.32E-01	-.35E-01	-.32E-01	-.21E-01	0.
0.	-.39E-02	-.92E-02	-.15E-01	-.21E-01	-.26E-01	-.27E-01	-.24E-01	-.13E-01	0.
0.	-.25E-02	-.62E-02	-.11E-01	-.15E-01	-.18E-01	-.18E-01	-.14E-01	-.70E-02	0.
0.	-.98E-03	-.29E-02	-.54E-02	-.79E-02	-.95E-02	-.94E-02	-.70E-02	-.28E-02	0.
0.	.31E-04	-.52E-03	-.15E-02	-.25E-02	-.33E-02	-.33E-02	-.22E-02	-.53E-03	0.
0.	0.	0.	0.	0.	0.	0.	0.	0.	0.

TABLE OF THE VORTICITY

0.	.19E+02	.19E+02	.18E+02	.17E+02	.17E+02	.16E+02	.16E+02	.15E+02	.20E+02
-.60E+00	.16E+00	.32E+00	.41E+00	.49E+00	.58E+00	.66E+00	.75E+00	.43E+01	-.53E+01
-.72E+00	-.15E+00	.20E-01	.14E+00	.28E+00	.42E+00	.51E+00	.56E+00	.33E+01	-.64E+01
-.87E+00	-.10E+00	.53E-01	.20E+00	.38E+00	.61E+00	.76E+00	.13E+01	.20E+01	-.57E+01
-.92E+00	-.57E-01	.72E-01	.22E+00	.44E+00	.74E+00	.10E+01	.11E+01	.88E+00	-.42E+01
-.79E+00	-.54E-01	.51E-01	.18E+00	.34E+00	.50E+00	.59E+00	.57E+00	.14E+00	-.27E+01
-.51E+00	-.82E-01	-.27E-01	.45E-01	.13E+00	.20E+00	.22E+00	.16E+00	-.20E+00	-.14E+01
-.20E+00	-.12E+00	-.12E+00	-.95E-01	-.57E-01	-.25E-01	-.14E-01	-.66E-01	-.28E+00	-.55E+00
.63E-02	-.13E+00	-.19E+00	-.21E+00	-.20E+00	-.17E+00	-.14E+00	-.16E+00	-.23E+00	-.11E+00
0.	.63E-02	-.10E+00	-.29E+00	-.51E+00	-.66E+00	-.66E+00	-.44E+00	-.11E+00	0.

TABLE 5--Flow Model Results

Reynolds No. = 10,000

TABLE OF VELOCITY U IN X-DIRECTION

.10E+01	.10E+01	.10E+01	.10E+01	.10E+01	.10E+01	.10E+01	.10E+01	.10E+01	.10E+01
0.	.18E-01	.44E-01	.73E-01	.10E+00	.13E+00	.15E+00	.16E+00	.16E+00	0.
0.	.69E-02	.21E-01	.39E-01	.58E-01	.75E-01	.82E-01	.72E-01	.10E-01	0.
0.	.50E-02	.99E-02	.17E-01	.25E-01	.30E-01	.28E-01	.41E-02	-.53E-01	0.
0.	-.22E-02	-.66E-02	-.11E-01	-.17E-01	-.25E-01	-.38E-01	-.61E-01	-.76E-01	0.
0.	-.10E-01	-.23E-01	-.37E-01	-.53E-01	-.70E-01	-.84E-01	-.89E-01	-.71E-01	0.
0.	-.15E-01	-.32E-01	-.50E-01	-.68E-01	-.83E-01	-.90E-01	-.83E-01	-.53E-01	0.
0.	-.13E-01	-.29E-01	-.46E-01	-.61E-01	-.72E-01	-.73E-01	-.61E-01	-.32E-01	0.
0.	-.49E-02	-.15E-01	-.27E-01	-.39E-01	-.47E-01	-.47E-01	-.35E-01	-.14E-01	0.
0.	0.	0.	0.	0.	0.	0.	0.	0.	0.

TABLE OF VELOCITY V IN Y-DIRECTION

0.	0.	0.	0.	0.	0.	0.	0.	0.	0.
0.	-.32E-01	-.34E-01	-.34E-01	-.32E-01	-.28E-01	-.27E-01	-.39E-01	.11E+00	0.
0.	-.44E-01	-.55E-01	-.58E-01	-.55E-01	-.44E-01	-.29E-01	-.13E-01	.16E+00	0.
0.	-.53E-01	-.66E-01	-.71E-01	-.68E-01	-.52E-01	-.24E-01	.33E-01	.18E+00	0.
0.	-.54E-01	-.67E-01	-.72E-01	-.68E-01	-.47E-01	-.28E-02	.68E-01	.16E+00	0.
0.	-.46E-01	-.57E-01	-.61E-01	-.53E-01	-.30E-01	.12E-01	.70E-01	.12E+00	0.
0.	-.31E-01	-.40E-01	-.43E-01	-.35E-01	-.16E-01	.16E-01	.54E-01	.72E-01	0.
0.	-.15E-01	-.22E-01	-.25E-01	-.20E-01	-.74E-02	.12E-01	.33E-01	.35E-01	0.
0.	-.26E-02	-.75E-02	-.10E-01	-.92E-02	-.38E-02	.55E-02	.14E-01	.11E-01	0.
0.	0.	0.	0.	0.	0.	0.	0.	0.	0.

TABLE 5 (cont.)--Flow Model Results

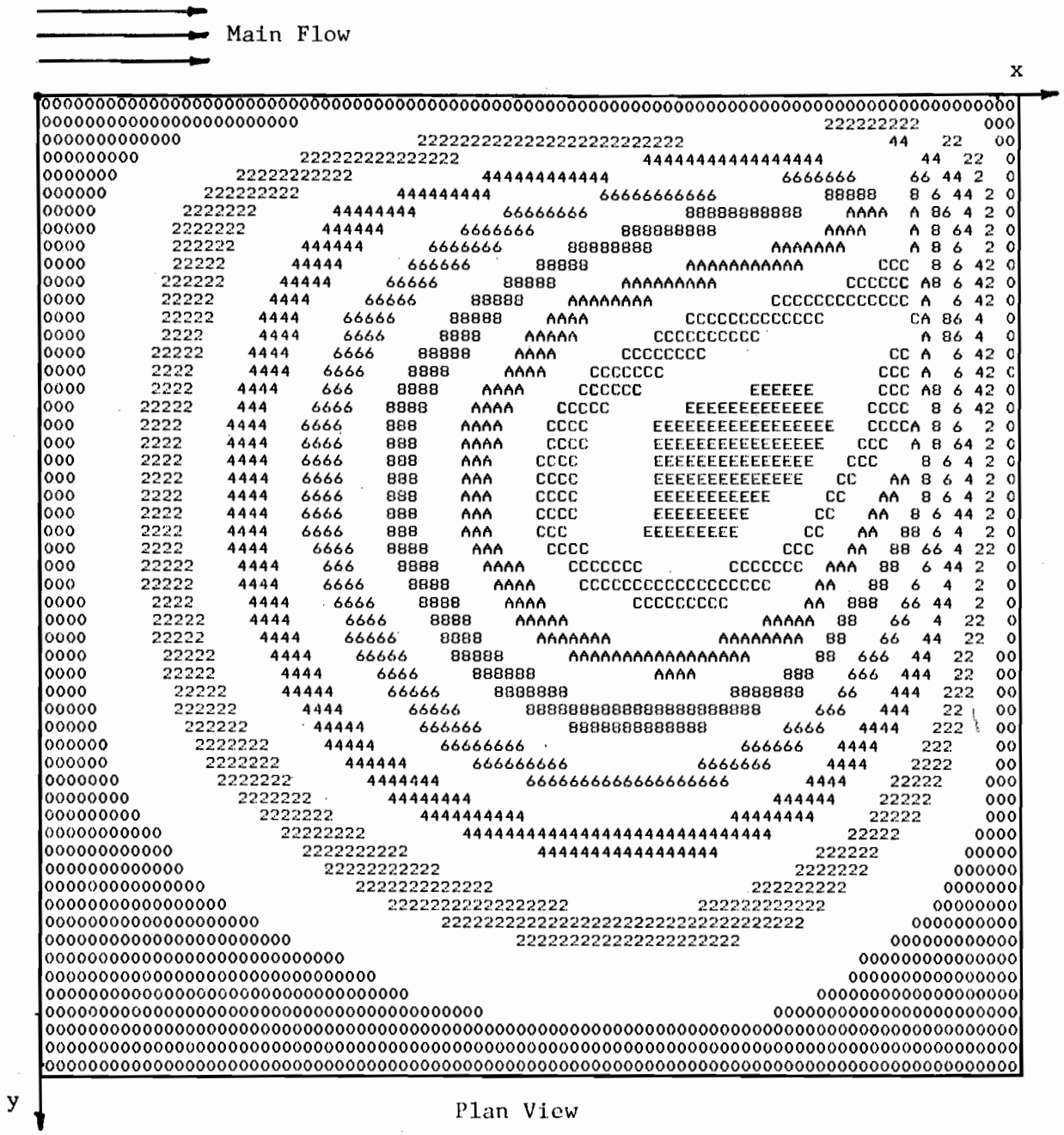

Plan View

Reynolds No. = 10,000

Fig. 12. Contour Plot of Streamlines

PROBLEM PARAMETERS

NUMBER OF SUBDIVITIONS IN EACH DIRECTION = 9
TIME INTERVALS = .0333
SPACE INTERVALS IN EACH DIRECTION = .1000
NUMBER OF ITERATIONS = 1640
ITERATION CRITERIA = .00005000
DIFFERENCE OF Z(T) AND Z(T-1) = .499E-04
REYNOLDS NUMBER RE = 15000.00

TABLE OF THE STREAMFUNCTION

0.	0.	0.	0.	0.	0.	0.	0.	0.	0.
0.	-.24E-02	-.54E-02	-.85E-02	-.12E-01	-.14E-01	-.17E-01	-.20E-01	-.25E-01	0.
0.	-.31E-02	-.79E-02	-.13E-01	-.19E-01	-.24E-01	-.27E-01	-.30E-01	-.30E-01	0.
0.	-.40E-02	-.96E-02	-.16E-01	-.23E-01	-.29E-01	-.33E-01	-.34E-01	-.27E-01	0.
0.	-.43E-02	-.10E-01	-.17E-01	-.24E-01	-.30E-01	-.33E-01	-.31E-01	-.21E-01	0.
0.	-.37E-02	-.87E-02	-.14E-01	-.20E-01	-.25E-01	-.26E-01	-.23E-01	-.13E-01	0.
0.	-.24E-02	-.59E-02	-.10E-01	-.14E-01	-.17E-01	-.17E-01	-.14E-01	-.69E-02	0.
0.	-.92E-03	-.28E-02	-.52E-02	-.76E-02	-.91E-02	-.91E-02	-.68E-02	-.27E-02	0.
0.	.44E-04	-.49E-03	-.14E-02	-.25E-02	-.32E-02	-.32E-02	-.22E-02	-.55E-03	0.
0.	0.	0.	0.	0.	0.	0.	0.	0.	0.

TABLE OF THE VORTICITY

0.	.20E+02	.19E+02	.18E+02	.18E+02	.17E+02	.17E+02	.16E+02	.15E+02	.20E+02
-.49E+00	.10E+00	.23E+00	.31E+00	.38E+00	.46E+00	.53E+00	.60E+00	.42E+01	-.51E+01
-.63E+00	-.14E+00	.76E-02	.12E+00	.25E+00	.39E+00	.48E+00	.51E+00	.32E+01	-.61E+01
-.79E+00	-.97E-01	.43E-01	.18E+00	.35E+00	.57E+00	.73E+00	.13E+01	.20E+01	-.55E+01
-.85E+00	-.50E-01	.62E-01	.21E+00	.41E+00	.71E+00	.10E+01	.10E+01	.87E+00	-.41E+01
-.74E+00	-.48E-01	.46E-01	.17E+00	.33E+00	.48E+00	.58E+00	.56E+00	.16E+00	-.26E+01
-.48E+00	-.76E-01	-.25E-01	.44E-01	.12E+00	.19E+00	.22E+00	.17E+00	-.18E+00	-.14E+01
-.18E+00	-.12E+00	-.11E+00	-.89E-01	-.52E-01	-.21E-01	-.97E-02	-.57E-01	-.27E+00	-.55E+00
.89E-02	-.13E+00	-.18E+00	-.20E+00	-.19E+00	-.15E+00	-.13E+00	-.15E+00	-.22E+00	-.11E+00
0.	.89E-02	-.97E-01	-.28E+00	-.49E+00	-.65E+00	-.65E+00	-.44E+00	-.11E+00	0.

TABLE 6--Flow Model Results

Reynolds No. = 15,000

TABLE OF VELOCITY U IN X-DIRECTION

.10E+01	.10E+01	.10E+01	.10E+01	.10E+01	.10E+01	.10E+01	.10E+01	.10E+01	.10E+01
0.	.16E-01	.39E-01	.66E-01	.93E-01	.12E+00	.14E+00	.15E+00	.15E+00	0.
0.	.76E-02	.21E-01	.39E-01	.57E-01	.74E-01	.81E-01	.72E-01	.10E-01	0.
0.	.56E-02	.11E-01	.18E-01	.26E-01	.32E-01	.30E-01	.69E-02	-.50E-01	0.
0.	-.14E-02	-.50E-02	-.87E-02	-.14E-01	-.22E-01	-.35E-01	-.57E-01	-.72E-01	0.
0.	-.94E-02	-.21E-01	-.34E-01	-.49E-01	-.65E-01	-.80E-01	-.85E-01	-.68E-01	0.
0.	-.14E-01	-.29E-01	-.47E-01	-.64E-01	-.79E-01	-.86E-01	-.80E-01	-.52E-01	0.
0.	-.12E-01	-.27E-01	-.43E-01	-.58E-01	-.69E-01	-.70E-01	-.59E-01	-.32E-01	0.
0.	-.46E-02	-.14E-01	-.26E-01	-.38E-01	-.46E-01	-.45E-01	-.34E-01	-.14E-01	0.
0.	0.	0.	0.	0.	0.	0.	0.	0.	0.

TABLE OF VELOCITY V IN Y-DIRECTION

0.	0.	0.	0.	0.	0.	0.	0.	0.	0.
0.	-.27E-01	-.30E-01	-.31E-01	-.30E-01	-.27E-01	-.27E-01	-.42E-01	.99E-01	0.
0.	-.39E-01	-.50E-01	-.54E-01	-.52E-01	-.44E-01	-.30E-01	-.16E-01	.15E+00	0.
0.	-.48E-01	-.61E-01	-.67E-01	-.65E-01	-.51E-01	-.25E-01	.29E-01	.17E+00	0.
0.	-.50E-01	-.62E-01	-.69E-01	-.66E-01	-.47E-01	-.46E-02	.64E-01	.15E+00	0.
0.	-.43E-01	-.54E-01	-.58E-01	-.52E-01	-.30E-01	.10E-01	.66E-01	.11E+00	0.
0.	-.29E-01	-.38E-01	-.41E-01	-.34E-01	-.16E-01	.15E-01	.52E-01	.70E-01	0.
0.	-.14E-01	-.21E-01	-.24E-01	-.20E-01	-.77E-02	.12E-01	.32E-01	.34E-01	0.
0.	-.24E-02	-.73E-02	-.99E-02	-.91E-02	-.38E-02	.52E-02	.13E-01	.11E-01	0.
0.	0.	0.	0.	0.	0.	0.	0.	0.	0.

TABLE 6 (cont.)--Flow Model Results

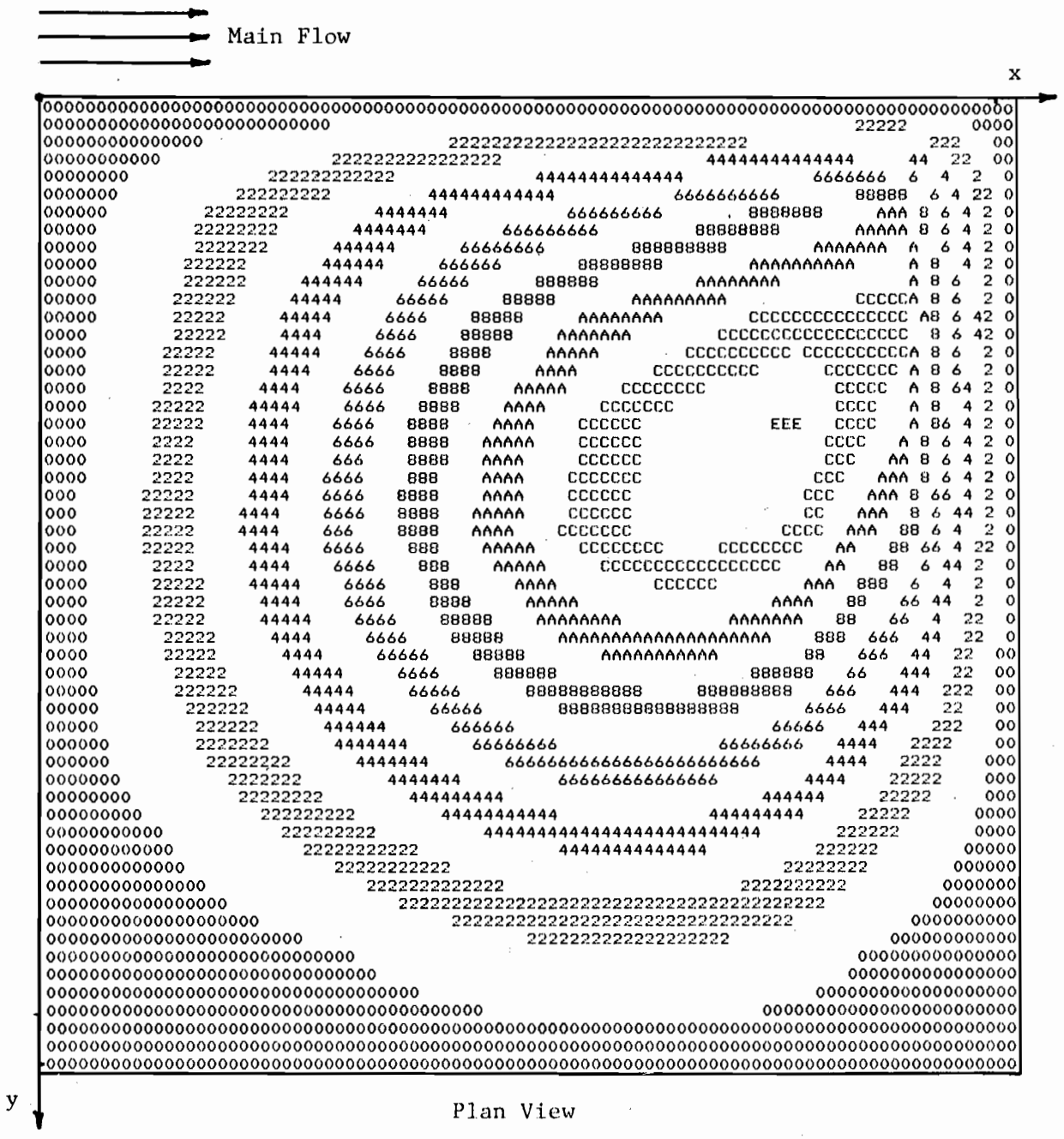

Plan View

Reynolds No. = 15,000

Fig. 13. Contour Plot of Streamlines

PROBLEM PARAMETERS

NUMBER OF SUBDIVITIONS IN EACH DIRECTION = 9
TIME INTERVALS = .0333
SPACE INTERVALS IN EACH DIRECTION = .1000
NUMBER OF ITERATIONS = 1727
ITERATION CRITERIA = .00005000
DIFFERENCE OF Z(T) AND Z(T-1) = .500E-04
REYNOLDS NUMBER RE = 20000.00

TABLE OF THE STREAMFUNCTION

0.	0.	0.	0.	0.	0.	0.	0.	0.	0.
0.	-.21E-02	-.48E-02	-.77E-02	-.11E-01	-.14E-01	-.16E-01	-.19E-01	-.25E-01	0.
0.	-.29E-02	-.73E-02	-.12E-01	-.18E-01	-.23E-01	-.26E-01	-.29E-01	-.30E-01	0.
0.	-.37E-02	-.91E-02	-.15E-01	-.22E-01	-.28E-01	-.32E-01	-.33E-01	-.27E-01	0.
0.	-.41E-02	-.95E-02	-.16E-01	-.23E-01	-.29E-01	-.32E-01	-.30E-01	-.20E-01	0.
0.	-.35E-02	-.83E-02	-.14E-01	-.20E-01	-.24E-01	-.26E-01	-.22E-01	-.13E-01	0.
0.	-.23E-02	-.57E-02	-.97E-02	-.14E-01	-.16E-01	-.17E-01	-.14E-01	-.68E-02	0.
0.	-.88E-03	-.27E-02	-.50E-02	-.73E-02	-.89E-02	-.89E-02	-.67E-02	-.27E-02	0.
0.	.52E-04	-.46E-03	-.14E-02	-.24E-02	-.32E-02	-.32E-02	-.22E-02	-.55E-03	0.
0.	0.	0.	0.	0.	0.	0.	0.	0.	0.

TABLE OF THE VORTICITY

0.	.20E+02	.19E+02	.18E+02	.18E+02	.17E+02	.17E+02	.16E+02	.15E+02	.20E+02
-.42E+00	.64E-01	.17E+00	.25E+00	.32E+00	.39E+00	.46E+00	.52E+00	.41E+01	-.50E+01
-.57E+00	-.13E+00	.89E-03	.11E+00	.23E+00	.37E+00	.46E+00	.48E+00	.31E+01	-.59E+01
-.74E+00	-.93E-01	.37E-01	.16E+00	.33E+00	.55E+00	.71E+00	.12E+01	.20E+01	-.54E+01
-.81E+00	-.46E-01	.57E-01	.19E+00	.39E+00	.69E+00	.10E+01	.10E+01	.87E+00	-.40E+01
-.70E+00	-.45E-01	.43E-01	.16E+00	.32E+00	.47E+00	.56E+00	.56E+00	.17E+00	-.26E+01
-.46E+00	-.72E-01	-.25E-01	.43E-01	.12E+00	.19E+00	.22E+00	.17E+00	-.17E+00	-.14E+01
-.18E+00	-.11E+00	-.11E+00	-.86E-01	-.50E-01	-.19E-01	-.80E-02	-.53E-01	-.26E+00	-.54E+00
.10E-01	-.13E+00	-.17E+00	-.19E+00	-.18E+00	-.15E+00	-.12E+00	-.14E+00	-.22E+00	-.11E+00
0.	.10E-01	-.93E-01	-.27E+00	-.48E+00	-.63E+00	-.63E+00	-.43E+00	-.11E+00	0.

TABLE 7--Flow Model Results

Reynolds No. = 20,000

TABLE OF VELOCITY U IN X-DIRECTION

.10E+01	.10E+01	.10E+01	.10E+01	.10E+01	.10E+01	.10E+01	.10E+01	.10E+01	.10E+01
0.	.14E-01	.36E-01	.62E-01	.88E-01	.11E+00	.13E+00	.14E+00	.15E+00	0.
0.	.80E-02	.21E-01	.38E-01	.57E-01	.73E-01	.81E-01	.72E-01	.10E-01	0.
0.	.59E-02	.11E-01	.18E-01	.26E-01	.32E-01	.31E-01	.82E-02	-.48E-01	0.
0.	-.10E-02	-.41E-02	-.74E-02	-.12E-01	-.20E-01	-.33E-01	-.55E-01	-.70E-01	0.
0.	-.88E-02	-.19E-01	-.32E-01	-.46E-01	-.63E-01	-.78E-01	-.82E-01	-.67E-01	0.
0.	-.13E-01	-.28E-01	-.45E-01	-.61E-01	-.76E-01	-.84E-01	-.78E-01	-.51E-01	0.
0.	-.12E-01	-.26E-01	-.42E-01	-.56E-01	-.67E-01	-.68E-01	-.58E-01	-.31E-01	0.
0.	-.44E-02	-.13E-01	-.25E-01	-.37E-01	-.45E-01	-.44E-01	-.34E-01	-.14E-01	0.
0.	0.	0.	0.	0.	0.	0.	0.	0.	0.

TABLE OF VELOCITY V IN Y-DIRECTION

0.	0.	0.	0.	0.	0.	0.	0.	0.	0.
0.	-.24E-01	-.28E-01	-.29E-01	-.29E-01	-.27E-01	-.27E-01	-.43E-01	.95E-01	0.
0.	-.36E-01	-.47E-01	-.52E-01	-.51E-01	-.43E-01	-.30E-01	-.17E-01	.14E+00	0.
0.	-.46E-01	-.58E-01	-.65E-01	-.64E-01	-.51E-01	-.26E-01	.27E-01	.17E+00	0.
0.	-.48E-01	-.60E-01	-.67E-01	-.65E-01	-.47E-01	-.58E-02	.61E-01	.15E+00	0.
0.	-.41E-01	-.52E-01	-.57E-01	-.51E-01	-.30E-01	.92E-02	.64E-01	.11E+00	0.
0.	-.28E-01	-.37E-01	-.40E-01	-.34E-01	-.16E-01	.14E-01	.50E-01	.68E-01	0.
0.	-.13E-01	-.21E-01	-.23E-01	-.20E-01	-.78E-02	.11E-01	.31E-01	.34E-01	0.
0.	-.23E-02	-.71E-02	-.97E-02	-.90E-02	-.39E-02	.49E-02	.13E-01	.11E-01	0.
0.	0.	0.	0.	0.	0.	0.	0.	0.	0.

TABLE 7 (cont.)--Flow Model Results

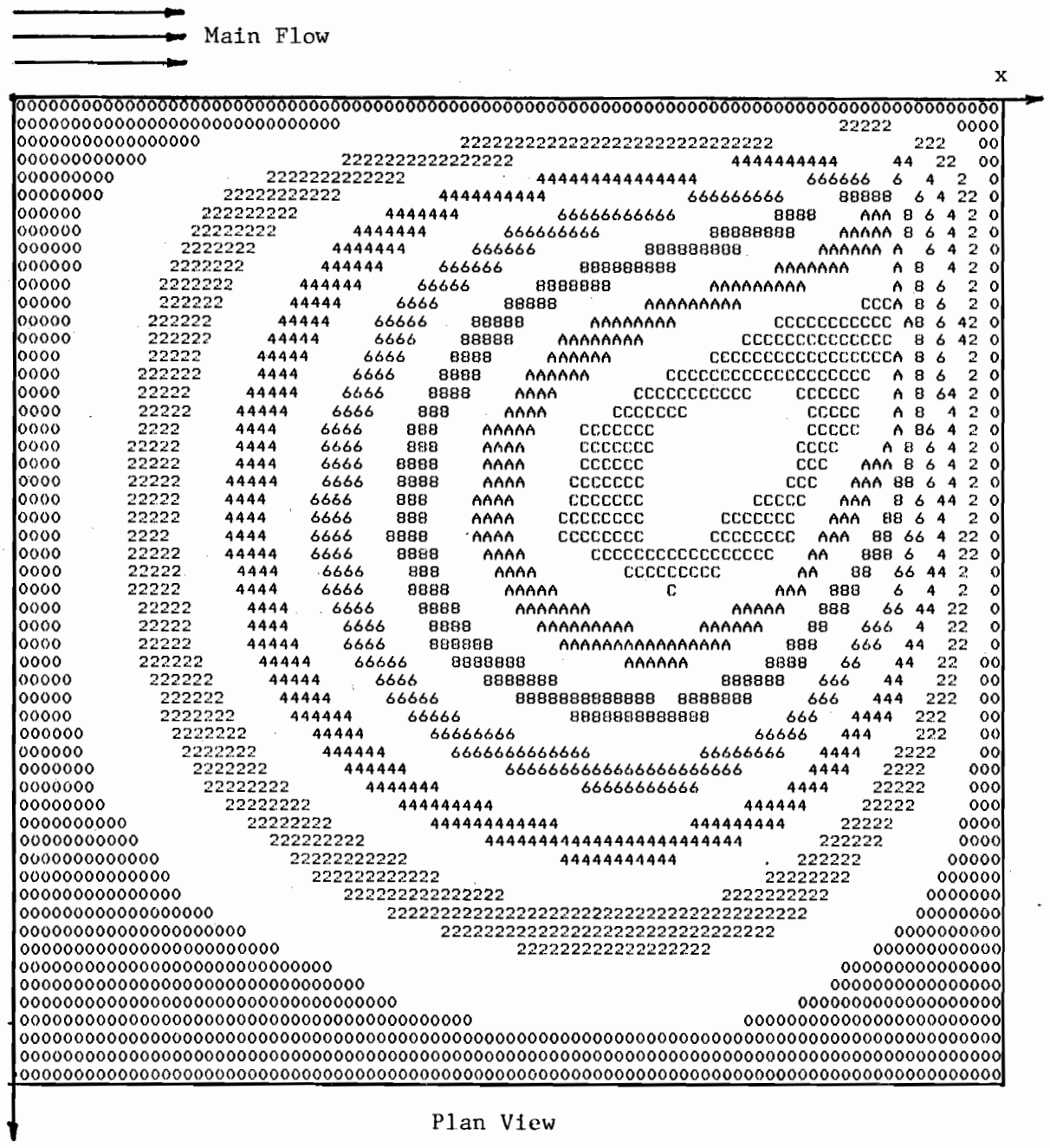

Plan View

Reynolds No. = 20,000

Fig. 14. Contour Plot of Streamlines

PROBLEM PARAMETERS

NUMBER OF SUBDIVITIONS IN EACH DIRECTION = 9
TIME INTERVALS = .0333
SPACE INTERVALS IN EACH DIRECTION = .1000
NUMBER OF ITERATIONS = 1840
ITERATION CRITERIA = .00005000
DIFFERENCE OF Z(T) AND Z(T-1) = .499E-04
REYNOLDS NUMBER RE = 30000.00

TABLE OF THE STREAMFUNCTION

0.	0.	0.	0.	0.	0.	0.	0.	0.	0.
0.	-.17E-02	-.42E-02	-.69E-02	-.97E-02	-.13E-01	-.15E-01	-.18E-01	-.24E-01	0.
0.	-.26E-02	-.66E-02	-.11E-01	-.17E-01	-.21E-01	-.25E-01	-.27E-01	-.29E-01	0.
0.	-.34E-02	-.85E-02	-.14E-01	-.21E-01	-.27E-01	-.31E-01	-.32E-01	-.26E-01	0.
0.	-.38E-02	-.90E-02	-.15E-01	-.22E-01	-.28E-01	-.31E-01	-.29E-01	-.20E-01	0.
0.	-.33E-02	-.79E-02	-.13E-01	-.19E-01	-.23E-01	-.25E-01	-.22E-01	-.13E-01	0.
0.	-.22E-02	-.54E-02	-.93E-02	-.13E-01	-.16E-01	-.16E-01	-.13E-01	-.67E-02	0.
0.	-.83E-03	-.25E-02	-.48E-02	-.71E-02	-.86E-02	-.86E-02	-.65E-02	-.27E-02	0.
0.	.59E-04	-.44E-03	-.13E-02	-.23E-02	-.31E-02	-.31E-02	-.21E-02	-.55E-03	0.
0.	0.	0.	0.	0.	0.	0.	0.	0.	0.

TABLE OF THE VORTICITY

0.	.20E+02	.19E+02	.19E+02	.18E+02	.17E+02	.17E+02	.16E+02	.15E+02	.20E+02
-.35E+00	.21E-01	.11E+00	.18E+00	.25E+00	.32E+00	.38E+00	.44E+00	.40E+01	-.48E+01
-.51E+00	-.13E+00	-.65E-02	.96E-01	.21E+00	.35E+00	.44E+00	.46E+00	.30E+01	-.58E+01
-.69E+00	-.88E-01	.30E-01	.15E+00	.31E+00	.53E+00	.69E+00	.12E+01	.19E+01	-.52E+01
-.76E+00	-.43E-01	.50E-01	.18E+00	.37E+00	.66E+00	.10E+01	.10E+01	.86E+00	-.39E+01
-.67E+00	-.42E-01	.39E-01	.16E+00	.30E+00	.45E+00	.55E+00	.55E+00	.17E+00	-.25E+01
-.43E+00	-.69E-01	-.25E-01	.41E-01	.12E+00	.18E+00	.21E+00	.17E+00	-.16E+00	-.13E+01
-.17E+00	-.11E+00	-.11E+00	-.83E-01	-.48E-01	-.18E-01	-.69E-02	-.48E-01	-.25E+00	-.54E+00
.12E-01	-.12E+00	-.16E+00	-.19E+00	-.17E+00	-.14E+00	-.12E+00	-.13E+00	-.21E+00	-.11E+00
0.	.12E-01	-.88E-01	-.26E+00	-.46E+00	-.61E+00	-.62E+00	-.43E+00	-.11E+00	0.

TABLE 8--Flow Model Results

Reynolds No. = 30,000

TABLE OF VELOCITY U IN X-DIRECTION

.10E+01	.10E+01	.10E+01	.10E+01	.10E+01	.10E+01	.10E+01	.10E+01	.10E+01	.10E+01
0.	.13E-01	.33E-01	.57E-01	.83E-01	.11E+00	.13E+00	.14E+00	.14E+00	0.
0.	.85E-02	.22E-01	.38E-01	.56E-01	.72E-01	.80E-01	.71E-01	.10E-01	0.
0.	.63E-02	.12E-01	.19E-01	.27E-01	.33E-01	.31E-01	.95E-02	-.46E-01	0.
0.	-.52E-03	-.31E-02	-.60E-02	-.11E-01	-.18E-01	-.31E-01	-.53E-01	-.68E-01	0.
0.	-.82E-02	-.18E-01	-.30E-01	-.44E-01	-.60E-01	-.75E-01	-.80E-01	-.65E-01	0.
0.	-.13E-01	-.27E-01	-.42E-01	-.59E-01	-.73E-01	-.81E-01	-.76E-01	-.49E-01	0.
0.	-.11E-01	-.25E-01	-.40E-01	-.54E-01	-.64E-01	-.66E-01	-.56E-01	-.31E-01	0.
0.	-.41E-02	-.13E-01	-.24E-01	-.35E-01	-.43E-01	-.43E-01	-.33E-01	-.13E-01	0.
0.	0.	0.	0.	0.	0.	0.	0.	0.	0.

TABLE OF VELOCITY V IN Y-DIRECTION

0.	0.	0.	0.	0.	0.	0.	0.	0.	0.
0.	-.21E-01	-.26E-01	-.28E-01	-.28E-01	-.27E-01	-.27E-01	-.45E-01	.90E-01	0.
0.	-.33E-01	-.44E-01	-.49E-01	-.50E-01	-.43E-01	-.30E-01	-.19E-01	.14E+00	0.
0.	-.42E-01	-.55E-01	-.62E-01	-.62E-01	-.51E-01	-.26E-01	.25E-01	.16E+00	0.
0.	-.45E-01	-.57E-01	-.64E-01	-.63E-01	-.47E-01	-.72E-02	.59E-01	.15E+00	0.
0.	-.39E-01	-.50E-01	-.55E-01	-.50E-01	-.30E-01	.78E-02	.62E-01	.11E+00	0.
0.	-.27E-01	-.35E-01	-.39E-01	-.33E-01	-.16E-01	.13E-01	.49E-01	.67E-01	0.
0.	-.13E-01	-.20E-01	-.23E-01	-.19E-01	-.78E-02	.10E-01	.30E-01	.33E-01	0.
0.	-.22E-02	-.69E-02	-.94E-02	-.88E-02	-.39E-02	.47E-02	.13E-01	.11E-01	0.
0.	0.	0.	0.	0.	0.	0.	0.	0.	0.

TABLE 8 (cont.)--Flow Model Results

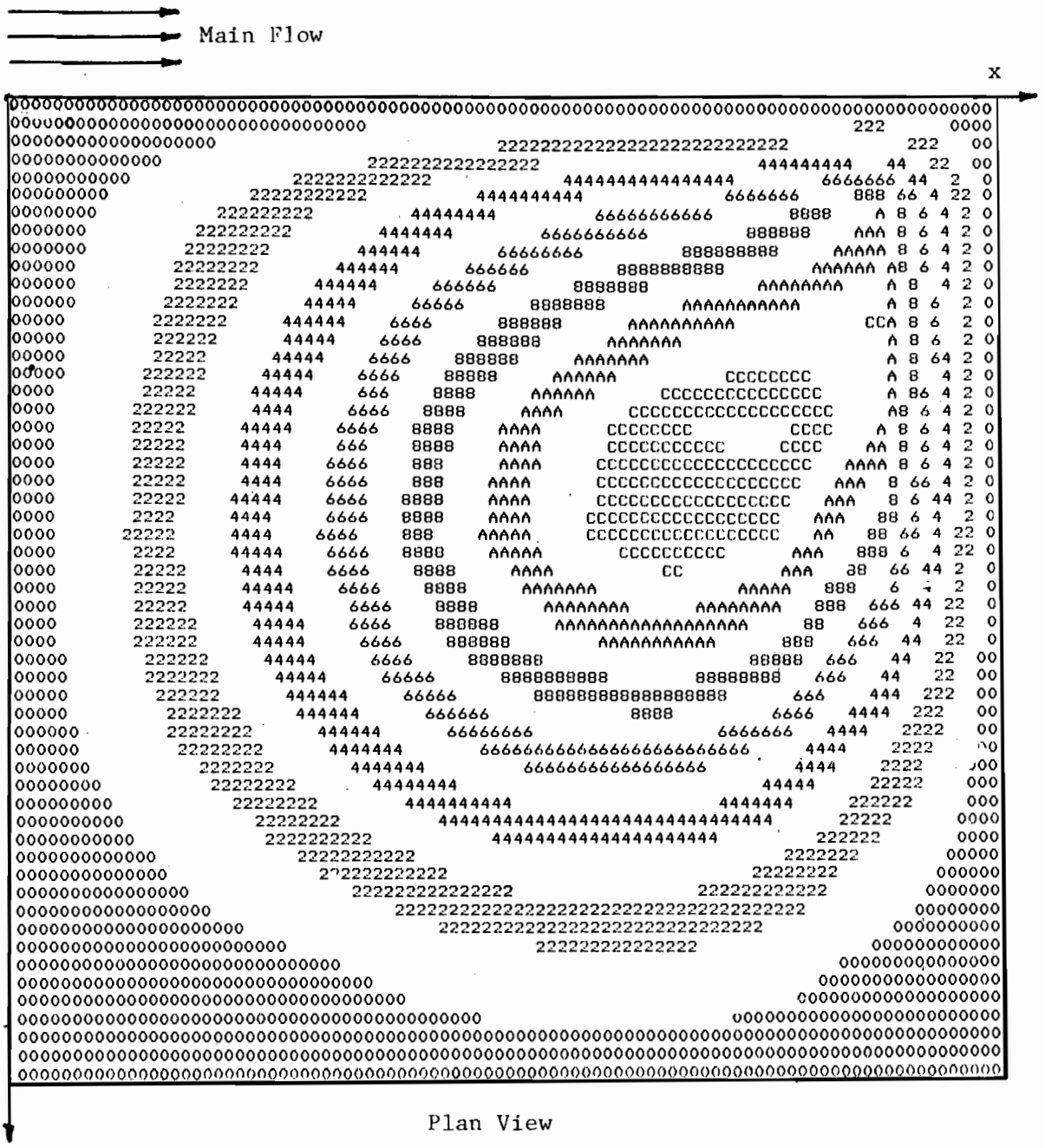

Plan View

Reynolds No. = 30,000

Fig. 15. Contour Plot of Streamlines

5.3 Results from the Mass Transport Model

5.3.1 Presentation

The thrust of the mass transport model numerical experiments was to examine the behavior of the solution for various values of dispersion coefficient, E, and finite difference time step, t. Versions I and II of the model were tested using identical data sets to make comparison easier. The simulation conditions for eleven runs are summarized in Table 9.

Instantaneous mass injection of a finite amount of mass at node 67 (see Fig. 3) was selected as initial condition for each simulation. This node is away from the boundaries as the flow velocity is moderate there. The quantity of mass injected was either 100.0 or 10.0 units. Mass quantity of 1.0 unit was also tried and resulted in very small concentration levels and instability partly caused by roundoff errors. Comparison of the experiments in which only the quantity of mass input varied revealed no difference in the normalized concentration levels. Therefore, in order to save computation cost, results for simulation with mass input of 10.0 units were scaled up by a factor of 10 for plotting and comparison purposes.

Results from Runs 2-7, 9, and 11 (see Table 9) are presented here. Runs 1 and 6 are identical except for the mass input and runs 8 and 10 became unstable after a few time steps and therefore are not included here. Simulations were terminated when mass loss, due to numerical diffusion, boundary effects, truncation errors, and other reasons, approached 10-15% of the mass input. A plot of computed mass increase or decrease versus time for each run is given in Fig. 16.

Maximum concentration level in the flow field is one measure of the relative degree of dispersion in a mass transport simulation exercise. A

TABLE 9--Summary of Simulation Conditions

Run Number	Program Version	Initial Mass Injected	Dispersion Coefficient E	Time Step ΔT	Clock Time	Mass Remaining	% Mass Loss
1	I	10.0	0.1	2.0	14.0	9.156	8.44
2	I	100.0	0.1	1.0	12.0	93.25	6.75
3	I	10.0	0.2	1.0	31.0	8.989	10.11
4	I	100.0	0.1	1.5	36.0	87.63	12.37
5	I	10.0	0.8	1.0	21.0	9.738	2.62
6	I	100.0	0.1	2.0	14.0	91.56	8.44
7	I	100.0	0.5	2.0	20.0	91.99	8.01
8	I	100.0	0.1	0.5	2.0	-467.33	--
9	II	100.0	0.1	2.0	6.0	81.92	18.08
10	II	100.0	0.1	0.5	2.0	85.02	14.98
11	II	100.0	0.5	2.0	14.0	97.46	2.54

Flow Reynolds No. 10,000
Finite Element Grid Spacing (ΔL) = 1.0
Injection Node Number 67

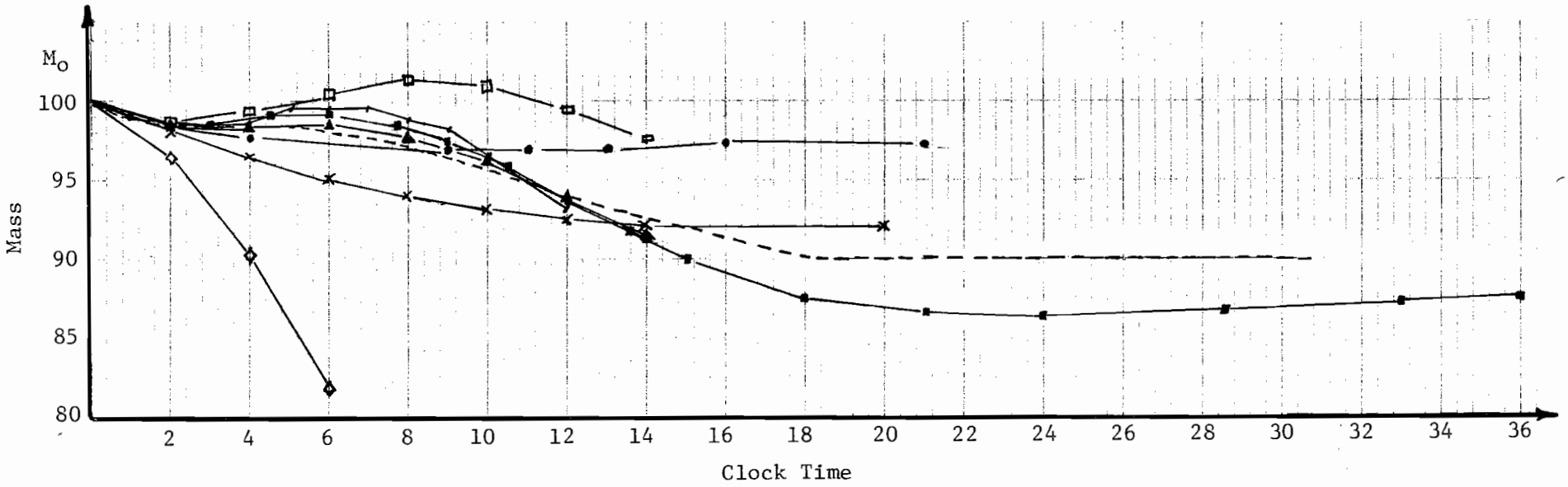

LEGEND:

Symbol	Run No.
—•—	2
- - - - -	3
—■—	4
—●—	5
—▲—	6
—×—	7
—◇—	9
—□—	11
M_o	Initial Mass Injected

Fig. 16. Total Mass versus Time

plot of maximum concentration C_{MAX}, found in the flow field versus time for each run is shown in Fig. 17.

Contour plots of normalized concentrations for Runs 2, 4, 6, 7, 9, and 11 are presented in Figs. 18-35. The contour plots are generated using subroutine PLOT as described in Chapter 4. The symbol * in Figs. 18-35 denotes concentration levels greater than or equal to 98% of the maximum nodal concentration.

A dispersion coefficient of 0.1 was specified for Runs 2, 4, and 6. The time step was set at 1.0, 1.5, and 2.0, respectively. Figs. 18-35 show the developing concentration patterns for each time step. Comparison of scalar and vectorized formulation of the dispersion coefficient can be made for identical input parameters by examination of Figs. 30-34. Another comparison can be made by viewing concentration contours for Run 6, Figs. 27-29, and Run 9, Fig. 35.

The influence of advection can be observed by tracking the path of the peak concentration as calculations progress in time. The path of maximum nodal concentration for Runs 4, 6, 7, and 11 is given in Figs. 36 and 37. The node of maximum concentration is denoted by a geometric symbol on the finite element node networks. The resident clock time is recorded at the node.

5.3.2 Discussion

The stability of calculations, degree of apparent numerical diffusion and ability of the model to simulate mass transport in a a range of flow conditions, (from advection dominance to dispersion dominated) have been examined. The plots and concentration contours must be examined together to develop a meaningful picture of the results.

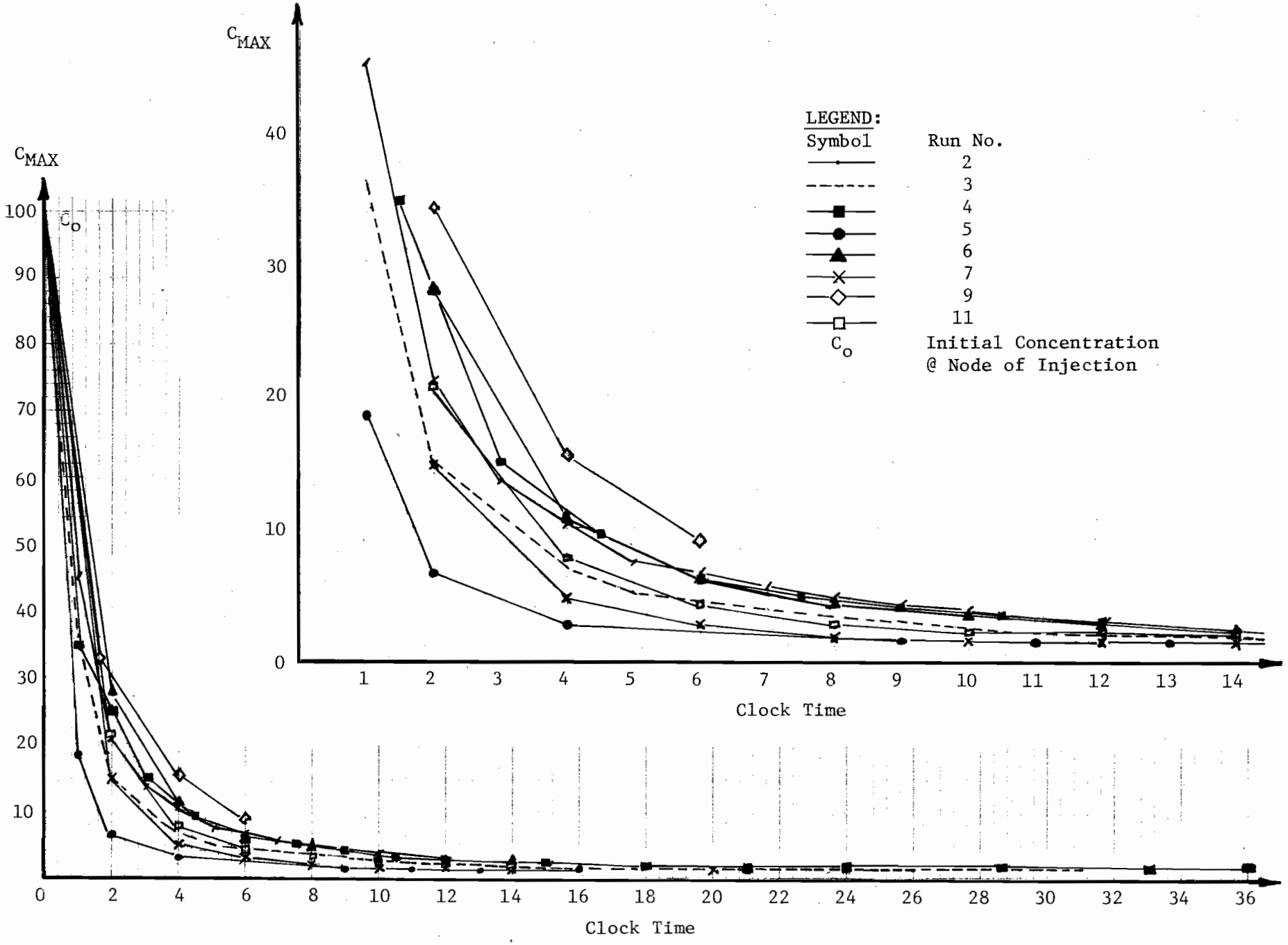

Fig. 17. Maximum Concentration versus Time

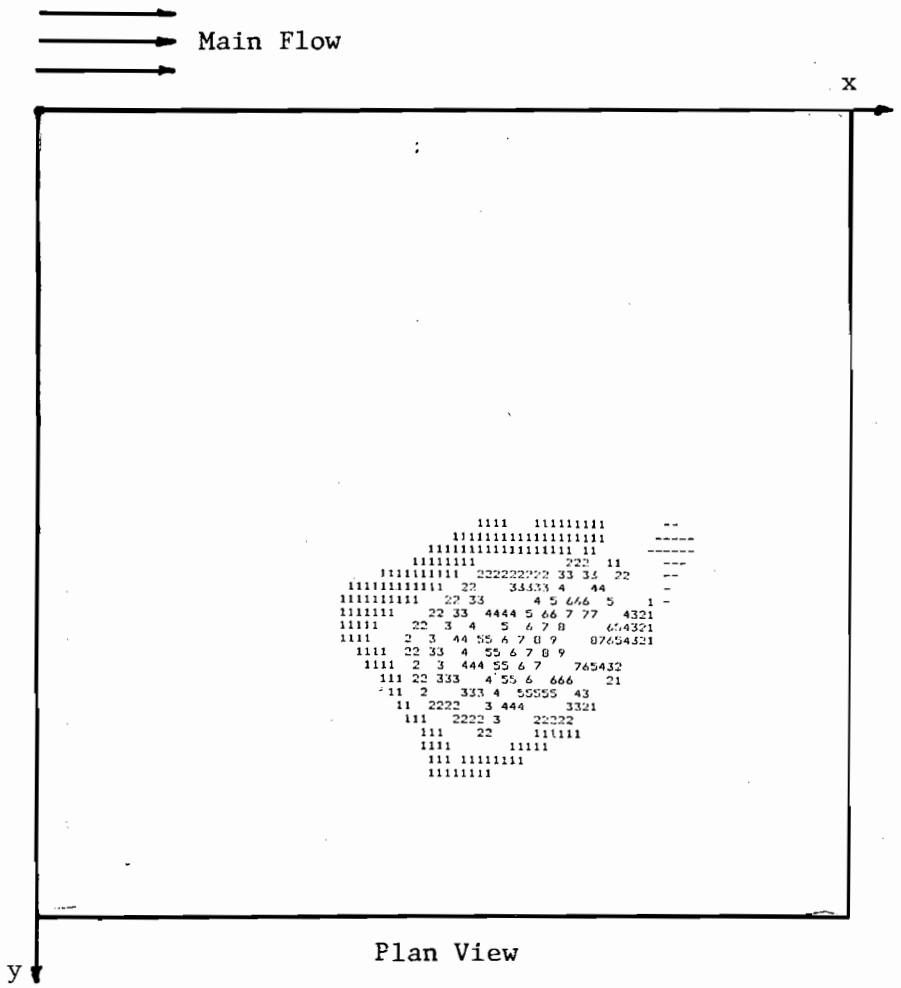

Run No. 2
Clock Time 1.0
C_{MAX} 44.9
Total Mass 99.09

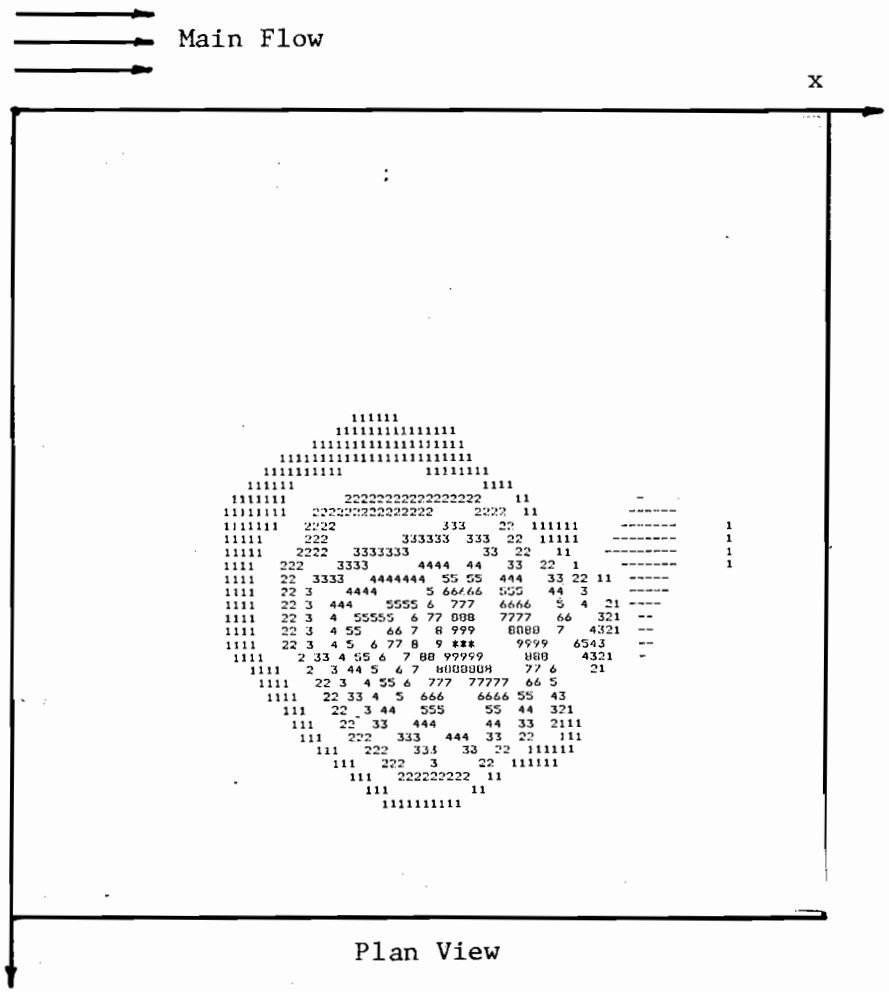

Run No. 2
Clock Time 2.0
C_{MAX} 21.0
Total Mass 98.62

Fig. 18. Normalized Concentration Contours

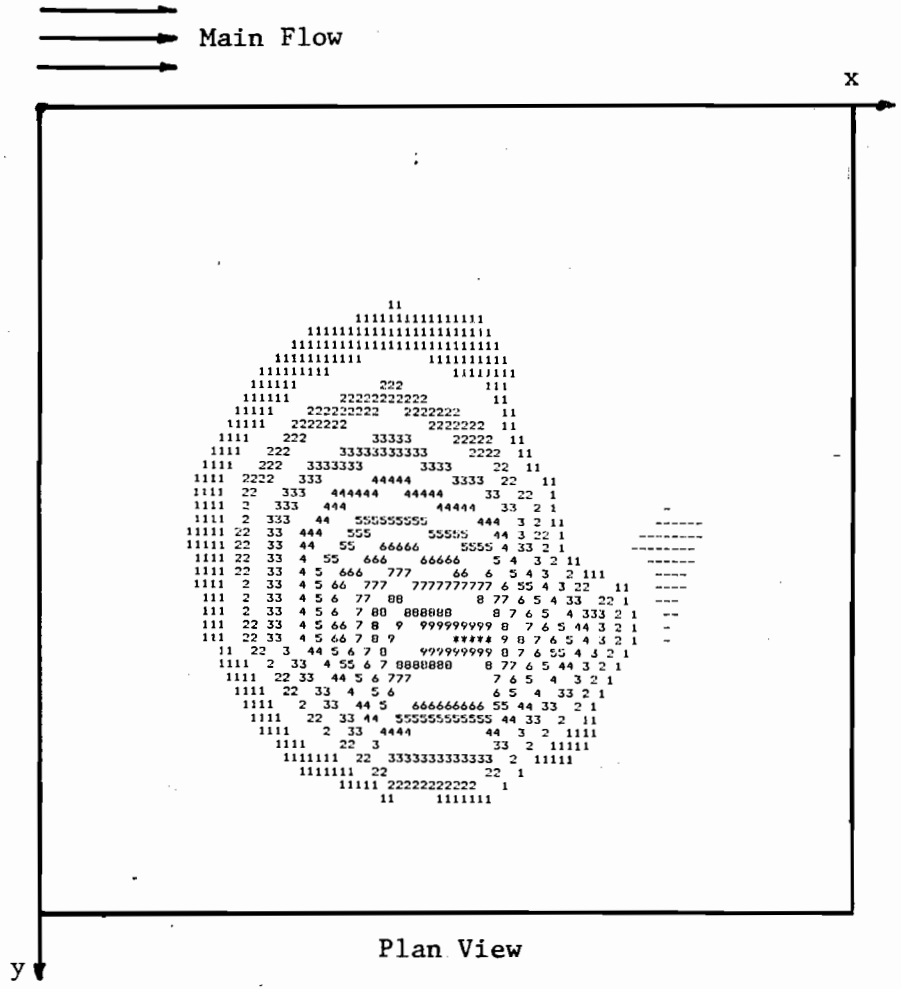

Plan View

Run No. 2
Clock Time 3.0
C_{MAX} 13.8
Total Mass 98.72

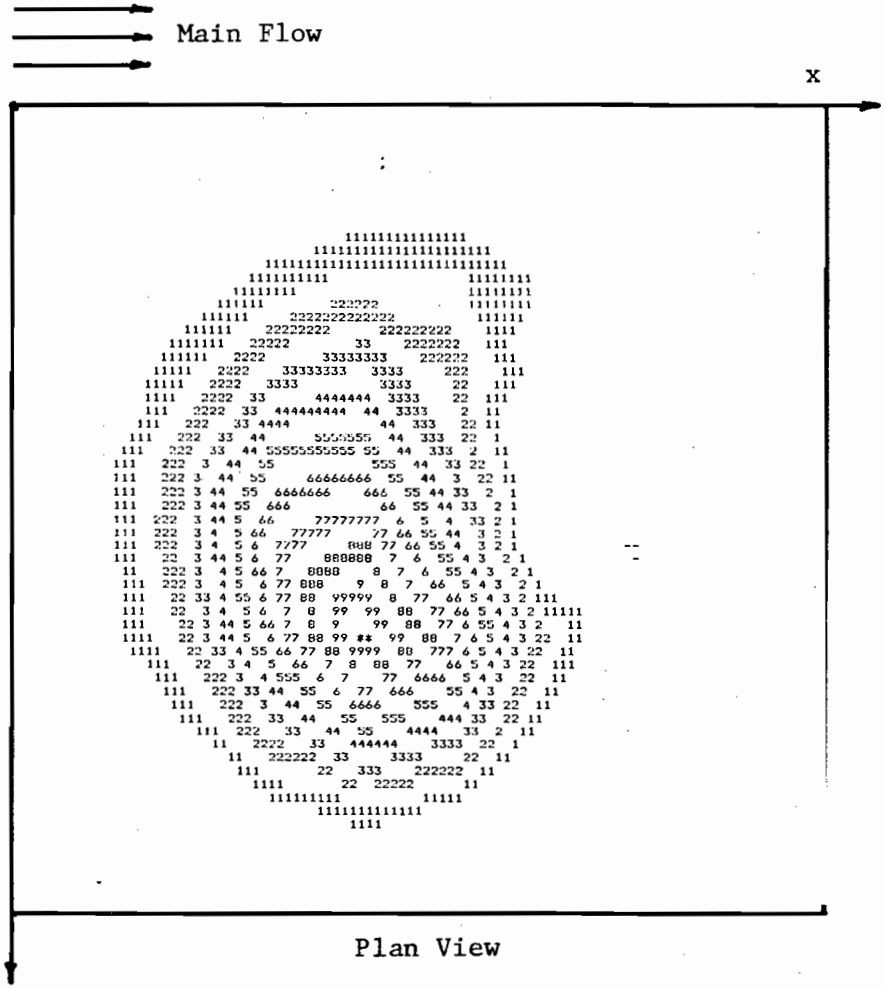

Plan View

Run No. 2
Clock Time 4.0
C_{MAX} 10.5
Total Mass 98.83

Fig. 19. Normalized Concentration Contours

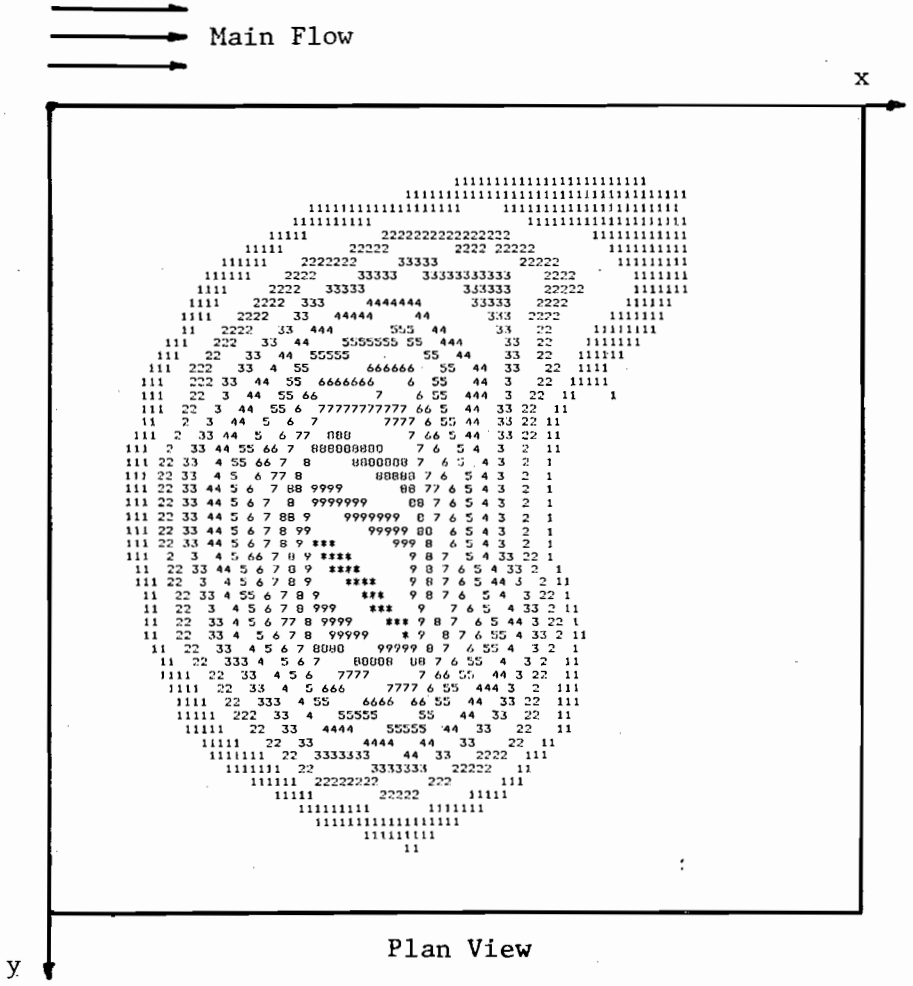

Run No. 2
Clock Time 5.0
C_{MAX} 7.48
Total Mass 99.37

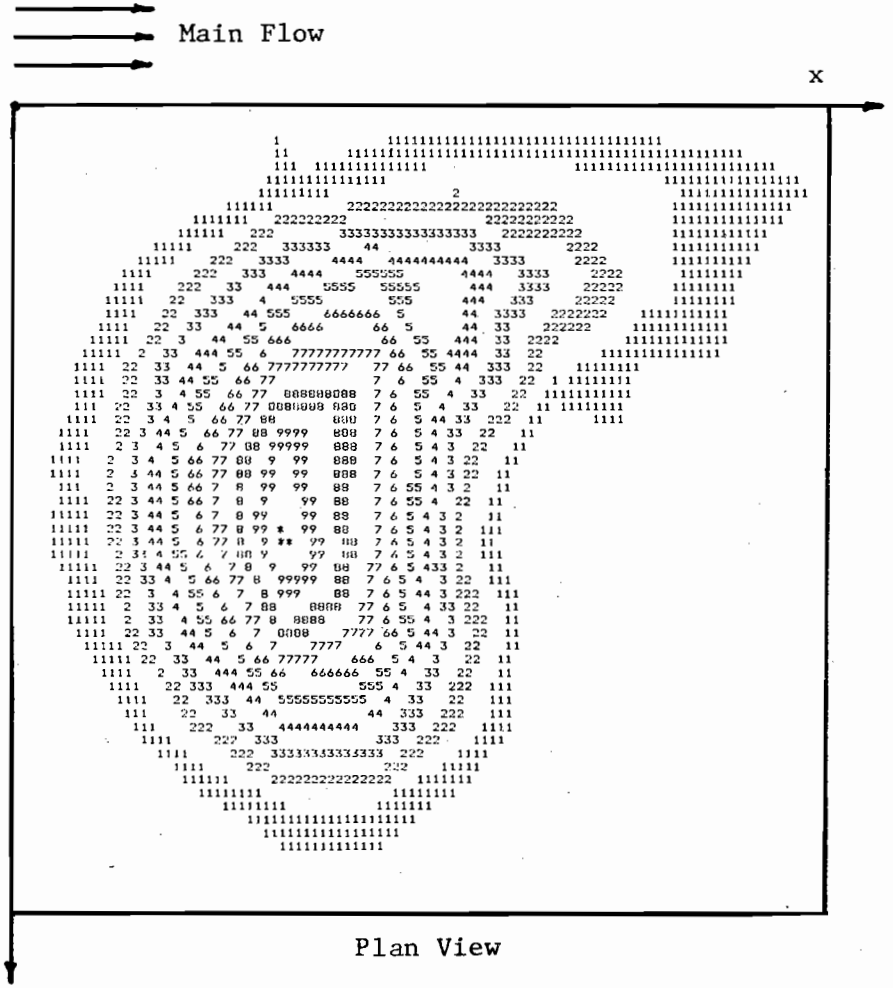

Run No. 2
Clock Time 6.0
C_{MAX} 6.72
Total Mass 96.51

Fig. 20. Normalized Concentration Contours

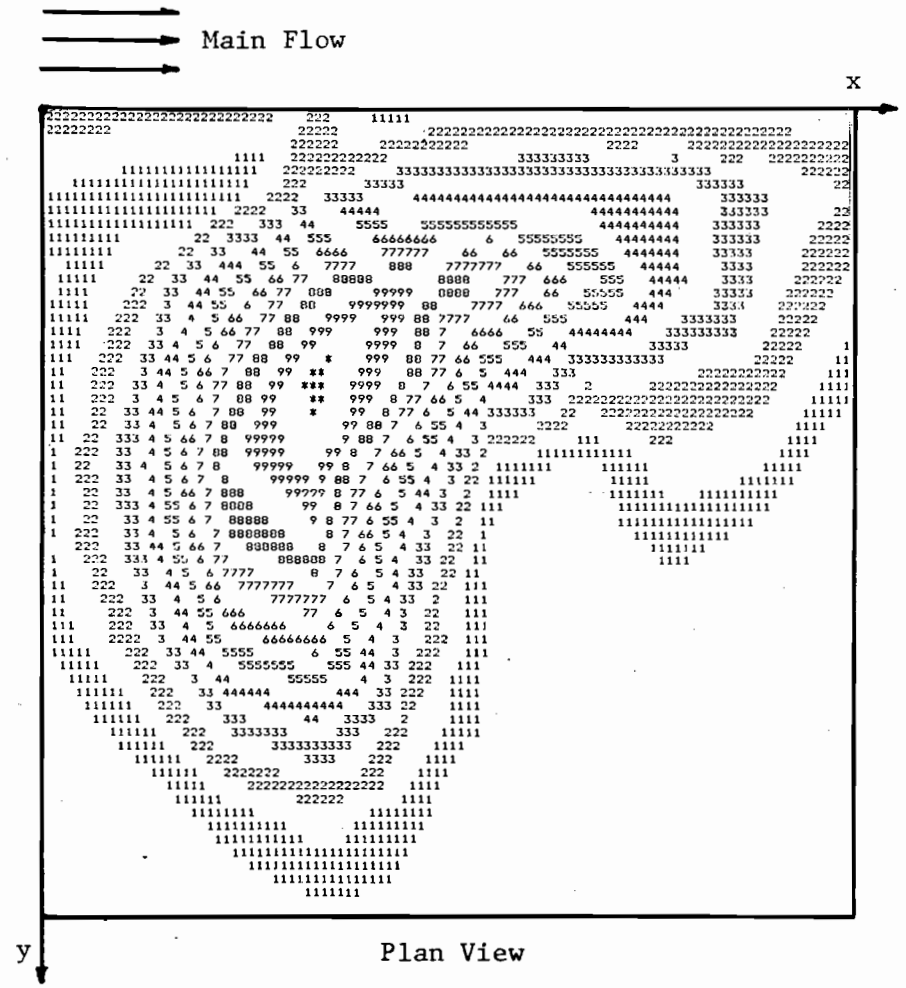

Run No.	2
Clock Time	8.0
C_{MAX}	4.86
Total Mass	98.82

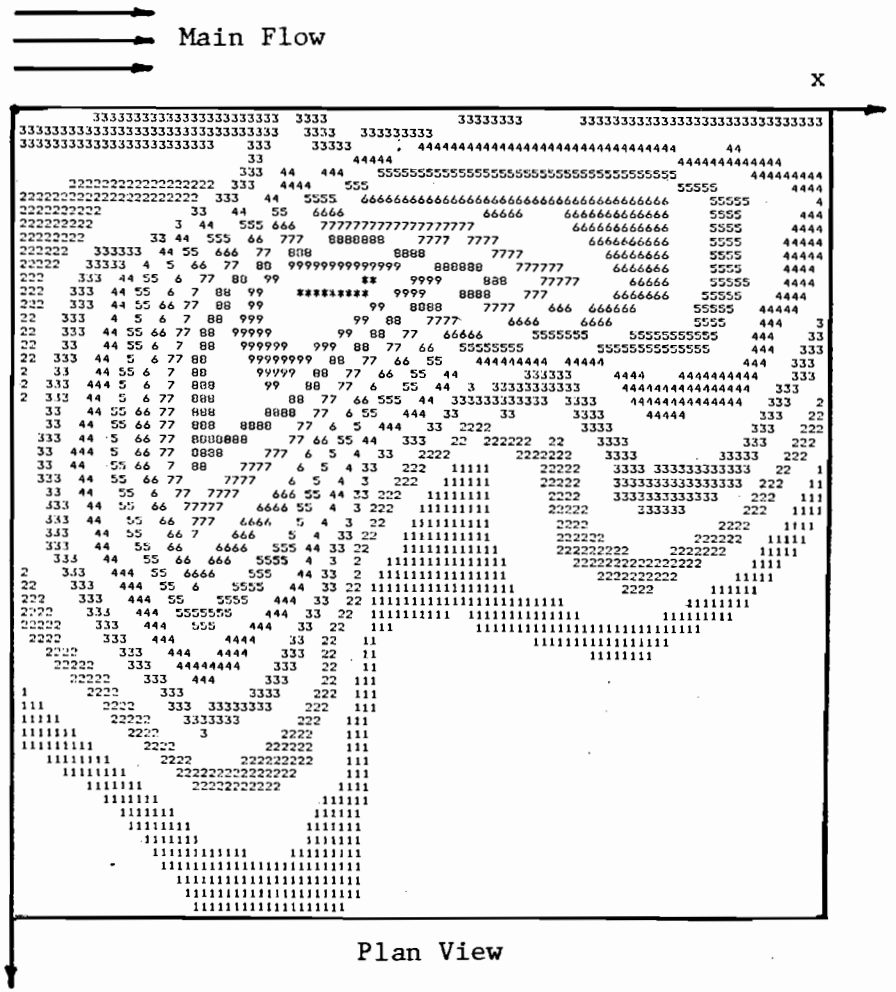

Run No.	2
Clock Time	10.0
C_{MAX}	3.94
Total Mass	96.51

Fig. 21. Normalized Concentration Contours

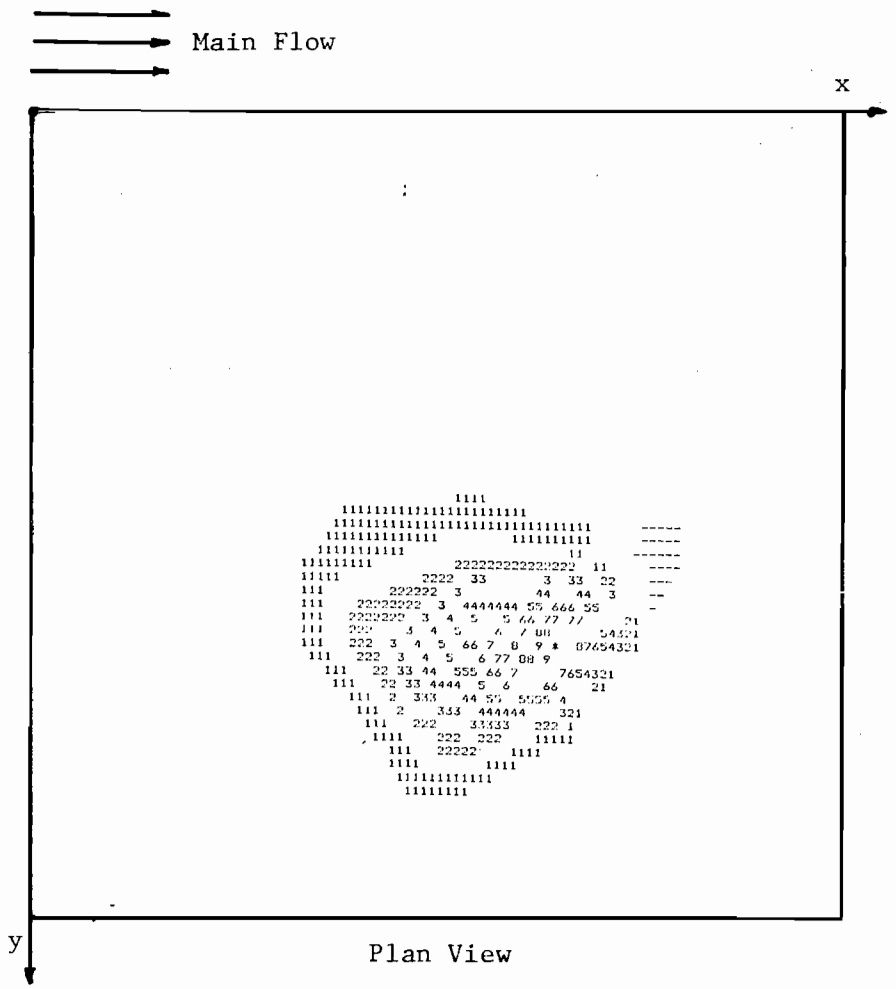

Plan View

Run No. 4
Clock Time 1.50
C_{MAX} 34.5
Total Mass 98.96

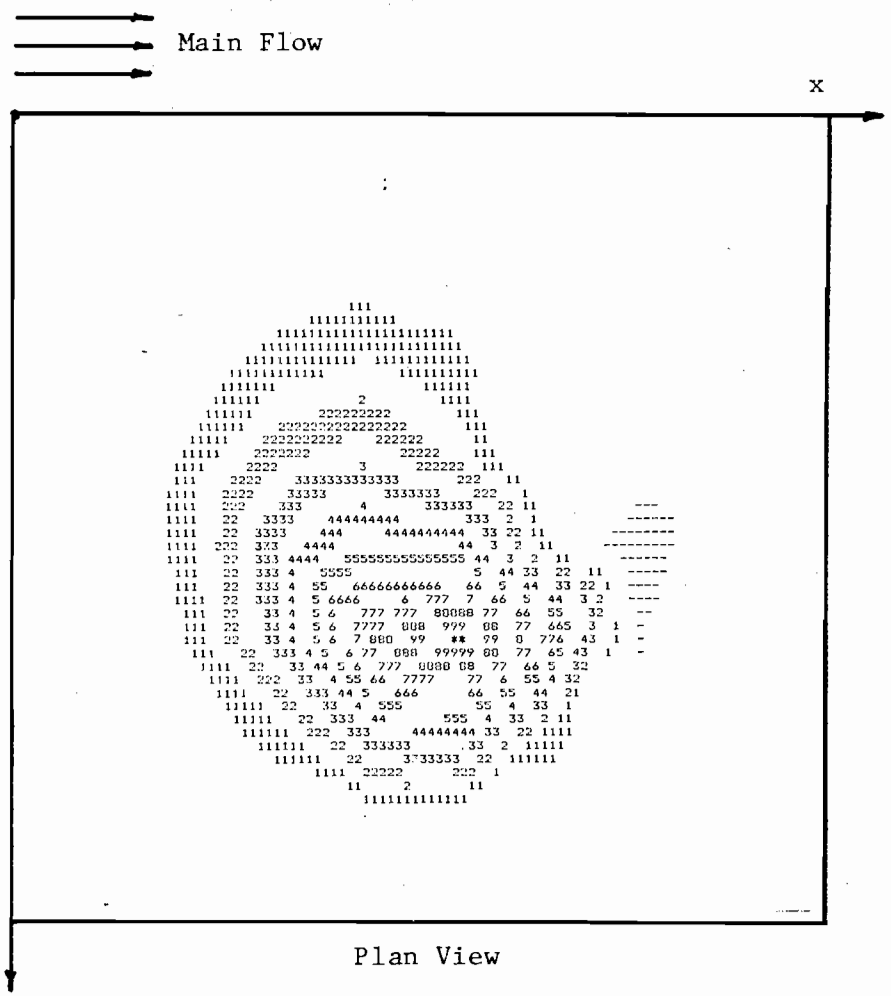

Plan View

Run No. 4
Clock Time 3.0
C_{MAX} 14.9
Total Mass 98.76

Fig. 22. Normalized Concentration Contours

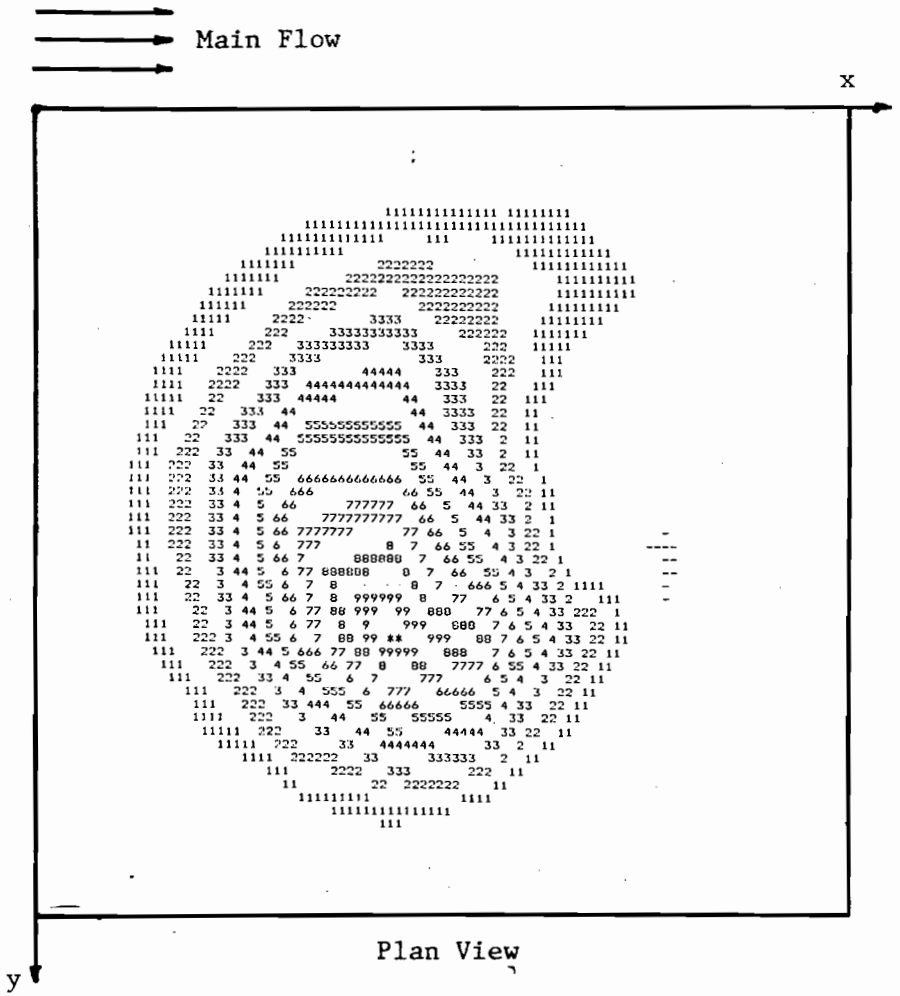

Plan View

Run No.	4
Clock Time	4.5
C_{MAX}	9.06
Total Mass	98.98

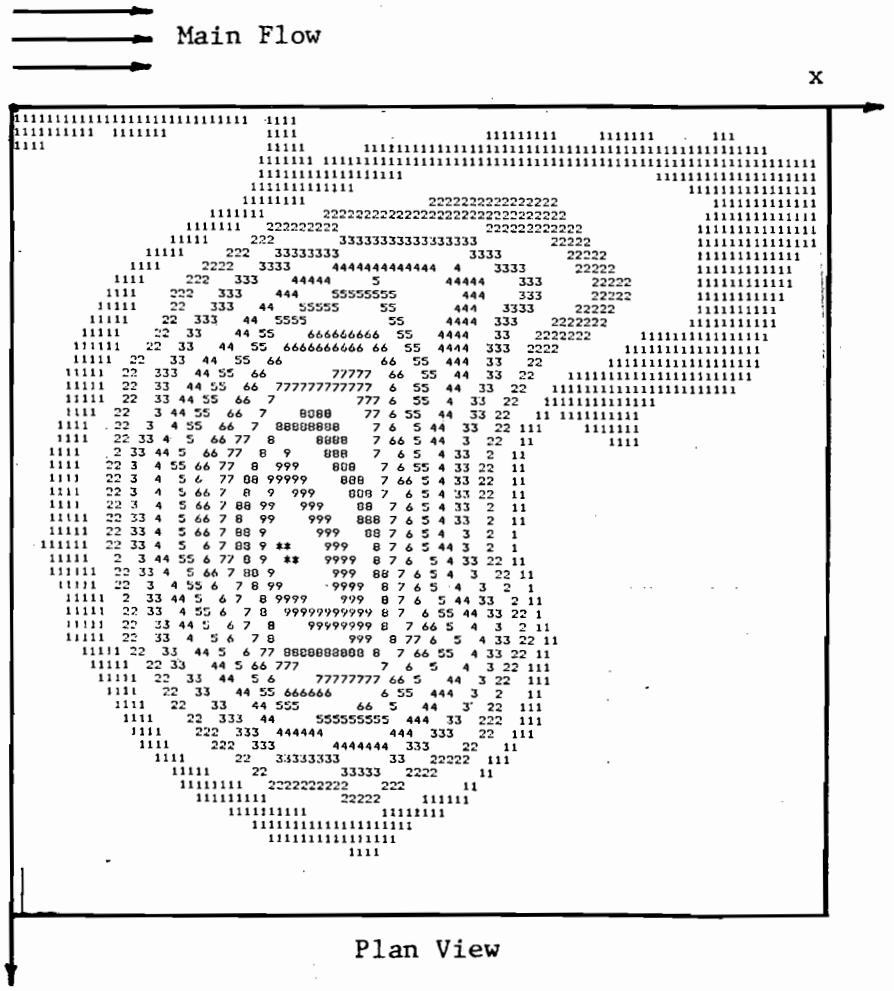

Plan View

Run No.	4
Clock Time	6.0
C_{MAX}	6.21
Total Mass	99.05

Fig. 23. Normalized Concentration Contours

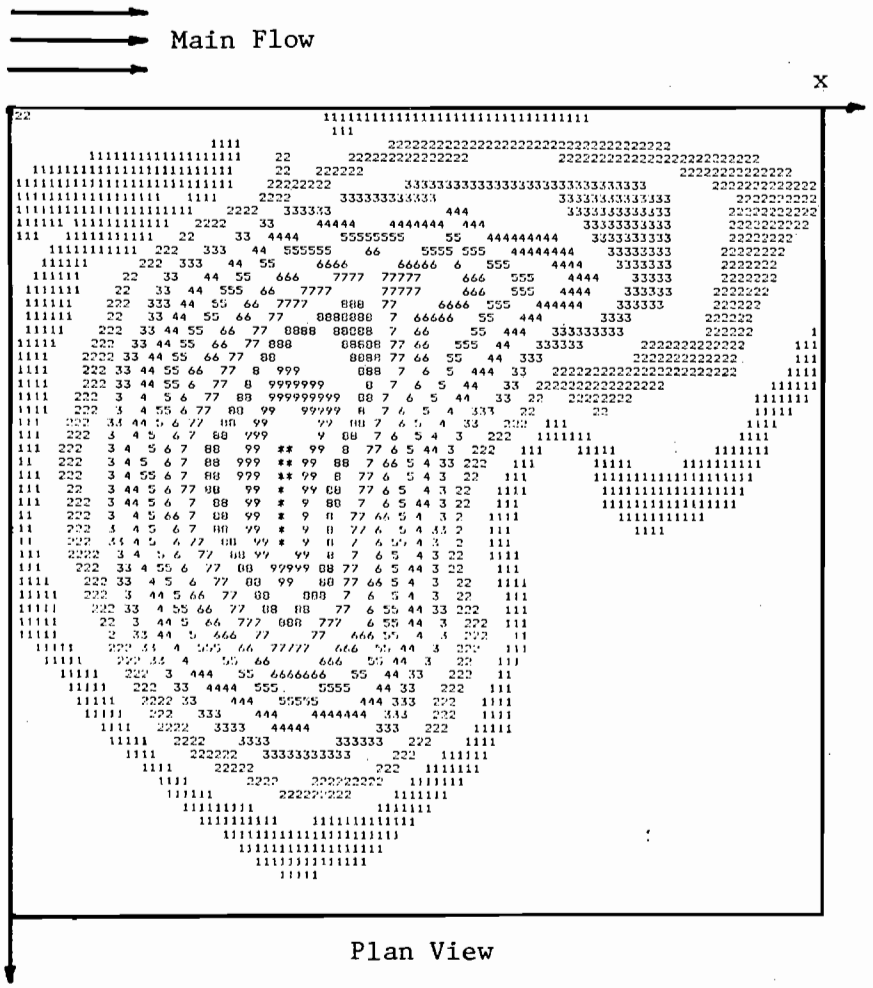

Run No. 4
Clock Time 7.5
C_{MAX} 4.97
Total Mass 98.60

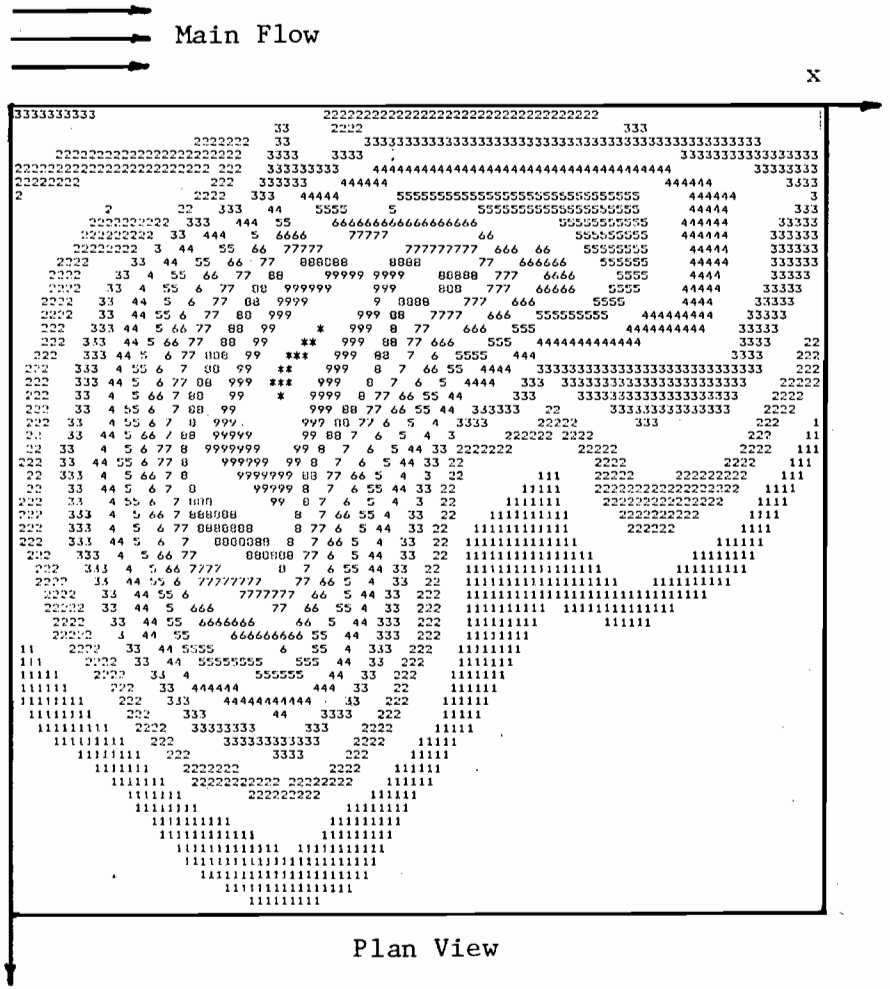

Run No. 4
Clock Time 9.0
C_{MAX} 4.04
Total Mass 97.46

Fig. 24. Normalized Concentration Contours

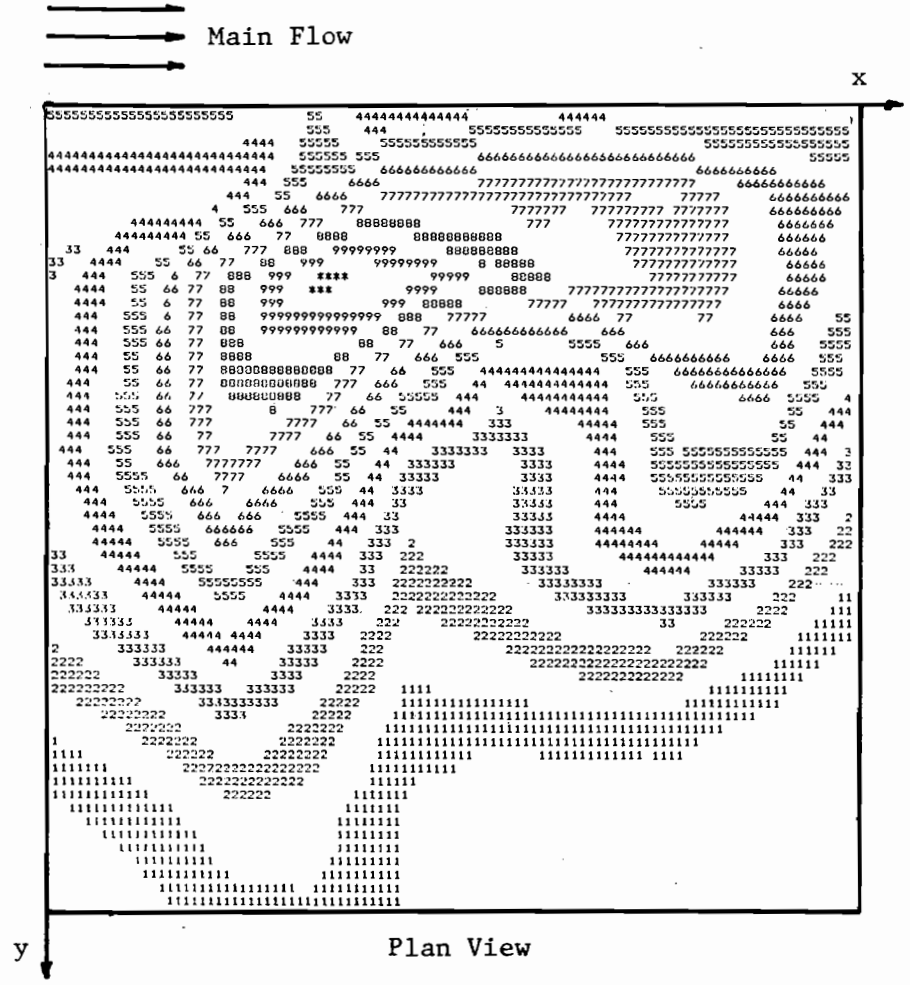

Run No. 4
Clock Time 12.0
C_{MAX} 3.07
Total Mass 93.76

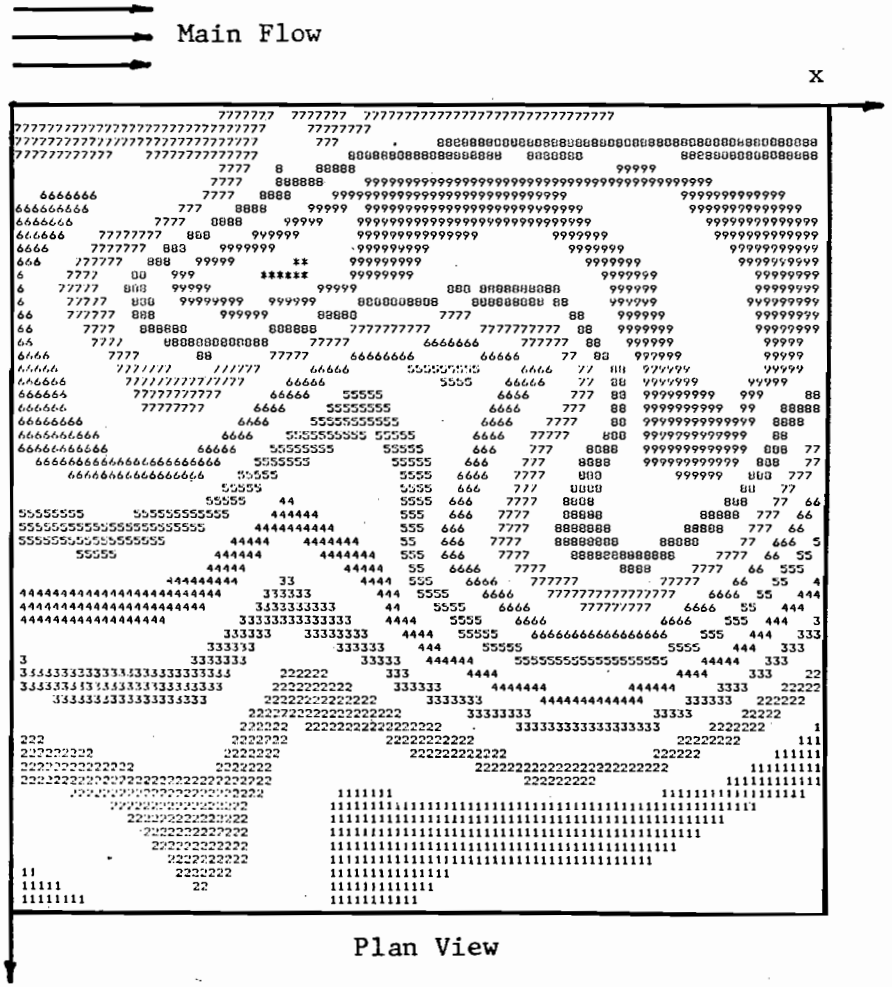

Run No. 4
Clock Time 15.0
C_{MAX} 2.08
Total Mass 89.98

Fig. 25. Normalized Concentration Contours

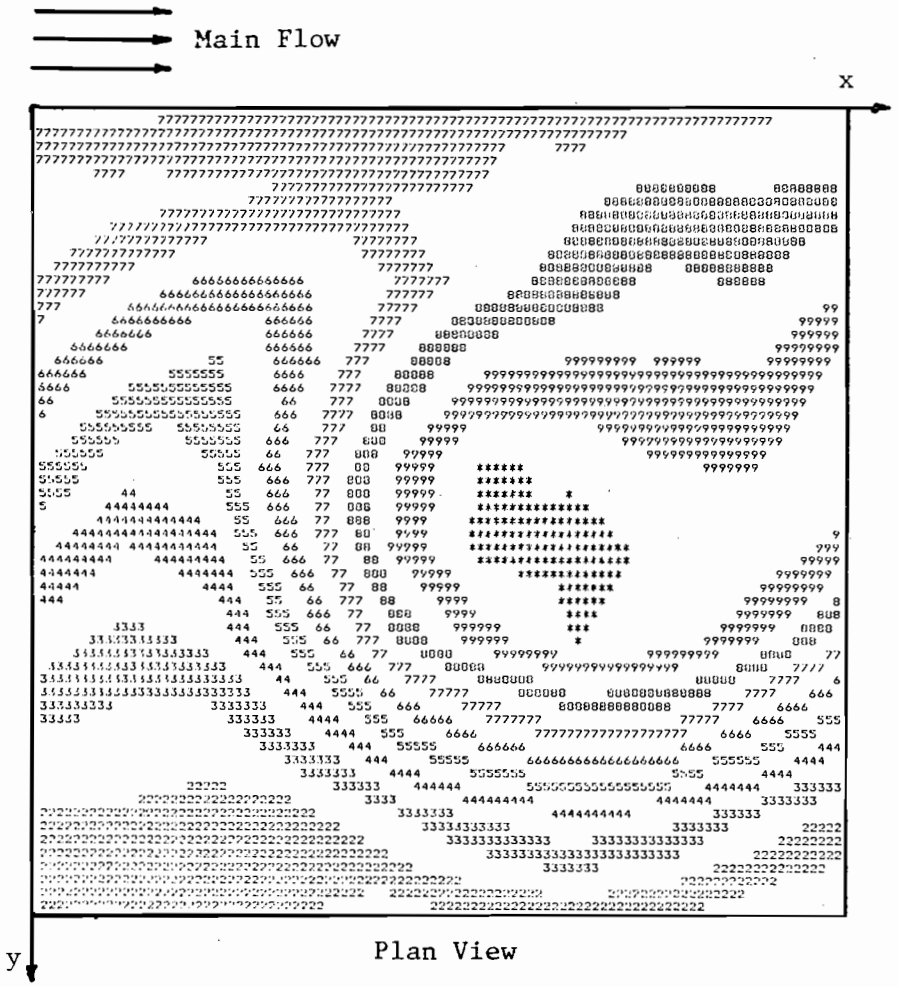

Run No. 4
Clock Time 21.0
C_{MAX} 1.70
Total Mass 86.43

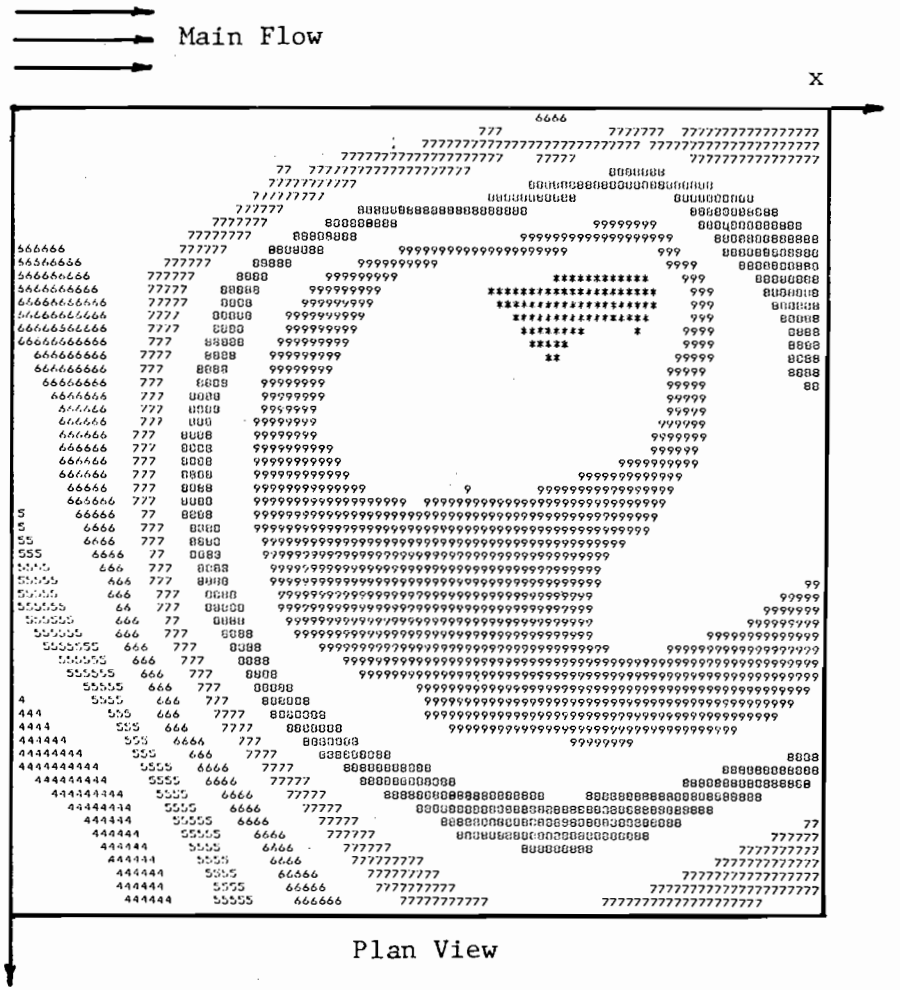

Run No. 4
Clock Time 86.0
C_{MAX} 1.40
Total Mass 87.63

Fig. 26. Normalized Concentration Contours

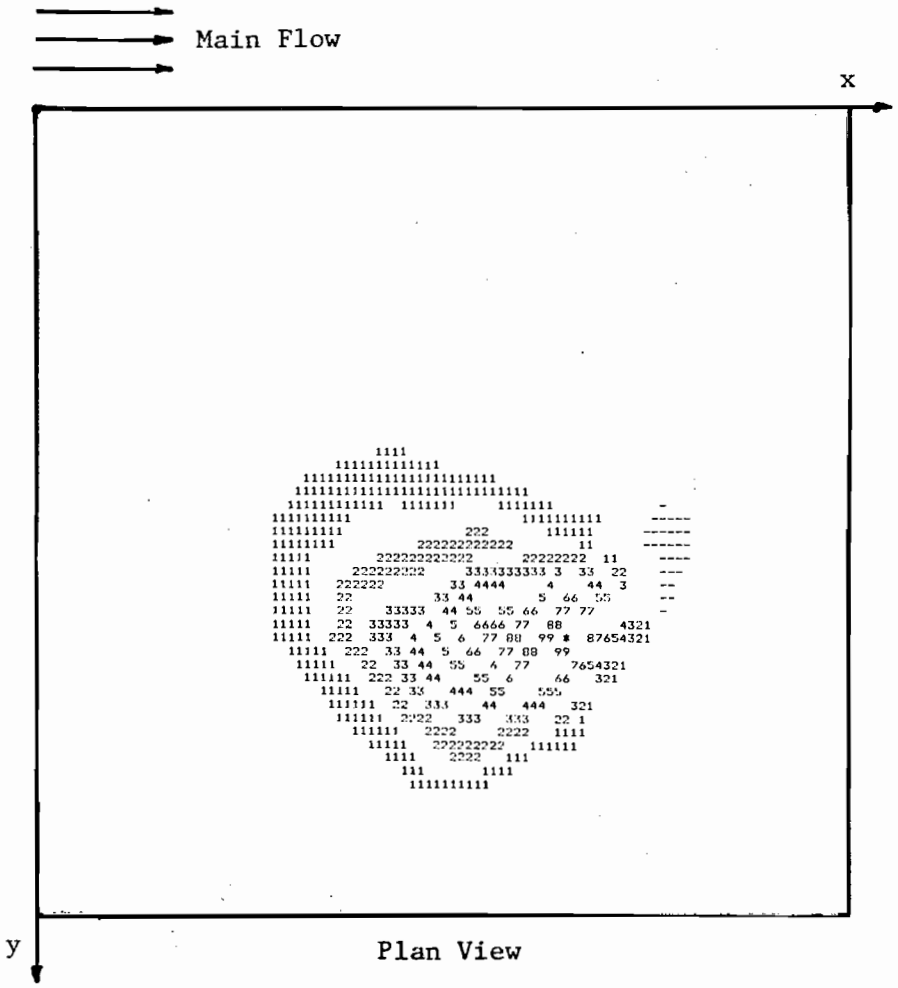

Run No. 6
Clock Time 2.0
C_{MAX} 28.0
Total Mass 98.92

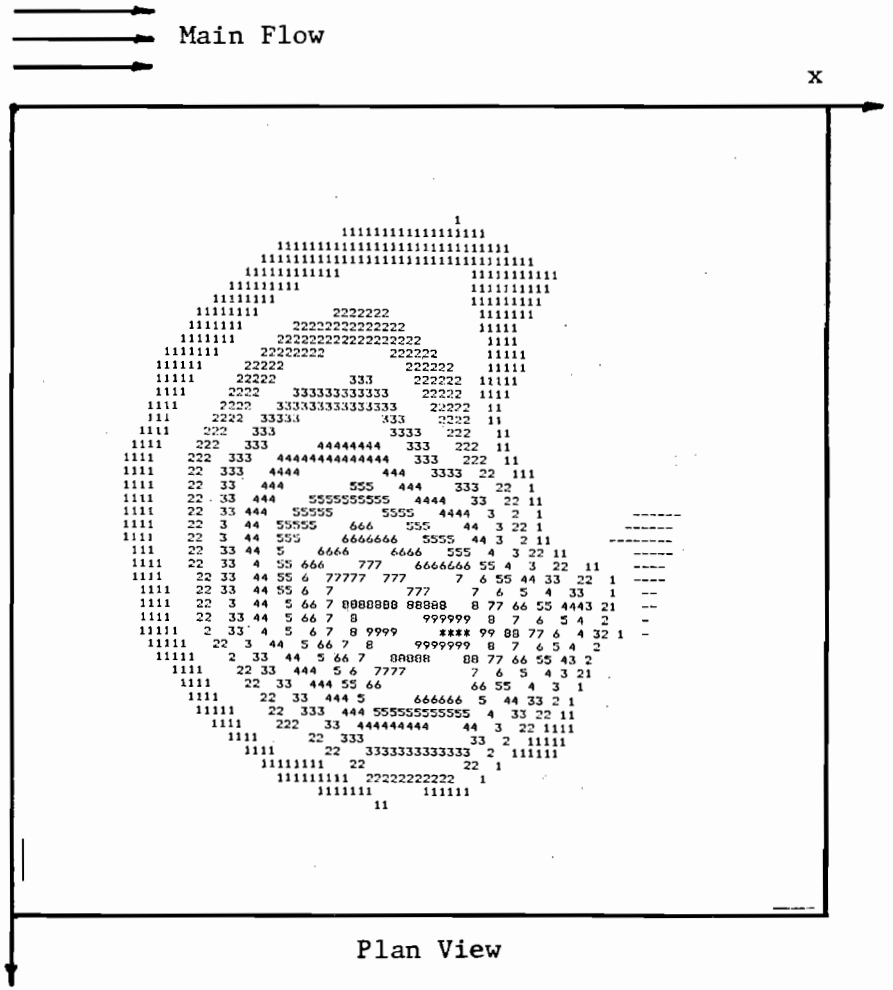

Run No. 6
Clock Time 4.0
C_{MAX} 10.8
Total Mass 98.82

Fig. 27. Normalized Concentration Contours

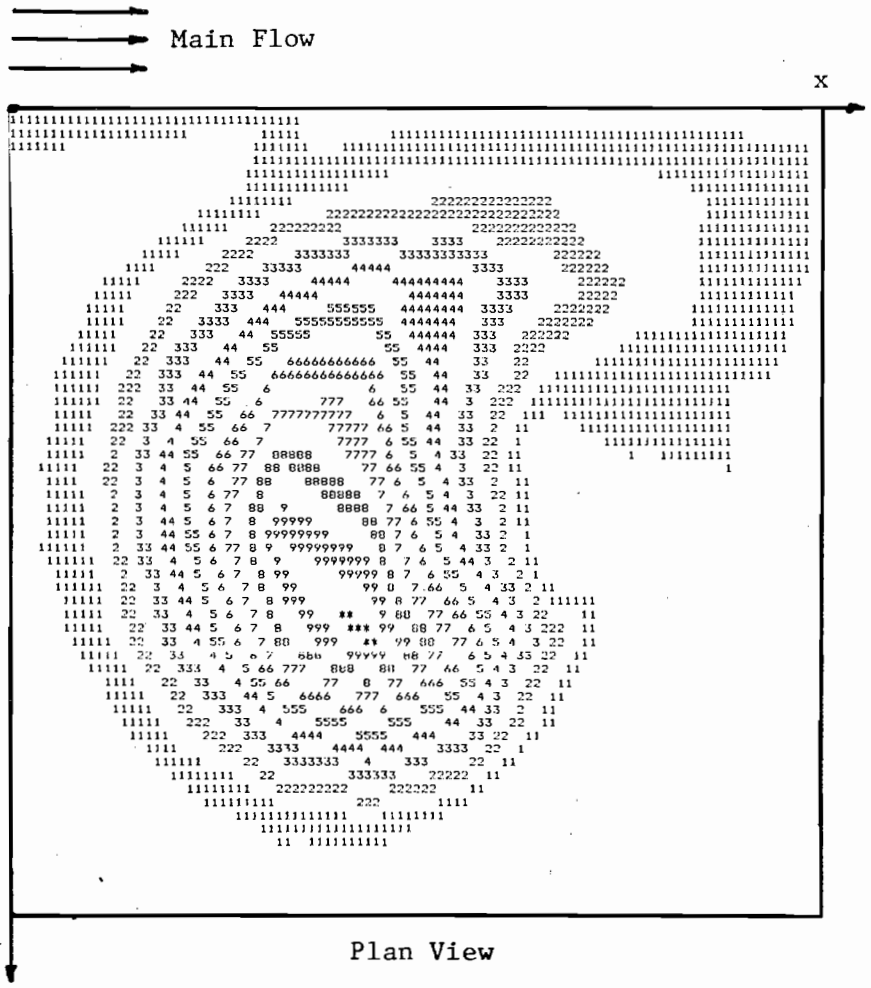

Plan View

Run No. 6
Clock Time 6.0
C_{MAX} 6.13
Total Mass 98.68

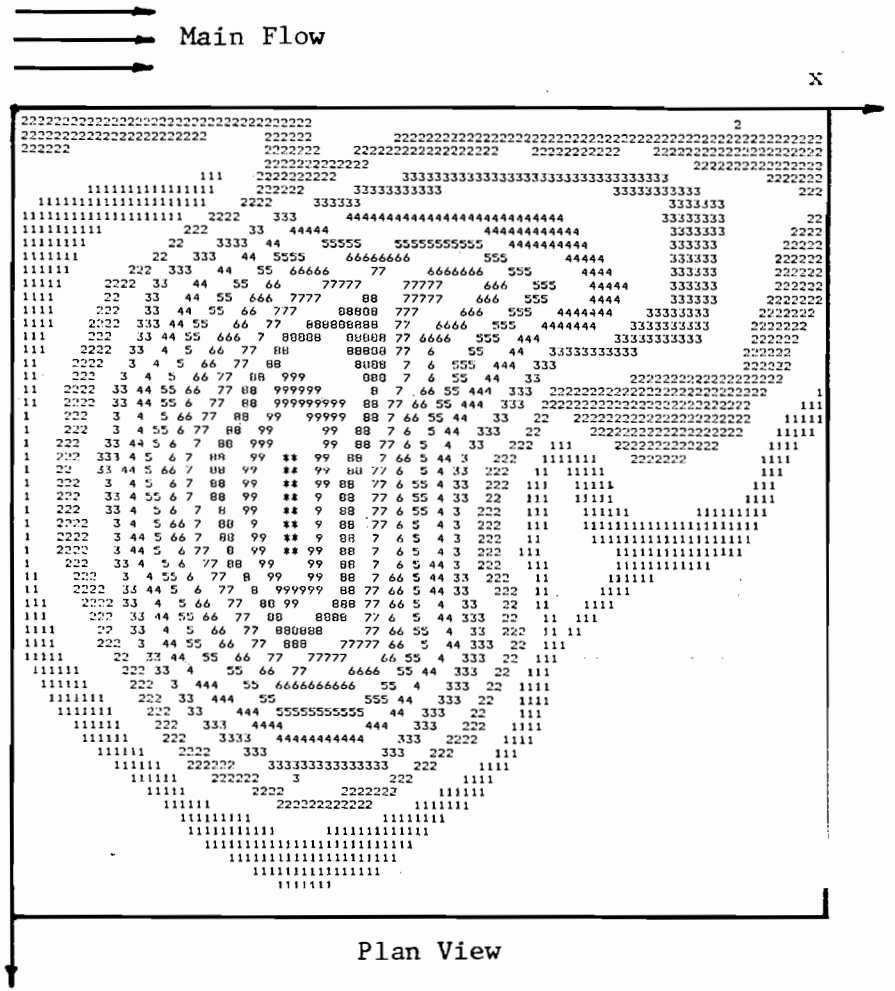

Plan View

Run No. 6
Clock Time 8.0
C_{MAX} 4.48
Total Mass 97.81

Fig. 28. Normalized Concentration Contours

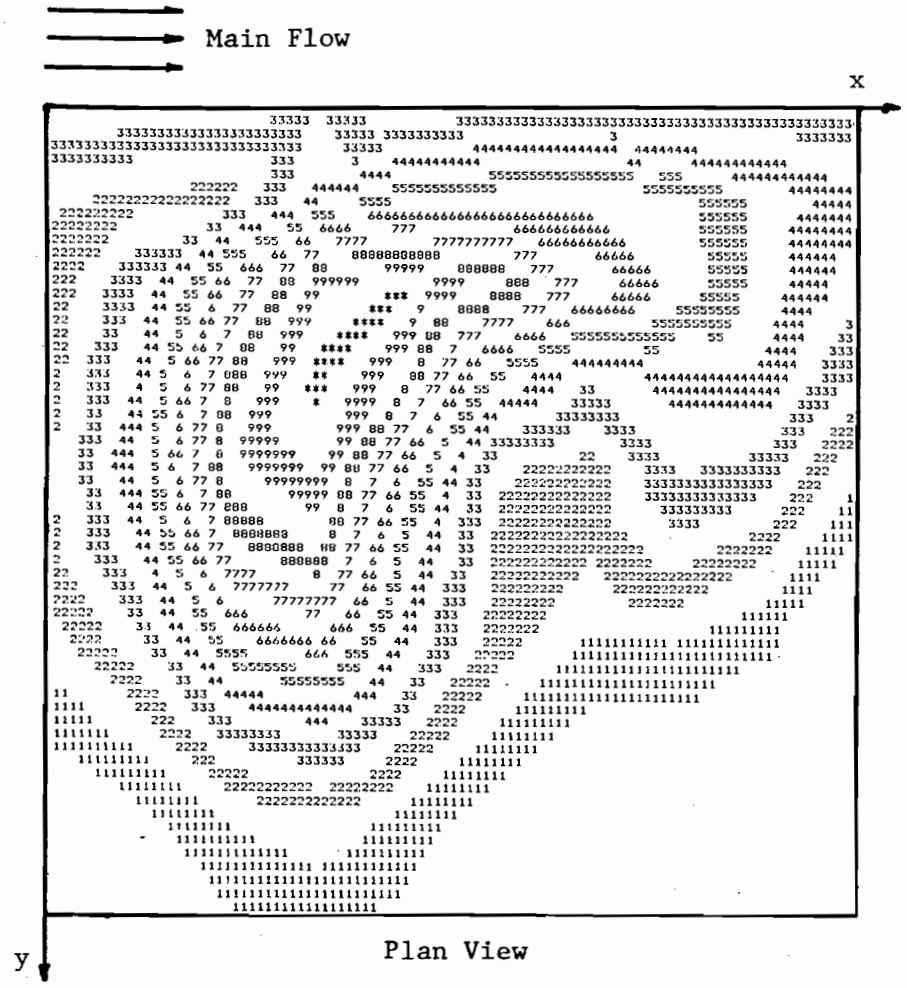

Run No. 6
Clock Time 10.0
C_{MAX} 3.49
Total Mass 96.10

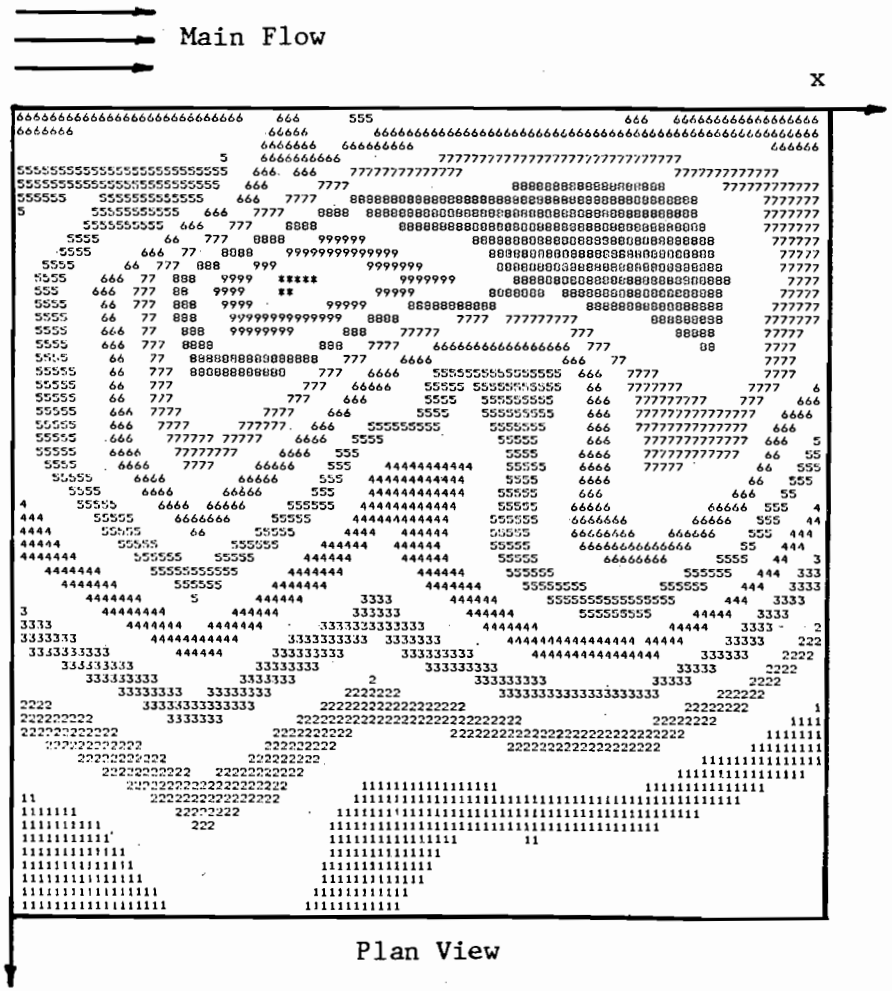

Run No. 6
Clock Time 14.0
C_{MAX} 2.46
Total Mass 91.56

Fig. 29. Normalized Concentration Contours

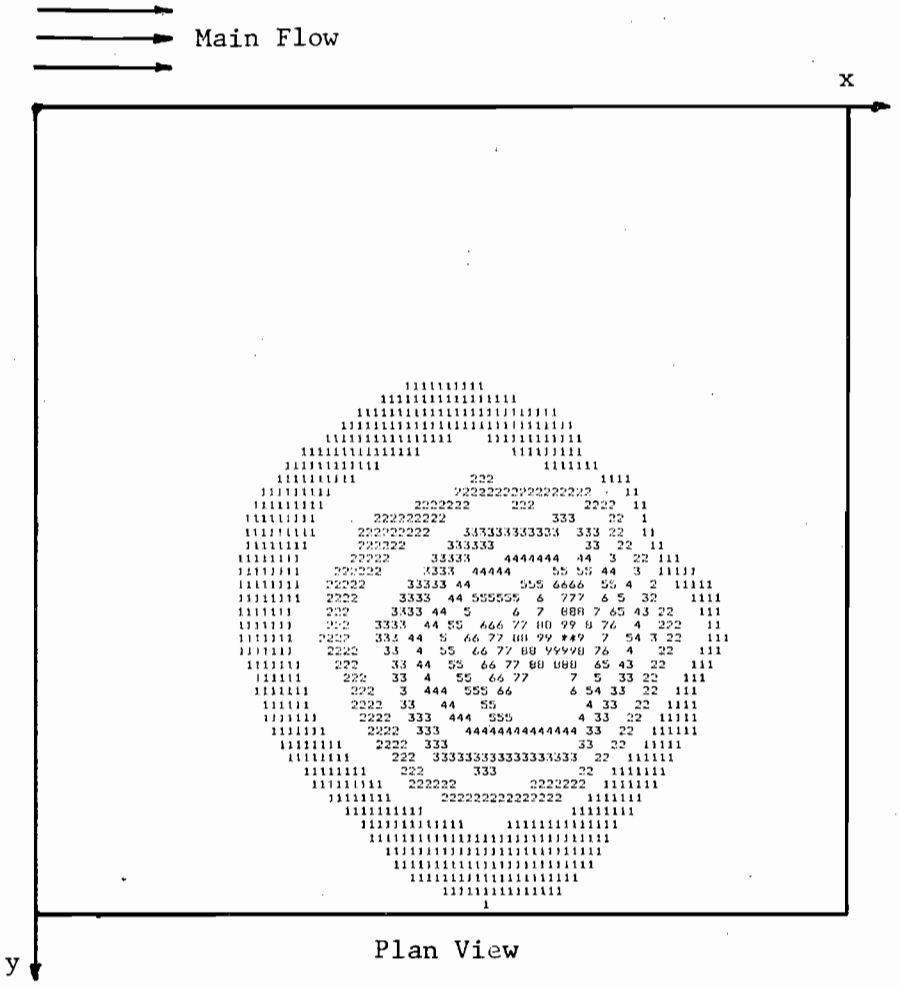

Run No.	7
Clock Time	2.0
C_{MAX}	14.8
Total Mass	97.88

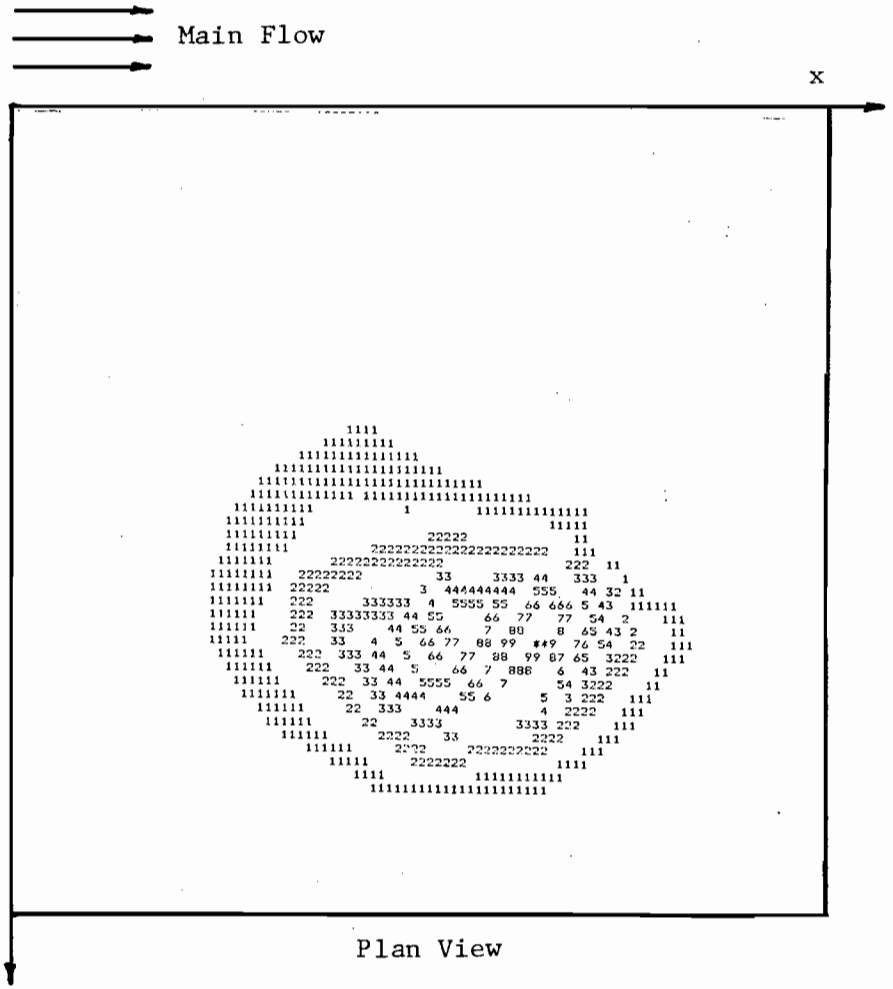

Run No.	11
Clock Time	2.0
C_{MAX}	20.8
Total Mass	98.80

Fig. 30. Normalized Concentration Contours

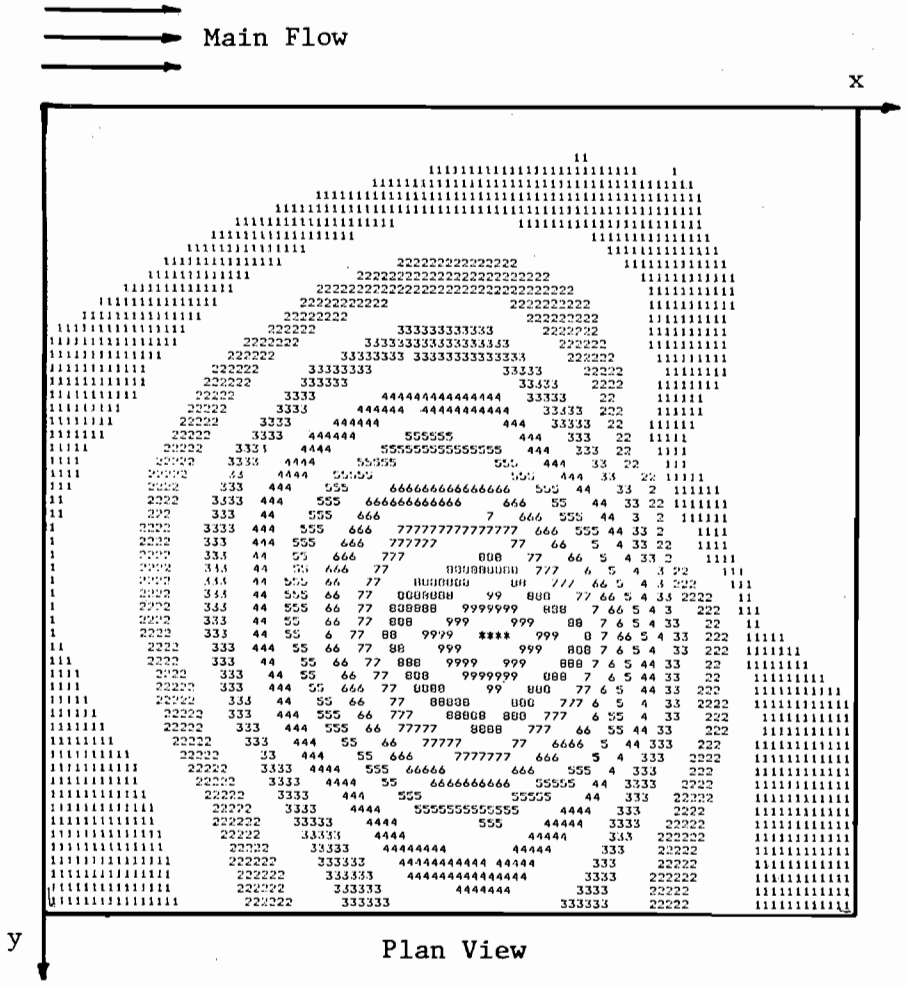

Run No. 7
Clock Time 4.0
C_{MAX} 4.78
Total Mass 96.41

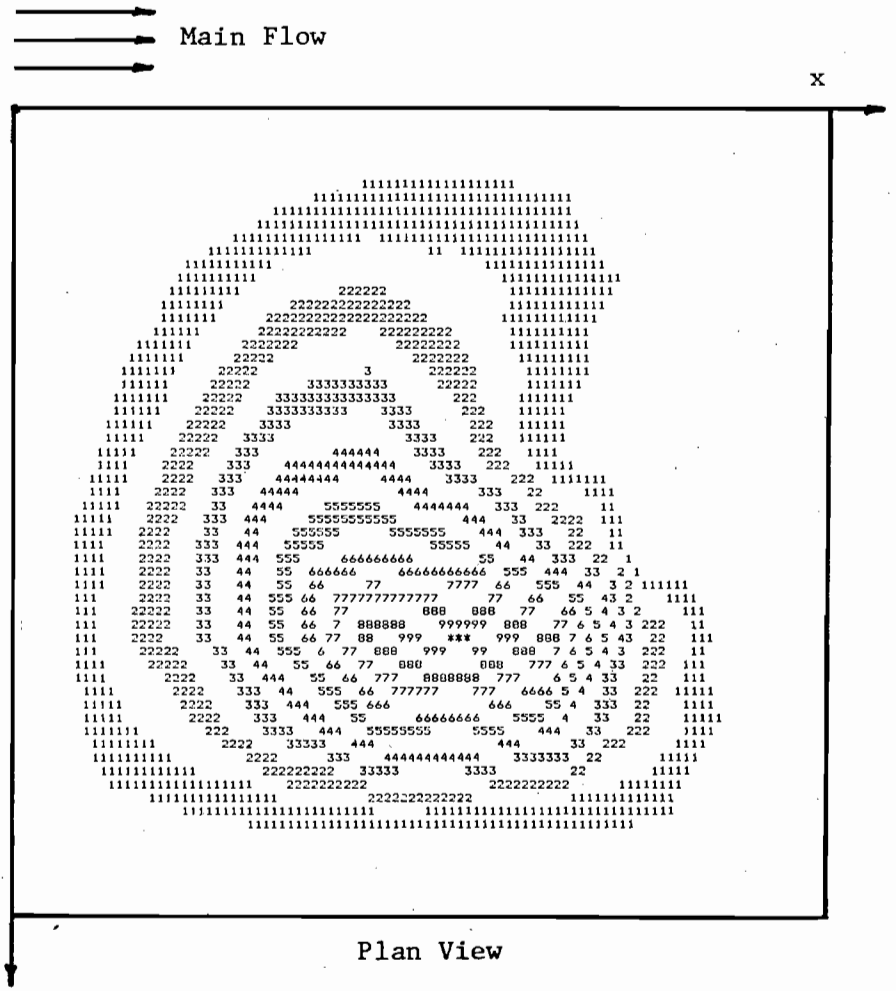

Run No. 11
Clock Time 4.0
C_{MAX} 7.75
Total Mass 99.40

Fig. 31. Normalized Concentration Contours

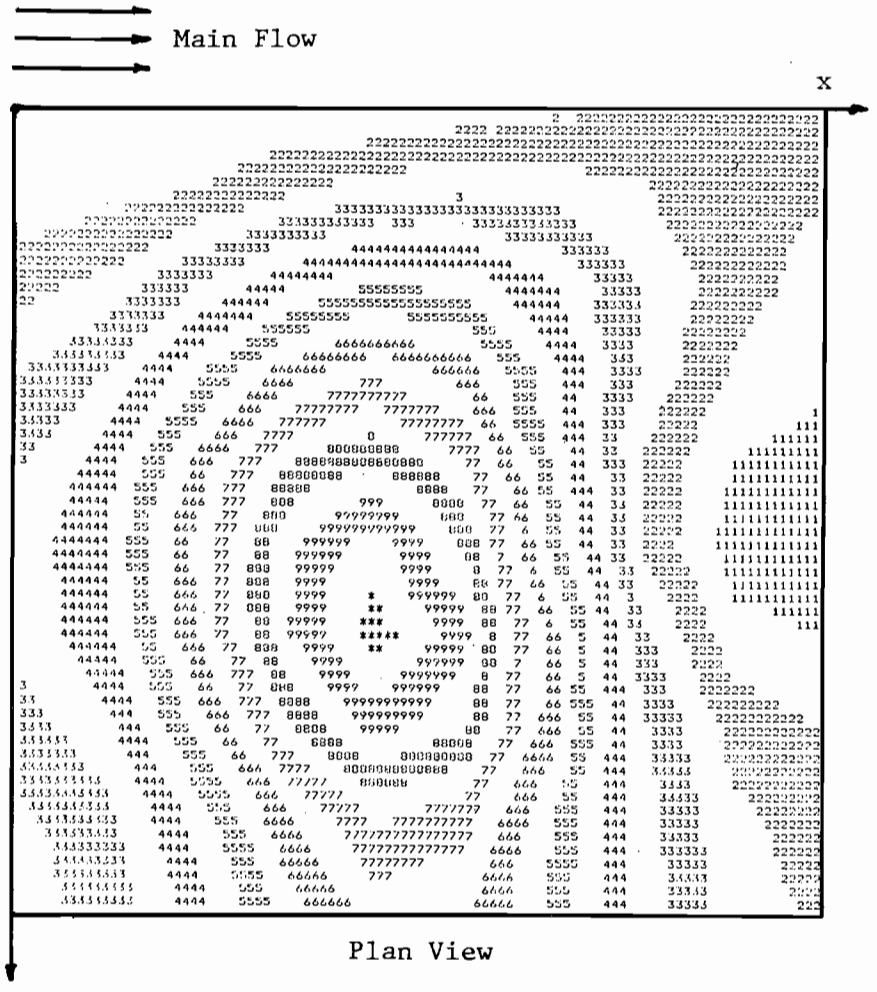

Run No. 7
Clock Time 6.0
C_{MAX} 2.80
Total Mass 95.07

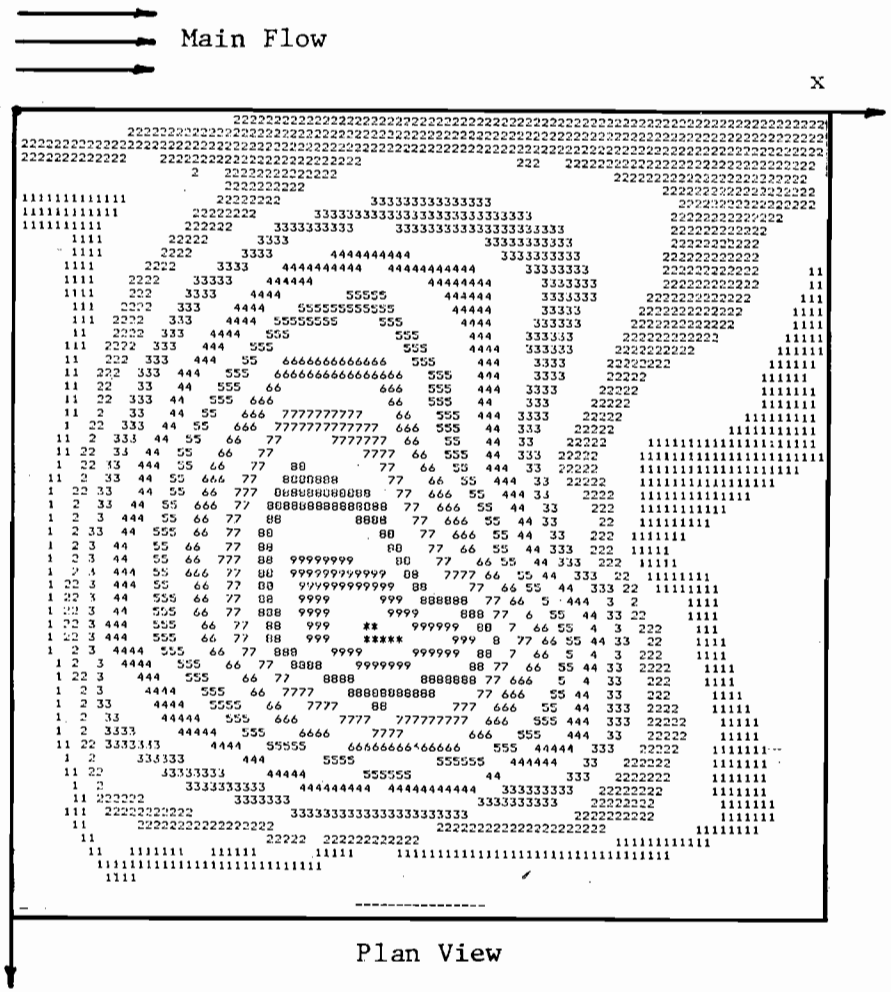

Run No. 11
Clock Time 6.0
C_{MAX} 4.12
Total Mass 100.56

Fig. 32. Normalized Concentration Contours

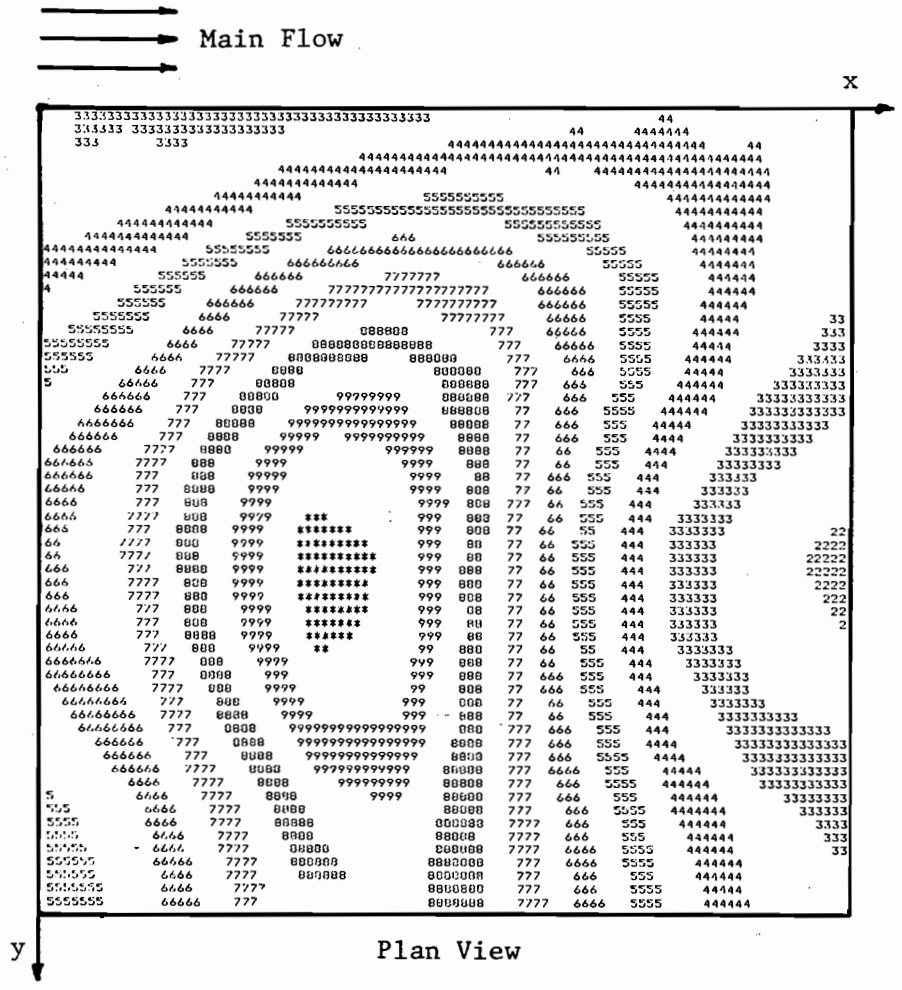

Run No. 7
Clock Time 8.0
C_{MAX} 2.03
Total Mass 93.96

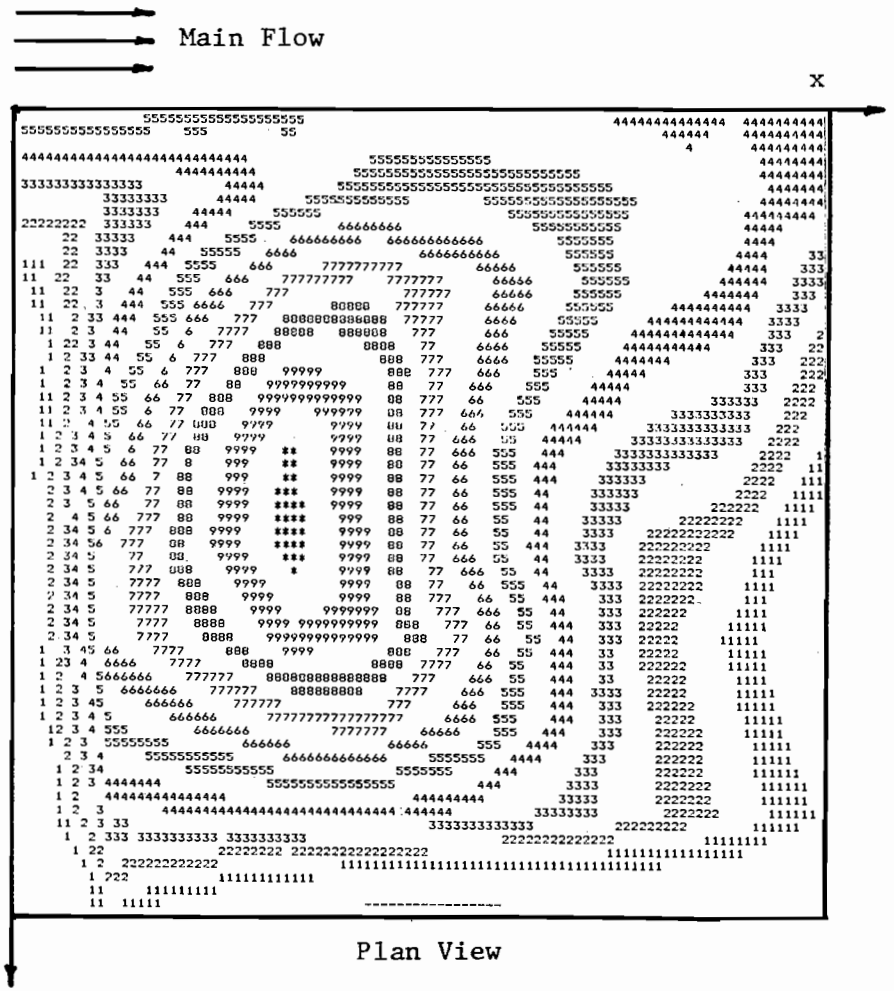

Run No. 11
Clock Time 8.0
C_{MAX} 2.88
Total Mass 101.21

Fig. 33. Normalized Concentration Contours

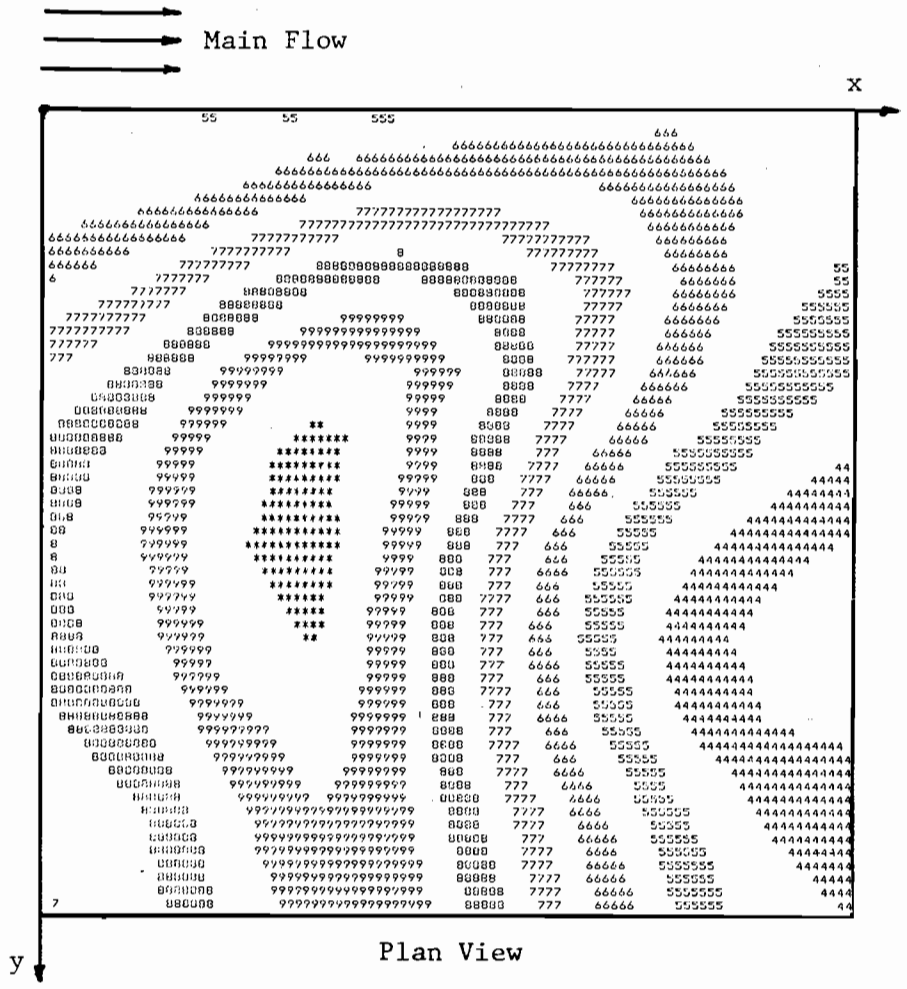

Run No. 7
Clock Time 10.0
C_{MAX} 1.67
Total Mass 93.17

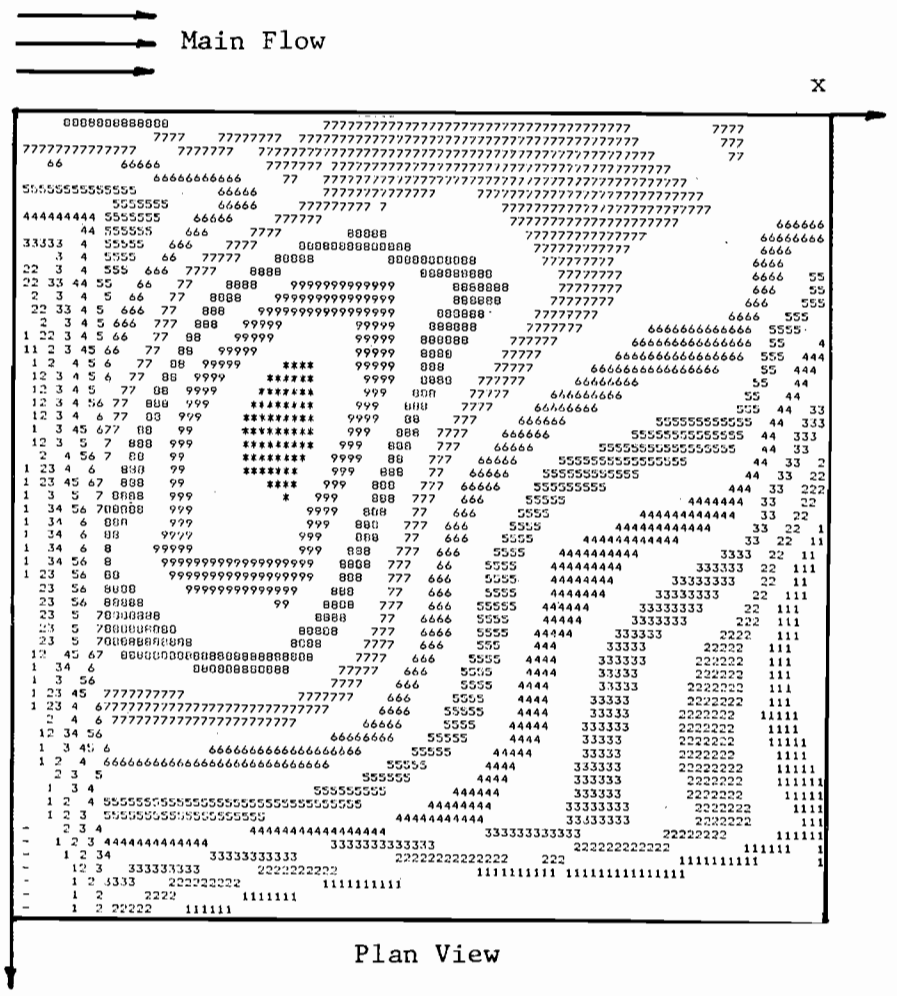

Run No. 11
Clock Time 10.0
C_{MAX} 2.33
Total Mass 100.82

Fig. 34. Normalized Concentration Contours

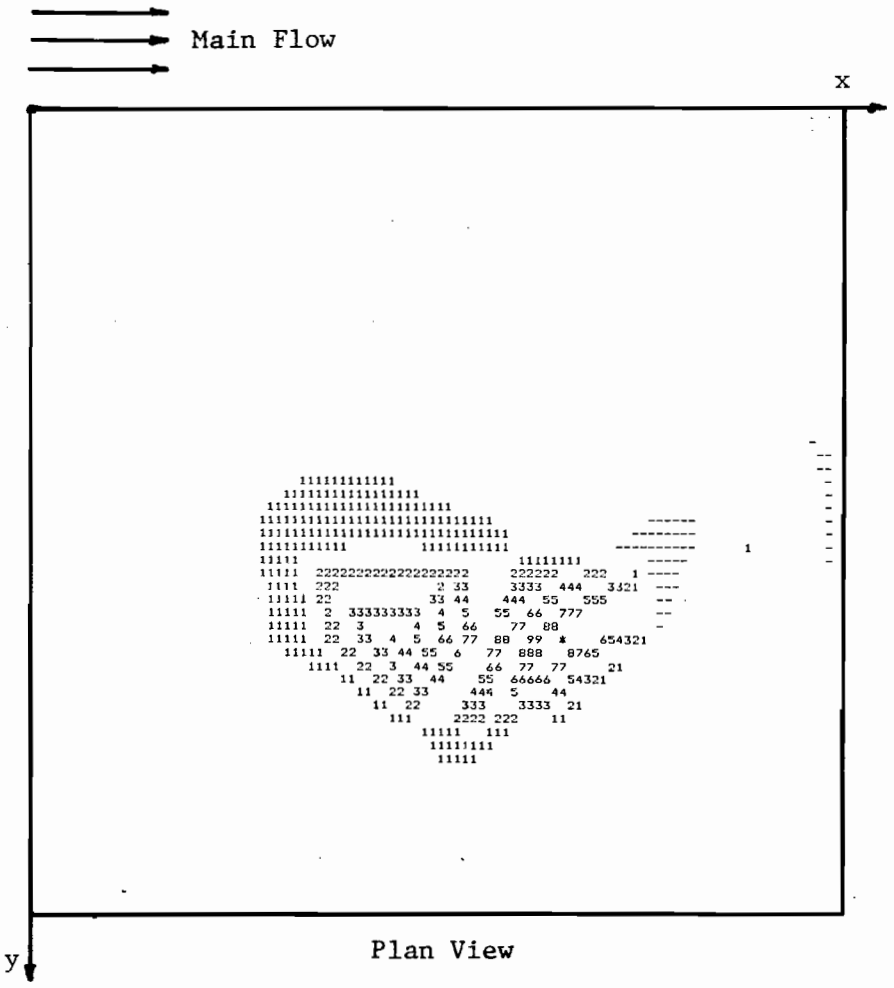

Plan View

Run No. 9
Clock Time 2.0
C_{MAX} 33.9
Total Mass 96.40

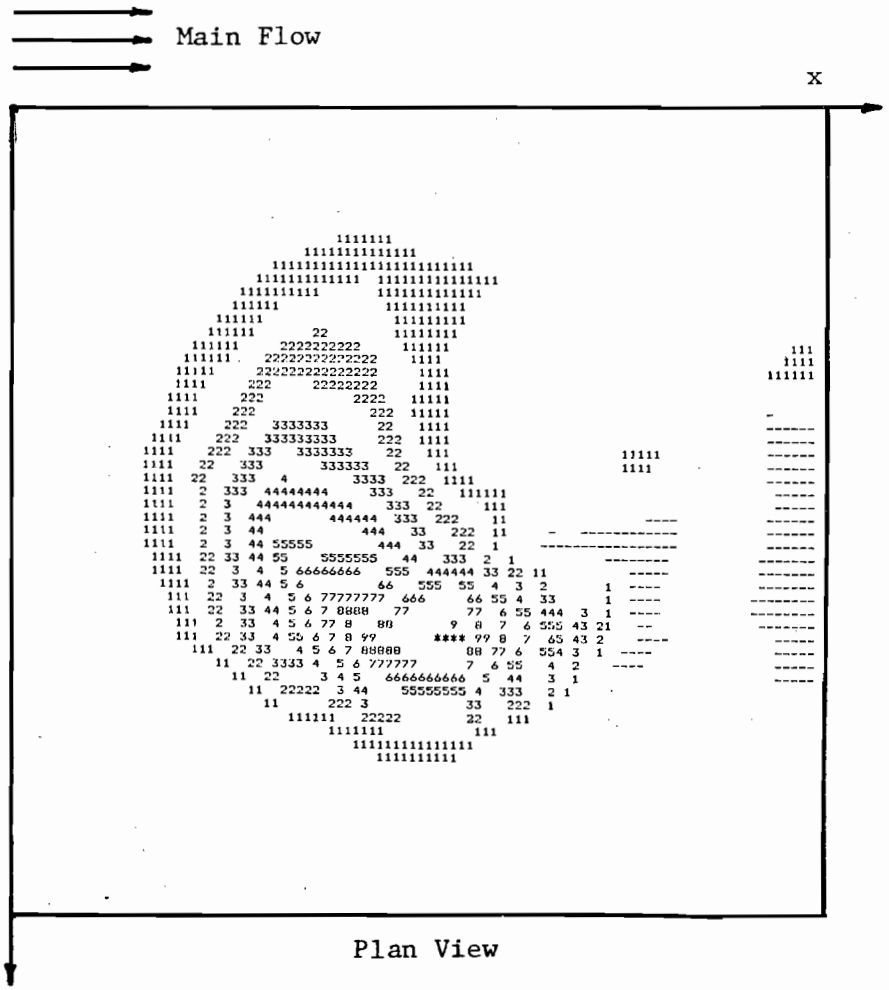

Plan View

Run No. 9
Clock Time 4.0
C_{MAX} 15.5
Total Mass 90.11

Fig. 35. Normalized Concentration Contours

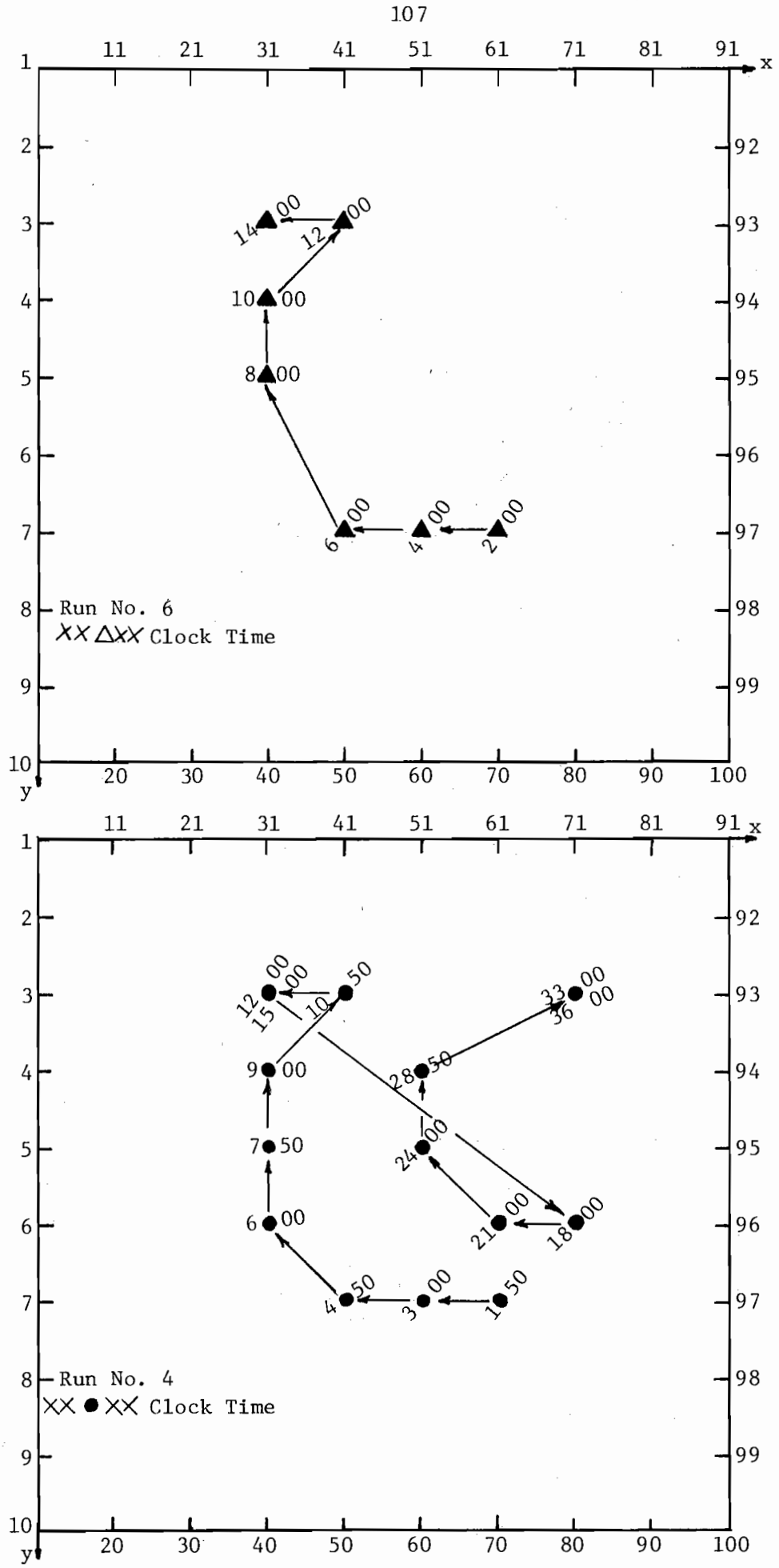

Fig. 36. Path of Maximum Concentration, C_{MAX}

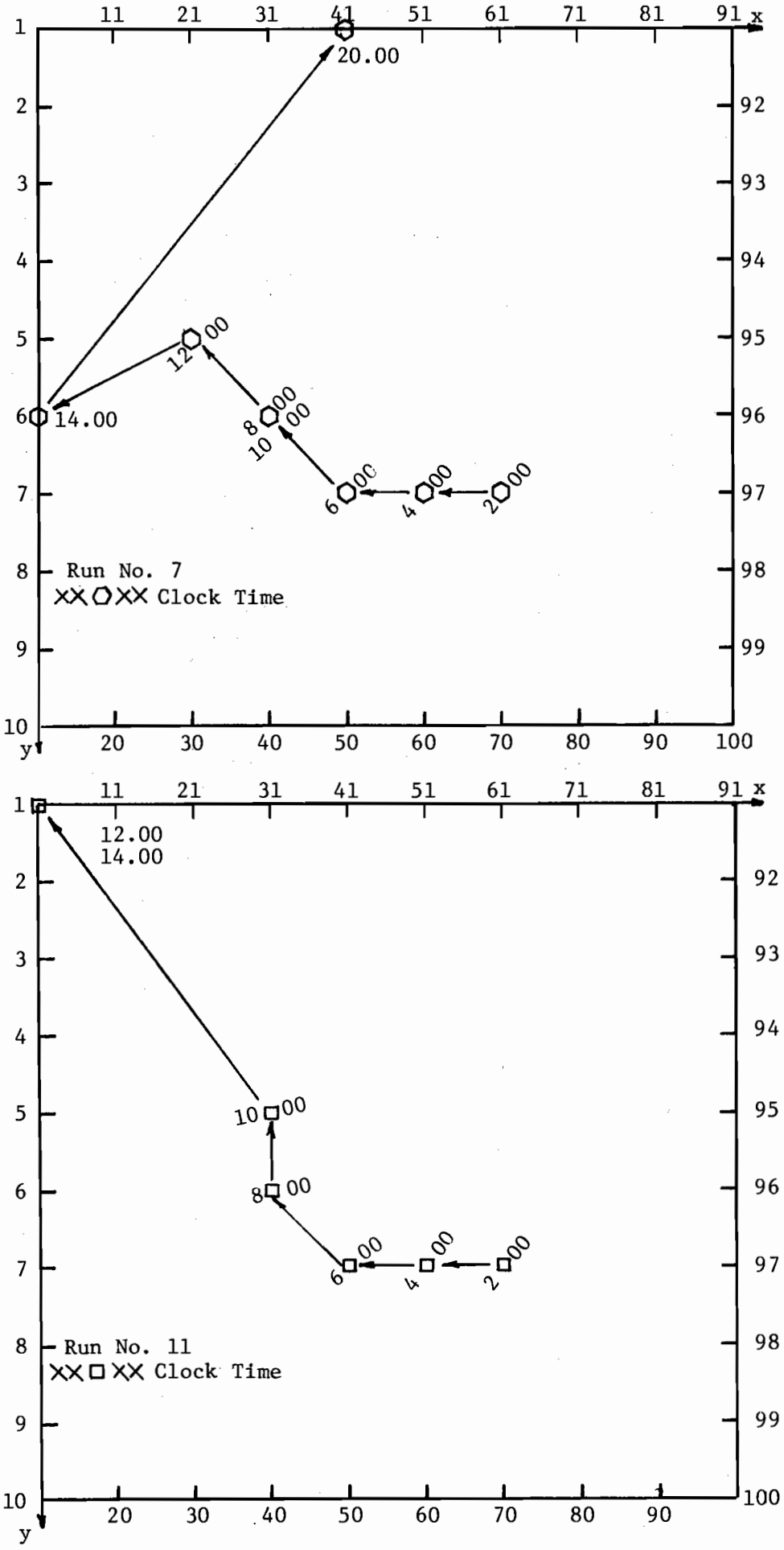

Fig. 37. Path of Maximum Concentration, C_{MAX}

The stability guidelines developed in section 4.3.3 for the scalar dispersion coefficient problem forecast the decisive role of the magnitude of the dispersion coefficient. Runs 3, 5, and 7 with dispersion coefficients of 0.2, 0.5, and 0.8, respectively proved to be stable. It can be seen in Fig. 16 that as the dispersion coefficient increases the rate mass loss decreases. Runs 2, 4, and 6 have been made with dispersion coefficient value of 0.1, but different time steps. They follow the same pattern, within 2%, of total mass change with time.

A simple test for the magnitude of the numerical diffusion does not appear to exist for the numerical model. However, as discussed in section 4.3.5, a ratio of ΔL to Δt having the same order of magnitude as the typical flow velocity may somewhat minimize the numerical diffusion. Specification of a typical velocity is not easy since velocity varies throughout the flow field. A time step of $\Delta t = 2.0$ units served well as a first approximation. The values of Δt may be chosen by using a typical velocity based on those in the region of highest mass concentration. Three values of Δt: 1.0, 1.5, and 2.0 units; were specified for Runs 2, 4, and 6 respectively with the same dispersion coefficient. The difference in concentration levels is most apparent during the early iterations, see Fig. 17. At the first common clock time of 2.0 units, the maximum concentration is highest for $\Delta t = 2.0$ and the lowest for $\Delta t = 1.0$. The maximum concentration value for all three time steps is with 1% after a clock time of 4.0 units. The highest concentration levels occurred in Run 9, program version II and $\Delta t = 2.0$. The calculated total mass shows losses over 18% of the initial mass but, examination of Fig. 35 reveals that numerical problems at the boundary may be the source of the mass loss. Interior element calculations may be stable. Run 5, with dispersion

coefficient of 0.8 has the lowest maximum concentration levels as would be expected.

The contour plots of Runs 2, 4, and 6; Figs. 18-29; clearly show the influence of advection in the mass transport process. The concentration contours are "stretched" in the direction of flow. The concentration patterns trailing the peak concentration show the influence of back dispersion. Note that the trailing concentrations for Run 6 ($\Delta t = 2$) are less dispersed than for Runs 4 ($\Delta t = 1.5$) or 2 ($\Delta t = 1.0$).

The method of dispersion vectorization implemented in Version II of the model reduces dispersion normal to the stream lines. This is substantiated by the concentration contour plot of Run 9, Fig. 35. Note, also, that in Fig. 35 the trailing contours are not smooth. The trailing concentration gradient for Run 9 is much higher than those for Runs 2, 4, and 6. The magnitude of the concentration gradient may be another source of numerical problems.

The comparison of concentration contours for Runs 7 and 11, Figs. 30-34, graphically demonstrates the effect of vectorizing the dispersion coefficient. The dispersion coefficient was at 0.5 for both runs to obtain stable computations for a sufficient clock time. Version I uses the values of 0.5 for the uniform scalar dispersion coefficient. Version II uses the product of 0.5 and the nodal velocity vector direction cosines to evaluate the location dependent components of the dispersion coefficient. The half cosine function used varies from 0 to 1, thus the effective dispersion calculated at each node will always be less than that used in Version I. The boundary element problems with Version II are notable after a clock time of 6.0 units.

The influence of advection is apparent in the path of maximum concentration for runs 4 and 6, Fig. 36. The path of maximum concentration for Runs 2 and 3 are similar. It is not clear at this time what induces the maximum concentration to consistently move from node 43 to node 33 before continuing in the direction of flow. The sudden movement of the maximum concentration from node 33 to node 76 in Run 2 may be in part due to higher velocities in the upper right sector of the flow field. In Run 7, the dispersion coefficient of 0.5 apparently was the leading factor which caused the path of maximum concentration to deviate from the results obtained from a lower dispersion coefficient.

Maximum concentration paths for Runs 7 and 11, Fig. 37, demonstrates another effect of vectorizing the dispersion coefficient.

The numerical experiments tend to support the stability and numerical diffusion analysis developed in the course of this study. Advection dominated transport has been simulated, but pure advection may not be achievable. The transport model, Version I, apparently has no difficulty generating a solution for very dispersive flow, (i.e. large dispersion coefficients).

The problem formulation tested in Run 2 was successfully simulated by the transport model. The dispersion coefficient of 0.1 appears to be sufficiently small so that the influence of advection can be observed. The stability guidelines suggest that a dispersion coefficient of 0.1 may be the threshhold of simulating advection dominated flow field having a characteristic Reynolds number of 10,000.

6. CONCLUSIONS AND RECOMMENDATIONS

6.1 Conclusions

Two-dimensional (depth averaged) numerical models have been developed to simulate streamline patterns and mass transport in a circulating flow generated and maintained by a uniform main flow. In the flow model, the vorticity transport equation has been numerically solved for the rotation of an incompressible fluid inside a square cavity. The velocity distribution generated by the flow model was subsequently used in the mass transport model to simulate mixing and movement of a finite quantity of mass introduced to the rotating flow at any location.

Results obtained from the simulation runs lead to the following conclusions:

1. Two-dimensional shear induced rotation can be generated by solving the vorticity transport equation subject to the appropriate boundary conditions. The numerical scheme used gives results comparable to those obtained by other researchers solving the same problem.
2. Characteristic Reynolds number based on the main stream velocity, width of the cavity, and viscosity can be used as a measure of the influence of the main flow on the water in the circulating region. Simulations show a stagnant region (eye) forming away from the geometric center of the flow field. At higher Reynolds numbers, this eye moves closer to the downstream wall of the cavity and at lower Reynolds numbers the eye moves closer to the center of the flow field. At very low Reynolds numbers (creeping flow), not simulated by the flow model developed here, the flow has been shown to be symmetrical about the center of the cavity.

3. The numerical scheme developed in this project is capable of simulating movement of a finite amount of mass in the circulating flow field. The scheme does not simulate the exchange of mass between the main flow and the circulating region.
4. Plot of total mass in the computation domain versus time (Fig. 16) show an initial oscillation of mass and eventual stabilization at a value below the initial input. This is in part due to the way total mass is computed after each iteration. Choice of dispersion coefficient, and computation time step are also responsible for gain or loss of mass in numerical simulations. It was found that the mass loss after stabilization becomes smaller as the dispersion coefficient gets larger.
5. No formal test of the magnitude and significance of numerical diffusion was conducted. However, inspection of the concentration contour plots may be used to provide qualitative guide for the level of numerical diffusion. Judicious grid spacing and selection of the computation time step can reduce numerical diffusion.
6. Variation of computation time step did not have significant effect on the maximum concentration level at equal clock times. However, the shape of the concentration contours away from the moving center of mass differed with variation in the computation time step.
7. Vectorization of the dispersion coefficient, weighted by the local velocity components, reduces the traverse spreading and increases the streamwise spreading of mass.

6.2 Recommendations

In order to further improve the mass transport model for application to more complex geometries and eventually field situations, the following recommendations are made:

1. Dispersion in circulating flow should be further investigated both in the laboratory and in the field. The relationship between the dispersion coefficients used in the numerical experiments reported here and those in actual flow situation must be determined in order to allow more realistic simulation of mass transport in circulating flows. Of particular interest is the role of the cross product terms in the dispersion coefficient tensor.
2. The exchange region between the circulating flow and the main flow must be investigated and incorporated in the model. Concentration distribution in the circulating region will be different from that given in this report if mass is allowed to escape from the circulating region into the main flow.
3. As an extension of recommendation 2 above, residence time of tracer mass entering the circulating region must be studied. Knowledge of the storage and release characteristics of circulating flows will help better estimate the longitudinal dispersion in streams with such regions. Furthermore, randomly spaced circulating regions can be incorporated in water quality models if their time dependent storage (build-up) and release (wash out) behavior are known.

4. The present geometry of the model (square) must be extended to other more complicated geometric shapes (e.g. trapazoid and semi-circle) and eventually to irregular shapes in preparation for simulation of field conditions.

Most of the above recommendations are presently being considered in a subsequent research project (No. 381502, Agreement No. INT CT 371500) funded by the U.S. Department of the Interior.

REFERENCES

1. Baker, A. J. 1976. The Finite Element Method Applied to Flow Field Predictions in Environmental Hydrodynamics. Proceedings of the First International Conference on Finite Elements in Water Resources, Princeton University, July, pp. 4.95-4.112.

2. Bear, J., 1972. Dynamics of fluids in porous media. New York: Am. Elsevier Publishing Co., 764 p.

3. Day, T. 1974. Dispersion in Natural Channels. Thesis presented to the University of Canterbury, New Zealand in partial fulfillment of the requirements for the degree of Doctor of Philosophy.

4. Fischer, H. B. 1966. A Note on the One-Dimensional Dispersion Model. International Journal of Air and Water Pollution, Vol. 10, Nos. 6/7, pp. 443-452.

5. Fischer, H. B. 1967. The Mechanics of Dispersion in Natural Streams. Journal of the Hydraulics Division, ASCE, Vol. 93, No. HY6, Nov., pp. 187-216.

6. Fischer, H. B. 1973. Longitudinal Dispersion and Turbulent Mixing in Open Channel Flow. Annual Review of Fluid Mechanics, Vol. 5, No. 8036, pp. 59-78.

7. Fischer, H. B., List, E. J., Koh, R.C.Y., Imberger, J., and Brooks, N.H.,1979. Mixing in Inland and Coastal Waters. New York: Academic Press, Inc., 285 pp.

8. Findikakis, A. N., and Street, R. L. 1982. Mathematical Description of Turbulent Flows. Journal of the Hydraulics Division, ASCE, Vol. 108, No. HY8, Aug., pp. 904-920.

9. Flokstra, C. 1977. The Closure Problem for Depth-Averaged Two-Dimensional Flow. Paper A106, 17th International Association for Hydraulic Research Congress, Baden-Baden, Germany, pp. 247-256.

10. Forsyth, G. E., and C. B. Moler. Coomputer Solution of Linear Algebraic Systems, Englewood Cliffs, N.J.: Prentice Hall, 1967.

11. Grove, D. 1977. The Use of Galerkin-Finite Element Methods to Solve Mass-Transport Equations. USGS, Water Resources Investigations 77-49.

12. Lam, D.C.L. 1976. Comparison of Finite-Element and Finite-Difference Methods for Nearshore Advection-Diffusion Transport Models. Proceedings of the First International Conference on Finite Elements in Water Resources, Princeton University, pp. 1.115-1.129.

13. Langley Research Center Staff. 1975. Numerical Studies of Incompressible Viscous Flow in a Driven Cavity. National Aeronautics and Space Administration, NASA SP-378.

14. Lean, G. H., and Weare, I. J. 1979. Modeling Two-Dimensional Circulating Flow. Journal of the Hydraulics Division, ASCE, Vol. 106, No. HY1, Jan., pp. 17-26.

15. Lokrov, V. P., and Shen, H. W. 1983. Analysis of the Charactistics of Flow in Sudden Expansion by Similarity Approach. Journal of Hydraulic Research, 21, No. 2, pp. 119-132.

16. Lozuik, L. A., Anderson, J. C., and Belytchko, T. 1972. Hydrothermal Analysis by Finite Element Method. Journal of the Hydraulic Division, ASCE, Vol. 98, No. HY11, Nov., pp. 1985-1998.

17. McGurik, J., and Rodi, W. 1979. Calculation of Unsteady Mass Exchange Between a Main Stream and a Dead Water Zone. Proceedings of International Conference on Hydraulic Engineering in Water Resources Development and Management, Vol. 3, Subject B, XVIII Congress of IAHR, Italy, pp. 25-32.

18. Pederson, F. B. 1977. Prediction of Longitudinal Dispersion in Natural Streams. Institute of Hydrodynamics and Hydraulic Engineering, Technical University of Denmark, Series Paper No. 14, Feb., 69 p.

19. Pinder, G. F., and Gray, W. G. 1977. Finite Element Simulation in Surface Sand Subsurface Hydrology. New York: Academic Press.

20. Ponce, V. M., and Yabusaki, S. B. 1981. Modeling Circulation in Depth-Averaged Flow. Journal of the Hydraulics Division, ASCE, Vol. 107, No. HY11, Nov., pp. 1501-1518.

21. Roberts, K. V., and Weiss, N. O. 1966. Convective Difference Schemes. Math. Comput., 20(94), pp. 272-297.

22. Sabol, G. V., and Nordin, C. F., Jr. 1978. Dispersion in Rivers as Related to Storage Zones. Journal of the Hydraulics Division, ASCE, Vol. 104, No. HY5, May, pp. 695-708.

23. Scheidegger, A. E. 1961. General Theory of Dispersion in Porous Media. Journal Geophysics Research, V. 66, No. 10, p. 3273-3278.

24. Schlichting, H. 1968. Boundary Layer Theory. 6th ed., New York: McGraw-Hill Book Co., 748 pp.

25. Shapine, L. F., and R. C. Allen. 1973. Numerical Computing: An Introduction. W. B. Saunders Company, 258 pp.

26. Siemons, J. 1970. Numerical Methods for the Solution of Diffusion-Advection Equations. Publ. 88, Delft Hydraulics Laboratory, The Netherlands, Dec., pp. 1-32.

27. Smith, I. M., Farraday, R. V., and O'Connor, B. A. 1973. Rayleigh-Rite and Galerkin Finite Elements for Diffusion-Convection Problems. Water Resources Research, Vol. 9, No. 3, June.

28. Tsai, Y. G., and Holley, E. R. 1979. Temporal and Spatial Moments for Longitudinal Mixing in Prismatic Channels with Storage in Separation Zones. Hydraulic Engineering Series No. 35, University of Illinois, Champaign-Urbana.

29. Valentine, E. M., and Wood, I. R. 1977. Longitudinal Dispersion with Dead Zones. Journal of the Hydraulics Division, ASCE., Vol. 103, No. HY9, Sept., pp. 975-990.

30. Westrich, B. 1976. Simulation of Mass Exchange in Dead Zones for Steady and Unsteady Flow Conditions. International Symposium on Unsteady Flow in Open Channels, Newcastle upon-tyne, England.

31. White, F. M.. 1968. Viscous Fluid Flow. New York: McGraw-Hill Book Co., 748 pp.

32. Zelazny, S. W., and Baker, A. J.. 1975. Predictions in Environmental Hydrodynamics Using the Finite Element Method. AIAA Journal, Vol. 13, No. 7, January, pp. 36-46.

APPENDIX I

Flow Model Algorithm

Available from University of Illinois
Water Resources Center Upon Request

APPENDIX II

Mass Transport Algorithm (Version I); and
Subroutine MATRIX for Mass Transport Algorithm (Version II)

Available from University of Illinois
Water Resources Center Upon Request

LIST OF OTHER PUBLICATIONS ON PROJECT

1. Schmitt, L. J. 1983. A Method of Improving Aquatic Habitat in the Navigation Channel of the Kaskaskia River, Illinois. Department of Civil Engineering, University of Illinois, Urbana, M.S. Thesis, Jan.

2. Schmitt, L. J., E. E. Herricks, and V. Alavian. 1982. Modeling Fisheries Habitat: Physical Hydraulic Simulation of Structural Modification to Rivers. Proceedings of the Third International Conference on State-of-the-Art in Ecological Modeling, Colorado State University, Fort Collins, May 24-28.